

Gamma SkyShine Calculations for Shielded Sources

by

Michael S. Bassett

B.S., Kansas State University, 1986

A MASTER'S THESIS

submitted in partial fulfillment of the

requirements for the degree

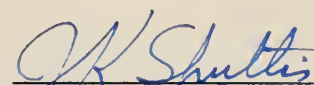
MASTER OF SCIENCE

Department of Nuclear Engineering

KANSAS STATE UNIVERSITY
Manhattan, Kansas

1989

Approved by:


Major Professor

LD
2662
.T4
NE
1887
B87
C. 2

ALL208 301702

TABLE OF CONTENTS

| | Page |
|--|------|
| 1. INTRODUCTION | 1 |
| 1.1 The Skyshine Problem | 1 |
| 1.2 Previous Skyshine Investigations | 2 |
| 1.3 Purpose of Study | 7 |
| 2. REVIEW AND MODIFICATION OF THE MICROSKEYSHINE METHOD | 10 |
| 2.1 Calculation of Detector Response to a Gamma Photon Beam | 10 |
| 2.2 Approximation of Beam Response Functions | 17 |
| 2.2.1 Interpolation of the Fitted Response Functions | 19 |
| 2.3 SkyShine Dose Calculations Using Beam Response Functions | 20 |
| 2.3.1 SkyShine Calculations for a Source in A Silo | 21 |
| 2.3.2 Unshielded Silo Calculation | 24 |
| 2.3.3 Shielded Silo Dose Calculation | 25 |
| 2.4 Extension to Polyenergetic and Anisotropic Point Sources | 27 |
| 3. A COMPOSITE SKYSHINE METHOD | 30 |
| 3.1 Decoupling the Shield and Air Transport Calculations | 31 |
| 3.1.1 Validity of Decoupling for Disk Shields | 31 |
| 3.2 The Composite Method for a Shielded-Silo SkyShine Problem | 37 |
| 3.2.1 Leakage from the Source Silo | 40 |
| 3.2.2 Approximation of Leakage by an Effective Point Source | 43 |
| 3.2.3 Use of a 1-D Model for Calculating the Effective Skyshine Source | 44 |
| 3.2.4 1-D Boundary Condition for a Point Collimated Source | 46 |
| 3.3 Transport Calculation of the Effective Point Skyshine Source | 49 |
| 3.3.1 Use of KSLAB for Shield Penetration Calculations | 50 |
| 3.3.2 Effective Skyshine Source for the Shielded Silo Problem | 55 |
| 3.4 Validation of the Composite Dose Calculation Method | 61 |
| 3.4.1 Benchmark Experimental Calculations | 61 |

| | Page |
|--|------|
| 4. ASSESSMENT OF THE MICROSKEYSHINE METHOD | 70 |
| 4.1 Nitrogen-16 Photon Test Case | 71 |
| 4.1.1 Nitrogen-16 Results for Concrete Shields | 71 |
| 4.1.2 Results for Nitrogen-16 Shielded by Iron | 79 |
| 4.2 Cobalt-60 Photon Test Cases in Concrete | 82 |
| 4.2.1 Results for Co-60 Photons and Concrete Shields | 82 |
| 4.3 0.5 MeV Photon Test Cases in Concrete | 90 |
| 4.3.1 Results for 0.5 MeV Photons in Concrete | 90 |
| 4.4 Composite Skyshine Results | 98 |
| 5. CONCLUSIONS | 104 |
| 5.1 Suggestions for Further Study | 107 |
| 6. ACKNOWLEDGEMENTS | 108 |
| 7. BIBLIOGRAPHY | 109 |
| Appendix A | 112 |

LIST OF FIGURES

| Figure | | Page |
|--------|---|------|
| 2.1 | Geometrical representation used to calculate the response functions for MicroSkyshine [Sh87] | 11 |
| 2.2 | Illustration of the variables representing the physical distances used in the MicroSkyshine method for a point source in a silo [Sh87] | 22 |
| 2.3 | Angular coordinate system used to transform the integral equation in MicroSkyshine [Sh87] | 23 |
| 2.4 | Effective slab thickness for a photon penetrating a slab of thickness t at an angle θ | 26 |
| 3.1 | Angular and geometrical illustration of the variables with a point source on the axis of a cylindrical shield used to calculate the reentrant flux into the shield | 33 |
| 3.2 | Fraction of photons from a point source on the axis of a cylindrical shield reflected back into a cylindrical shield | 38 |
| 3.3 | Photon scattering paths from a point source into a silo causing a radiation field outside the silo | 39 |
| 3.4 | Roof-air interface coordinate system used in estimating the source condition on the silo shield's top surface | 42 |
| 3.5 | Discrete ordinates coordinate system defined inside a slab shield as used in the one-dimensional transport code KSLAB [Ry79] | 52 |
| 3.6 | Example breaking apart the angular coordinate system into six distinct regions which will allow different source collimation angles | 53 |
| 3.7 | Emergent angular flux densities spline fit for the eighth energy group of the N-16 source for a source collimation angle of 120° | 58 |
| 3.8 | Emergent angular flux densities for the source energy group spline fit at intermediate points (i.e. between the KSLAB values) over the outward angular directions (i.e. out of the slab face) for the N-16 source collimated at 120° | 59 |

| | | |
|------|---|------|
| | | Page |
| 3.9 | Emergent angular flux densities for the source energy group spline fit in two regions (one above the source collimation angle and the other below it) for the N-16 source collimated at 120° | 60 |
| 3.10 | MicroSkyshine results (---), Composite Method results (—), and DOT results —·—·—) compared to the experimental data from the K-State Benchmark experiment [C178] for shield thicknesses of 21 and 42.8 cms | 66 |
| 3.11 | Comparison using Koch and Herchonroder's data [Ke82] (---) with the composite method results (—) and the K-State benchmark experimental results[C178] | 68 |
| 4.1 | Fractional difference between the MicroSkyshine method with the composite method for concrete shields of various mfp thicknesses using a N-16 source collimated at 160° | 73 |
| 4.2 | Fractional difference results comparing the MicroSkyshine method with the composite method for concrete shields of various mfp thicknesses using a N-16 source collimated at at 120° | 75 |
| 4.3 | Fractional difference results concerning the MicroSkyshine method with the composite method for concrete shields of various mfp thicknesses using a N-16 source collimated at 80° | 76 |
| 4.4 | Fractional difference results comparing the MicroSkyshine method with the composite method for concrete shields of various mfp thicknesses using a N-16 source collimated at 40° | 77 |
| 4.5 | Plot of the skyshine dose rate at 1000 m for various mfp concrete shields illuminated by N-16 gamma photons. The solid line (—) is the composite method and the dashed line (---) is the MicroSkyshine method | 78 |
| 4.6 | Fractional difference results comparing the Micro-Skyshine method with the composite method for iron shields of various mfp thicknesses using a N-16 source collimated at 160° | 80 |

| | Page |
|------|---|
| 4.7 | Fractional difference results comparing the Micro-Skyshine method with the composite method for concrete shields of various mfp thicknesses using a Co-60 point source collimated at 160° |
| | 84 |
| 4.8 | Fractional difference results comparing the Micro-Skyshine method with the composite method for concrete shields of various mfp thicknesses using a Co-60 point source collimated at 120° |
| | 85 |
| 4.9 | Fractional differences between MicroSkyshine and the composite method results for concrete shields of various mfp thicknesses using a Co-60 point source collimated at 80° |
| | 87 |
| 4.10 | Fractional differences between MicroSkyshine and the composite method results for concrete shields of various mfp thicknesses using a point Co-60 source collimated at 40° |
| | 88 |
| 4.11 | Plot of the skyshine dose rate at 600 m for various concrete shield thicknesses illuminated by Co-60 gamma photons. The solid line (—) is the composite method and the dashed line (— —) is the Micro-Skyshine method |
| | 89 |
| 4.12 | Fractional differences between MicroSkyshine and the composite method results for concrete shields of various thicknesses using a point .5 MeV source collimated at 160° |
| | 92 |
| 4.13 | Fractional difference results comparing the Micro-Skyshine method with the composite method for concrete shields of various mfp thicknesses using a .5 MeV source collimated at 120° |
| | 93 |
| 4.14 | Fractional differences between MicroSkyshine and the composite method results for concrete shields of various mfp thicknesses using a point .5 MeV source collimated at 80° |
| | 95 |
| 4.15 | Fractional differences between MicroSkyshine and the composite method results for concrete shields of various mfp thicknesses using a point .5 MeV source collimated at 40° |
| | 96 |

| | | Page |
|------|--|------|
| 4.16 | Plot of the skyshine doses at 300 m for various thicknesses of concrete shields illuminated by .5 MeV gamma photons. The solid line (—) is for the composite method and the dashed line (— —) is for the MicroSkyshine method | 97 |
| 4.17 | Example plot showing the source-energy dependence of the composite skyshine dose with source-to-detector distance for the sources collimated at 160° and covered by a 1.5 mfp shield (with respect to each of the source energies) | 99 |
| 4.18 | Example plot showing the variation of the composite skyshine dose with various degrees of source collimation for a N-16 point source at a source-to-detector distance of 475 m | 100 |
| 4.19 | Example plot showing the variation of the composite skyshine dose with various source collimation angles for the Co-60 source with a source-to-detector distance of 475 m | 101 |
| 4.20 | Example plot showing the variation of the composite skyshine dose with various source collimation angles for the .5 MeV source with a source-to-detector distance of 475 m | 102 |

LIST OF TABLES

| Table | | Page |
|-------|--|------|
| 2.1 | Energy group structure used in deriving the beam response functions used in MicroSkyshine [Sh87] | 16 |
| 2.2 | The discrete beam directions used by Faw and Shultis in deriving the new beam response functions used in MicroSkyshine [Sh87] | 16 |
| 3.1 | Material composition of the concrete used in preparing the group-to-group cross sections used in K-SLAB [Ch87] | 62 |
| 3.2 | Angular directions and angular weights used in calculating the exact kernel cross sections for the Co-60 benchmark calculations. This quadrature set is designed for a source collimation angle of 150.5 degrees | 63 |
| 3.3 | Energy group ranges and average energies used in the Co-60 benchmark calculations. The average energies were generated by PHOGROUP [Ry79] and were used by SKYCALC [Ba88] | 63 |
| 3.4 | Fraction of the total dose each energy group contributes to the skyshine dose for source-to-detector mass thickness for the 21 and 42.8 cm benchmark cases | 69 |
| 4.1 | Energy group structure and average group energies Used with the 6.129 MeV N-16 photon in generating the exact kernel group-to-group cross sections for iron and concrete. The generated cross sections will support source collimation angles of 160, 120, 80 and 40 degrees | 72 |
| 4.3 | Comparison of the normalized SkyShine dose calculated with the composite method for an iron and a concrete shield of 1 mfp thickness. The fraction difference is calculated using (iron-dose - concrete-dose)/concrete-dose | 81 |
| 4.4 | Energy group structure and average group energies used with the two Co-60 photons to generate the exact kernel group-to-group cross sections for iron and concrete. The generated cross sections will support source collimation angles of 160, 120, 80, and 40 degrees | 83 |

| | Page |
|-----|---|
| 4.5 | Angular direction cosines and Gaussian weights used to generated the exact kernel group-to-group cross sections for the Co-60 photon energies of 1.33 and 1.17 MeV in concrete. The direction cosines and Gaussian weights will allow angular source collimation angles of 160, 120, 80, and 40 degrees |
| | 83 |
| 4.6 | Energy group structure and average group energies used with the 0.5 MeV photons to generate the exact kernel group-to-group cross sections for iron and concrete. The generated cross sections will support source collimation angles of 160, 120, 80, and 40 degrees |
| | 91 |
| 4.7 | Angular direction cosines and Gaussian weights used to generate the exact kernel group-to-group cross sections for the 0.5 MeV photons in concrete. The direction cosines and Gaussian weights will allow angular source collimation angles of 160, 120, 80, and 40 degrees |
| | 91 |

1. INTRODUCTION

1.1 The Skyshine Problem

Gamma-ray doses outside of areas containing nuclear materials can generally be broken into two components. The first component is the direct dose contribution arising from gamma photons that travel directly from the source to the detector location. The direct component can usually be evaluated easily using ray analysis techniques [Ch84]. The second dose component, which is generally more difficult to calculate, is due to indirectly scattered radiation and includes skyshine radiation, radiation streaming through ducts, and radiation reflected from surfaces (albedo radiation) [Ch84]. Skyshine dose refers to the dose caused by the reflection of photons in the air back to a ground target. In this study, approximate methods for calculating the indirect skyshine gamma dose are considered.

Outside of nuclear facilities, the skyshine dose can become an important component of the total offsite dose rate [Pe84, An87] and has become an important concern in the radiological assessment of these facilities. Skyshine dose calculations are required for accident analysis calculations at PWR and BWR nuclear power plants [Pe84, An87]. In BWR power plants the movement of nitrogen-16 from the reactor to the turbine room also requires an estimate of the skyshine dose to be made during normal operations [An87]. The storage of nuclear waste both above ground, in buildings, and below ground will likewise require an analysis of the skyshine dose during the design of the disposal facility.

Evaluation of the skyshine dose is, in general, more complicated than the ray-analysis techniques used for analyzing the direct dose [Fa87]. The techniques

used to evaluate the skyshine dose can range from engineering approximations [Pe84] to complete numerical solutions of the multigroup transport equation.

1.2 Previous Skyshine Investigations

Using a Monte-Carlo method, Lynch et al. [Ly58] calculated (at various source-to-detector distances) the dose rate caused by multiply scattered gamma photons emitted by a monoenergetic monodirectional beam of gamma photons into an infinite air medium. The dose rates caused by photons of a given direction and energy were normalized to unit source strength (1 photon per unit time) to yield a response function for a source photon of a given energy and direction of travel. Lynch's Monte-Carlo calculations were carried out for specific photon energies, specific source-detector distances, and specific directions of travel relative to the source-detector axis [Ly58]. The response functions generated from the Monte Carlo results are valid for source-to-detector distances from 5 m to 100 m, for energies from 0.6 MeV to 12 MeV, and for beam angles from 1 to 180 degrees relative to the source-detector axis [Ly58].

Trubey [Tr61] proposed an approximate method for calculating the skyshine flux by considering only a single scatter for the gamma photons. This single-scatter approximation ignored the contribution of multiply scattered gamma photons as well as the attenuation and buildup of photons in the air. Moreover, it was not considered suitable for a shielded source. However, the single scatter approximation for a bare source agreed well with the Monte-Carlo results calculated by Lynch [Tr61].

Kitazume [Ki68] later extended the single scattering approximation by incorporating exponential attenuation and a Taylor-type buildup factor.

Exponential attenuation was included along both the uncollided photon path and the scattered photon path. The Taylor buildup factor was applied only along the scattered photon path. The inclusion of exponential attenuation and photon buildup in the single scattering formulation allowed this method to be used beyond the 100m source-to-detector lengths considered by Trubey [Ki68]. Kitazume's results were in good agreement with Lynch's Monte Carlo results for beam angles less than 60 degrees at all energies and source-to-detector distances considered. At angles greater than 60 degrees, Kitazume's method was in better agreement with Lynch's results than were Trubey's results, being at most 20% lower than results reported by Lynch et al. [Ki68].

With these successful point-kernel approaches for estimating the photon skyshine dose, general purpose codes were developed for use in complex physical geometries. One such widely used point-kernel code is G^3 [Ma73] which uses surfaces defined by quadratic equations to define the geometry of the problem. G^3 uses exponential attenuation of the direct (uncollided) beam and has the option of using buildup of scattered photons in the scattered leg to account for multiple scattering [Ma73]. However at present, G^3 cannot deal with buildup in shielding structures along the unscattered photon's path of travel.

A specialized extension of the single-scattering approximation accounting for overhead shielding above a point isotropic source was proposed by Roseberry and Shultis [Ro80, Ro82]. Roseberry and Shultis proposed a point-kernel model with exponential direct beam attenuation, buildup of scattered photons in the scattered air leg, and an infinite-medium buildup factor for the overhead shield. The infinite-medium buildup factor was introduced to approximate the scattered photons produced in the shield. Their model gave reasonably good agreement

when compared to experimental data obtained from a shielded skyshine benchmark experiment [Cl78, Sh78, Na81].

A more accurate way of calculating the skyshine dose for an overhead shielded gamma source would be to use a calculational technique based on an exact transport description of the particular skyshine problem. The solution of the transport equation for skyshine geometries normally requires a multidimensional geometric representation and a multigroup energy formulation. One way for solving such a multidimensional, multigroup transport equation is to use Monte Carlo techniques. General purpose Monte Carlo codes that are available to solve skyshine problems include COHORT [So75] and OGRE [Pe65].

Discrete ordinates codes such as DOT [My73] and ANISN [En67] have also been used to solve some skyshine problems. The discrete ordinates procedure can give very accurate solutions for a geometry (usually simple) that it is capable of modeling. Unfortunately, both multidimensional discrete-ordinates solutions and multidimensional Monte-Carlo results require large computational effort, thereby limiting the usefulness of these codes for preliminary or routine design and safety studies.

To reduce the computational effort, and yet maintain acceptable accuracy for the estimation of skyshine doses from shielded sources, codes based on semi-empirical skyshine methods have been developed. Such specifically designed skyshine codes use response functions (obtained by fitting an empirical formula to Monte Carlo skyshine results) to calculate the skyshine dose. Examples of such codes include SKYSHINE [Pr76], SKYSHINE-II [La79], and SKYSHINE-III [La88]. These three codes consider radiation sources (photons or neutrons) in a rectangular structure with four walls, a roof, and a floor. The codes break each of

the containment surfaces up into a series of different sections, each with its own attenuation properties. With a Monte Carlo sampling technique, the radiation energy and location on the containment surface through which the radiation will stream are chosen. After a correction for attenuation as the beam penetrates through the structure, the contribution to the skyshine dose made by the transmitted beam is then calculated with the use of the beam response formulas.

To reduce the computational effort of running multidimensional transport codes for shielded skyshine problems, a one-dimensional transport code can be run to determine the photon distribution leaving the shielding around a source. This source distribution can then be used with any skyshine calculational method suitable for treating the unshielded skyshine problem. This hybrid approach was used by Keck and Herchenroder [Ke82] who combined the ANISN and the SKYSHINE II codes to calculate skyshine dose for the K-State Benchmark experiment [Cl78]. Peng [Pe84] also followed this two-stage approach by using ANISN and COHORT to calculate the skyshine dose rate outside of a nuclear power plant during a LOCA accident analysis.

To reduce the cost of analyzing shielded skyshine doses, Faw and Shultis [Fa87, Sh87] recently modified the original SKYSHINE-II method [La79]. They developed improved beam response-function formulas by fitting a three-parameter formula to skyshine results obtained with a point-kernel technique which accounted for gamma-ray attenuation, photon pair production, and buildup in the scattered leg. Unlike the SKYSHINE-II method (which used Monte Carlo techniques to account for different source emission directions), the skyshine dose was found by numerically integrating over all emission directions. This revised skyshine method was incorporated in the microcomputer code MicroSkyshine

[Gr87]. The MicroSkyshine method also added an interpolation scheme to make the beam response functions continuously variable in both energy and angle. The new response functions also eliminated the stochastic variations observed in the response functions used in the original SKYSHINE-II method.

MicroSkyshine can treat point, isotropic, polyenergetic, gamma sources with or without overhead shielding in two basic geometries. The first geometry MicroSkyshine treats is the case of a gamma photon source located on the axis of a cylindrical silo. The second geometry has the source and detector located on opposite sides of a vertical wall which may be oriented obliquely to the source-detector axis.

MicroSkyshine calculates the skyshine dose by integrating the fitted beam response functions over all directions allowed by the geometry of the problem. The effect of any overhead shielding is accounted for by exponentially attenuating the beam through the shield and then correcting the attenuation in the shield by multiplying by a buildup factor to obtain an estimate of all the gamma-rays (uncollided or scattered) passing through the shield. The MicroSkyshine method was found to be in good agreement with other methods and with the K-State benchmark skyshine experiment [Cl78] for the unshielded cases.

For shielded skyshine problems, there is a sparsity of published calculations and skyshine experimental measurements. The K-State benchmark skyshine experiment included two shielded silo configurations. Although the MicroSkyshine code gave better agreement with these experimental results than did other calculational methods [Fa87], the accuracy and robustness of the MicroSkyshine method for treating sources of different energies and degrees of collimation and shields of different materials and thicknesses was largely uncertain.

1.3 Purpose of Study

This study was motivated by the need to investigate the capabilities and limitations of the MicroSkyshine method for treating skyshine sources with a slab overhead shield. Inherently accurate methods for calculating the skyshine dose are methods based on a complete multidimensional description of the radiation field using the photon transport equation. However, the large computational cost needed to solve numerically the multidimensional transport equation precludes using this approach to obtain the many benchmark calculations needed to assess the MicroSkyshine method.

Less expensive approaches for calculating the skyshine dose from a shielded source include (1) the buildup factor approach for the shield used by Roseberry [Ro80, Ro82] and Faw and Shultis [Fa87, Sh87], and (2) the composite method used by Keck and Herchenroder [Ke82] and Peng [Pe84].

Although, the buildup factor approach is the simplest approach to the shielded skyshine problems, the magnitude of the error introduced by this method's approximations remains unexplored and unverified. Consequently, in this study a composite method, similar to Keck and Herchenroder's [Ke82], was developed. The composite method uses an accurate one-dimensional transport code to compute the emergent energy-angle distribution of photons on the outer shield's surface. Then a modified MicroSkyshine method uses this emergent distribution of photons as a bare skyshine source to calculate the skyshine dose at the detector location. This composite method, once verified, is used to investigate the accuracy of the buildup-factor approach used by MicroSkyshine to estimate the skyshine dose arising from a shielded point source in a silo.

The MicroSkyshine method for calculating the skyshine dose is reviewed in Chapter 2. The discussion of the MicroSkyshine method focuses on the generation of the fitted beam response functions, the energy and angular interpolation of the response functions, and the process by which the response functions are integrated to obtain the skyshine dose at the detector. In addition, an extension of the original MicroSkyshine method to treat sources with variable angular intensities is presented in Chapter 2.

In Chapter 3, the concept of using a two-step composite method to calculate the skyshine dose is explored. Specifically, this composite method combines a one-dimensional, discrete-ordinates, transport equation for the source shield with an extension of the MicroSkyshine method for calculating the skyshine dose from unshielded sources. The validity of using this two-step scheme for calculating the skyshine dose is explored and shown to be very reasonable for the class of skyshine problems considered in this study.

Also, in Chapter 3, a procedure to allow the use of a one-dimensional transport equation for the inherently two-dimensional transport problem of a point source shielded by a cylindrical slab is presented. This transformation technique allows the use of a one-dimensional, discrete-ordinates, transport calculation, rather than a two-dimensional calculation, to estimate the source distribution emerging from the slab shield, i.e. the distribution needed by the modified MicroSkyshine method. The basic outline of the discrete ordinates method for solving a one-dimensional transport problem is reviewed. The needed boundary source term for the one-dimensional discrete ordinates transport solution is then derived for the case of slab shielding over the skyshine source, and the process of linking the output from the discrete ordinates code to the modified MicroSkyshine

method is explained. Finally in Chapter 3, comparisons are given between the composite method to results from the K-State Benchmark Experiment. Comparisons to other skyshine calculation methods are also presented.

In Chapter 4, the composite method is used to investigate the accuracy of the MicroSkyshine method (exponential attenuation with buildup in the shield) for estimating the skyshine dose from a shielded point source. In this investigation gamma ray energies of 6.129 MeV, 1.25 MeV, and 0.5 MeV, and 4 different silo geometries with various shield thicknesses are considered.

Finally, Chapter 5 presents conclusions reached during this investigation as well as suggestions for further study.

2. REVIEW AND MODIFICATION OF THE MICROSKYSHINE METHOD

The beam response functions used by Faw and Shultis [Fa87, Sh87] to calculate the skyshine dose in the MicroSkyshine method were generated by fitting an empirical, three-parameter, response-function formula to results obtained by applying the point kernel method to a monoenergetic monodirectional beam of photons. Figure 2.1 shows the geometry used in estimating the response at a point isotropic detector caused by the monoenergetic monodirectional beam of photons in an infinite, homogeneous, air environment. The response produced by the detector will depend upon the photon's initial energy, the photon's initial direction of travel with respect to source-detector axis, the material in which the photon travels, and the source-to-detector distance.

In this chapter, the MicroSkyshine methodology for calculating the skyshine dose is studied. In particular, the review of the MicroSkyshine method examines the generation of the beam response functions, the fitting of an empirical formula to these response functions, and the use of the response functions in calculating the skyshine dose. The MicroSkyshine method is then extended to treat anisotropic point sources with variable source energies.

2.1 Calculation of Detector Response to a Gamma Photon Beam

The probability a photon (see Fig. 2.1) of energy E travels a distance y in air without interaction and then, while traveling a further distance dy , scatters through an angle θ_s into a unit solid angle is [Ch84]

$$Z N_e \sigma_c(E, \theta_s) e^{-\mu y} dy, \quad (2.1)$$

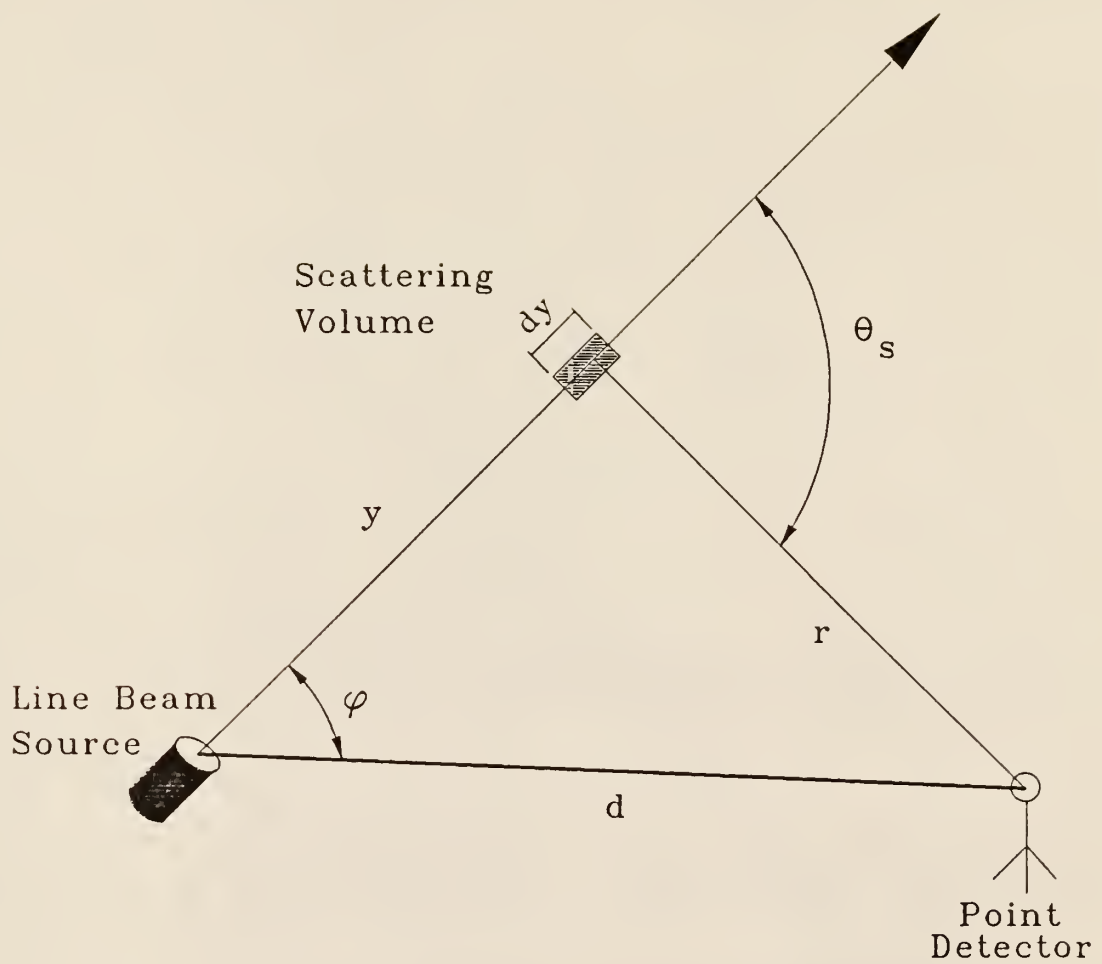


Figure 2.1. Geometrical representation used in calculating the response functions for MicroSkyshine [Sh87].

where ZN is the electron density of the air, μ is the total interaction coefficient at energy E , and ${}_e\sigma_c(E, \theta_s)$ is the Klein–Nishina differential scattering cross section. This differential scattering cross section can be approximated by the free–electron Klein–Nishina differential scattering cross section, and is given by [Ch84]

$${}_e\sigma_c(E, \theta_s) = \frac{1}{2} r_e^2 p [1 + p^2 - p (1 - \cos \theta_s)], \quad (2.2)$$

where

$$p = \frac{m_e c^2}{m_e c^2 + E - E \cos \theta_s}, \quad (2.3)$$

$m_e c^2 = 0.511$ MeV, and r_e is the classical electron radius. Source photons with energies greater than 1.02 MeV can produce annihilation photons. The probability that a source photon while traveling a distance dy after traveling a distance y produces an annihilation photon traveling towards the detector is [Sh87]

$$\frac{1}{2\pi} N \sigma_{pp}(E) e^{-\mu y} dy, \quad (2.4)$$

where N is the atomic density of the material being travelled through and $\sigma_{pp}(E)$ is the microscopic pair production cross section at energy E .

The response at the detector, without buildup, due to a beam of photons with energy E and with direction of travel ϕ can be found by integrating Eqs. (2.2) and (2.4) along the path of the photon beam to obtain

$$\begin{aligned} \mathcal{R}(E, \phi, x) = N \int_0^\infty \frac{e^{-\mu y}}{r^2} [Z e \sigma_c(E, \theta_s) R(E') e^{\mu' r} \\ + \frac{1}{2\pi} \sigma_{pp}(E) e^{-\mu_a r} R(E_a)] dy . \end{aligned} \quad (2.5)$$

The scattered photon energy is denoted by E' , the photon annihilation energy by E_a , the scattering point to detector distance by r and, the detector "response function" at a scattered energy E_d by $R(E_d)$. The scattered energy E' is found using the Compton formula for free electron scattering [Ch84], namely,

$$E' = \frac{E}{1 + (E/m_e c^2)(1 - \cos \theta_s)} . \quad (2.6)$$

To account for subsequent buildup of scattered photons along the second (or scattered) leg, the scattering source term and the pair production term in Eq. (2.5) was multiplied by an appropriate buildup factor $B(E, r)$. Thus, the total detector response is estimated by

$$\begin{aligned} \mathcal{R}(E, \phi, d) = N \int_0^\infty \frac{e^{-\mu y}}{r^2} [Z e \sigma_c(E, \theta_s) R(E') B(E', r) e^{-\mu' r} \\ + \frac{B(E_a, r)}{2\pi} \sigma_{pp}(E) R(E_a) e^{-\mu_a r}] dy . \end{aligned} \quad (2.7)$$

A change in the variables of integration using $\hat{y} = \mu y$, $r' = \mu' r$, $r'' = \mu_a r$, and $z = \mu r$ results in a detector response of, [Sh87]

$$\begin{aligned} \mathcal{R}(E, \phi, d) = N \int_0^{\infty} \frac{e^{-\hat{y}}}{\hat{z}^2} [Z e \sigma_c(E, \theta_s) B(E', r') \\ + \frac{B(E_a, r'')}{2\pi} R(E_a) \sigma_{PP}(E) e^{-\Gamma}] d\hat{y} . \end{aligned} \quad (2.8)$$

To evaluate Eq. (2.8), the buildup factor and interaction coefficients must first be selected. The total mass interaction coefficients were taken from Hubbell [Hu82] and the annihilation microscopic cross section data were taken from Storm and Israel [St67]. The buildup factor $B(E, \mu x)$ was assumed equal to the infinite medium exposure buildup factor as approximated by the geometric progression model [Ha83, Ha86] for a point isotropic source. The geometric buildup-factor model, used in evaluating the beam response functions, is given by

$$B(E, X) = \begin{cases} 1 + (b-1)(K^X - 1) , & \text{for } k \neq 1 \\ 1 + (b-1) X & , \text{for } k = 1 \end{cases} , \quad (2.9)$$

where $X = \mu x$ is the source-to-detector distance in mean-free-path (mfp) lengths, and K is evaluated from

$$K(X) = cX^a + d \frac{[\tanh(X/X_k - 2) - \tanh(-2)]}{[1 - \tanh(-2)]} . \quad (2.10)$$

Values for the coefficients a , b , c , d , and X_k were taken from a recent revision of QAD [Rs86] and depend on the photon energy and the shielding material [Sh87].

Evaluation of the integral in Eq. (2.8), once the integrand was known, was performed using Gaussian quadrature [Sh87]. A 16-point Gaussian quadrature routine integrated the detector response for each mfp of interest along the beam

path of the source photon. The integration procedure started at the source and continued along the photon path-of-travel until the change in the value of the integral was less than a prescribed value [Sh87]. In this manner the detector response function was evaluated at a given set of energies and for each energy at a given set of angular directions. Table 2.1 shows the energy set and Table 2.2 shows the angular set used in evaluating the beam response functions [Sh87].

Several important approximations were made in deriving Eq. (2.7) for the beam response functions [Sh87]. First, the Klein–Nishina differential scattering cross section ignores all electron binding effects on the cross sections [Ch87]. Errors caused by the Klein–Nishina approximation over the energy range of interest ($0.1 < E < 10$ MeV) are expected to be very small since electron binding effects are relatively small at these relatively high energies. Second, the buildup factors used were based on an isotropic point source, a situation not rigorously realized for this analysis, since photons which scatter in dy are preferentially scattered in a forward direction. Thus, use of the buildup factor for a point isotropic source will tend to overestimate the dose at the detector.

However, the errors introduced by the model assumptions discussed above appear to be quite small because of the excellent agreement between benchmark experimental data and the skyshine calculations using the above beam response functions [Sh87].

Table 2.1. Energy group structure used in deriving the beam response functions used in MicroSkyshine [Sh87].

| Energy Group i | Group Energy (MeV) |
|---------------------|-----------------------|
| 1 | 9.5 |
| 2 | 8.5 |
| 3 | 7.5 |
| 4 | 6.5 |
| 5 | 5.5 |
| 6 | 4.5 |
| 7 | 3.5 |
| 8 | 2.5 |
| 9 | 1.5 |
| 10 | 0.75 |
| 11 | 0.325 |
| 12 | 0.055 |

Table 2.2 The discrete beam directions used by Faw and Shultis in deriving the new beam response functions used in MicroSkyshine [Sh87].

| Angular Group | Angle ϕ_j | Angular Group | Angle ϕ_j |
|---------------|-------------------|---------------|-------------------|
| 1 | 0.5 | 11 | 45.0 |
| 2 | 1.5 | 12 | 55.0 |
| 3 | 2.5 | 13 | 65.0 |
| 4 | 4.0 | 14 | 75.0 |
| 5 | 6.0 | 15 | 85.0 |
| 6 | 8.5 | 16 | 95.0 |
| 7 | 12.5 | 17 | 110.0 |
| 8 | 17.5 | 18 | 130.0 |
| 9 | 25.0 | 19 | 150.0 |
| 10 | 35.0 | 20 | 170.0 |

A third important approximation in the MicroSkyshine method is the use of an infinite air medium for evaluating the beam responses. A more correct approach would include the effect of the ground in the beam response calculations. However, the complications involved in adding an air-ground interface are considerable and include changes in the detector response for different detector heights above the ground and different soil compositions. However, since the average Z number for most soils is reasonably close to that of air, and since photon reflection from the ground is typically small compared to the contribution of photons approaching the detector from above, the neglect of the air-ground interface is felt to be justified [Sh87].

2.2 Approximation of Beam Response Functions

To simplify the use of beam response functions, Faw and Shultis [Fa87, Sh87] fit a semi-empirical formula to their calculated values of the detector response. The detector responses calculated by the point kernel were approximated using [Sh87]

$$\mathcal{R}(E, \phi, x) = E \mathcal{F}(E, \phi, x) , \quad (2.11)$$

where the fit formula was

$$\mathcal{F}(E, \phi, x) = \mathcal{K}(\rho/\rho_0)^2 [x (\rho/\rho_0)]^b e^{(a-cx \rho/\rho_0)} . \quad (2.12)$$

The fit parameters a , b , and c depend only upon source energy E and beam direction ϕ . The reference air density is given by ρ_0 and the air density to be used in a dose calculation by ρ . The reference air density was 0.001225 g/cm³ [Sh87].

The detector response $\mathcal{R}(E, \phi, x)$ as calculated has units of rad per photon when $\mathcal{K} = 1.308 \times 10^{-11}$ rad m²/MeV [Sh87].

Values of the fit parameters a, b, and c were found for a fixed E_i and ϕ_j by minimizing the squared sum of the difference between the calculated response functions and the prediction from Eq. (2.11) for all calculated source-to-detector distances [Sh87]. Since, the response at the detector was found to vary over many orders of magnitude as the source-to-detector distance x changed, the least squares fits were actually performed by fitting the natural log of Eq. (2.11) to the natural log of the calculated responses [Sh87]. Using the logarithmic fitting procedure for $\rho = \rho_0$ results in the following least squares fit function.

$$S_{ij}(a, b, c) = \sum_{m=1}^M [G + b \ln(X_m) + a - cx_m - \ln\{R_m(E_i, \phi_j, x_m)\}]^2, \quad (2.13)$$

where $G = \ln(E_i)$ and $\mathcal{R}(E_i, \phi_j, x_n)$ is the beam response at a detector distance of x_m . The parameters a, b, and c that minimized S were then found using the simplex method [Sh87].

The point-kernel beam responses were calculated out to source-to-detector distances of 2500m. Then, the fitted response parameters were calculated for all energy and angular values given in Tables 2.1 and 2.2. Comparison of the fitted (approximate) response functions with the calculated values indicated that the poorest agreement always occurred at small source-to-detector distances. The error associated with the fitted response functions was, for almost all the cases, less than an absolute deviation of 16%. The detailed results calculated by Faw and Shultis are in reference works by those authors [Sh87].

2.2.1 Interpolation of the Fitted Response Functions

An interpolation scheme was used in MicroSkyshine to evaluate the beam response functions at energies and angular directions different from those used to approximate the response functions [Sh87]. The interpolation scheme results in beam response functions that are continuously variable in energy and direction.

The beam response function for a photon with energy E and direction of travel ϕ is found using a linear interpolation scheme. The beam response function is first interpolated in energy at all discrete angular directions ϕ_j using [Sh87]

$$\mathcal{F}(E, \phi_j, x) = \mathcal{F}_{i+1, j} \left[\frac{E_i - E}{E_i - E_{i+1}} \right] + \mathcal{F}_{ij} \left[\frac{E - E_{i+1}}{E_i - E_{i+1}} \right], \quad (2.14)$$

where

$$\mathcal{F}_{ij} \equiv \mathcal{F}(E_i, \phi_j, x), \quad (2.15)$$

and

$$\mathcal{F}_{i+1, j} \equiv \mathcal{F}(E_{i+1}, \phi_j, x). \quad (2.16)$$

For energies between 9.5 and 10.0 MeV, the following extrapolation scheme is used [Sh87]

$$\mathcal{F}(E, \phi_j, x) = \mathcal{F}_{1, j} (E - 8.5) + \mathcal{F}_{2, j} (9.5 - E) \quad (2.17)$$

Then, the response function for photons of energy E with direction ϕ (where $\phi_j \leq \phi \leq \phi_{j+1}$) is estimated, using linear interpolation, as [Sh87]

$$\mathcal{F}(E, \phi, x) = \mathcal{F}(E, \phi_j, x) + \frac{\mathcal{F}(E, \phi_{j+1}, x) - \mathcal{F}(E, \phi_j, x)}{\phi_{j+1} - \phi_j} [\phi - \phi_j]. \quad (2.18)$$

For directions in the two end intervals, linear extrapolation is used, namely, for $170^\circ \leq \phi \leq 180^\circ$,

$$\mathcal{F}(E, \phi, x) = \mathcal{F}(E, \phi_{20}, x) + \frac{\mathcal{A}(E, \phi_{19}, x) - \mathcal{A}(E, \phi_{20}, x)}{\phi_{19} - \phi_{20}} (\phi - \phi_{19}) . \quad (2.19)$$

and $0^\circ \leq \phi \leq .5^\circ$

$$\mathcal{F}(E, \phi, x) = \mathcal{F}(E, \phi_1, x) + \frac{\mathcal{A}(E, \phi_2, x) - \mathcal{A}(E, \phi_1, x)}{\phi_2 - \phi_1} (\phi - \phi_2) . \quad (2.20)$$

2.3 Skyshine Dose Calculations Using Beam Response Functions

The skyshine dose at a source-to-detector distance of d arising from a collimated, bare, isotropic, point source can be found by integrating the response functions over all source energies and over all possible photon beam directions Ω_s . The skyshine dose can thus, be calculated from

$$R(d) = \int_0^\infty dE' \int_{\Omega_s} d\Omega S(E', \vec{\Omega}) \mathcal{R}(E', \phi, d) , \quad (2.21)$$

where $S(E', \vec{\Omega})$ is the energy and directional distribution of the point skyshine source, Ω_s is the source's solid angle of collimation, and $\mathcal{R}(E', \phi, d)$ is the beam response function which may be approximated by Eq. (2.11). Often, the source $S(E', \vec{\Omega})$ is a monoenergetic isotropic point source with energy E . For this case $S(E', \vec{\Omega})$ becomes

$$S(E', \vec{\Omega}) = \frac{S_E}{4\pi} \delta(E' - E) , \quad (2.22)$$

and Eq. (2.21) reduces to

$$R(d) = \frac{S_P}{4\pi} \int_{\Omega_s} \mathcal{R}(E, \phi, d) d\Omega . \quad (2.23)$$

2.3.1 Skyshine Calculations for a Source in a Silo

The geometry of the silo problem is illustrated in Fig. 2.2. For the silo problem, the various geometric variables are defined as

- y_s \equiv the source height below the silo top,
- y_d \equiv the detector height below the silo top,
- x \equiv the horizontal source-to-detector distance,
- r \equiv the silo radius,
- ω_o $\equiv \sqrt{1 + r^2/y_s^2} = \cos \theta_o \equiv$ the source collimation angle,
- d $= \sqrt{x^2 + (y_d - y_s)^2} \equiv$ the source-to-detector distance,

and

- α $= \cos^{-1}(x/d) \equiv$ the angle between the horizontal and the source-detector axis.

The solid angle of collimation for the source is given by $2\omega_o$. Evaluation of Eq. (2.23) for the Skyshine dose for the silo problem first requires that the angle ϕ be expressed in terms of the integration variables. From Figure 2.3 it is seen that $\cos \phi$ is the dot product of a unit vector along the photon's initial path and the unit vector along the source-to-detector axis. The angle ϕ in terms of θ , ψ , and α is thus found to be

$$\phi = \cos^{-1}(\sin \theta \cos \psi \cos \alpha - \cos \theta \sin \alpha) . \quad (2.24)$$

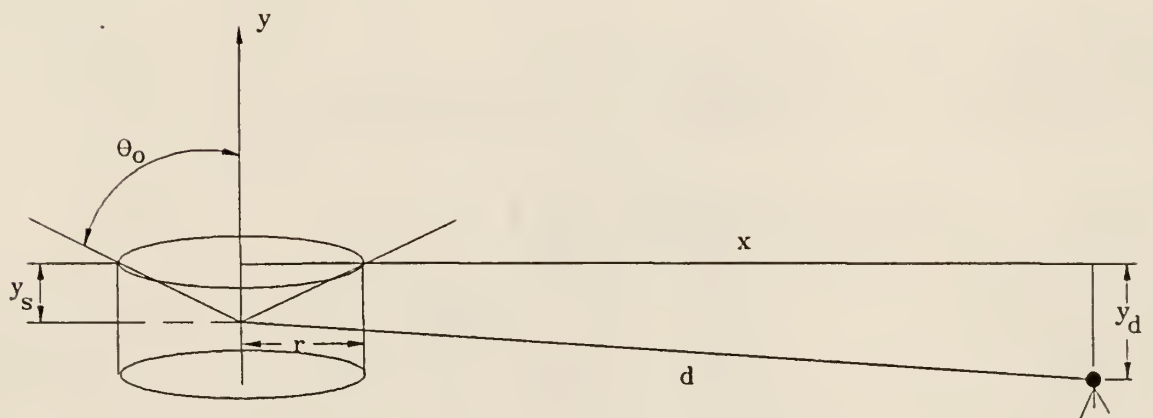


Figure 2.2. Illustration of the variables representing the physical distances used in the MicroSkyshine method for a point source in a silo [Sh87].

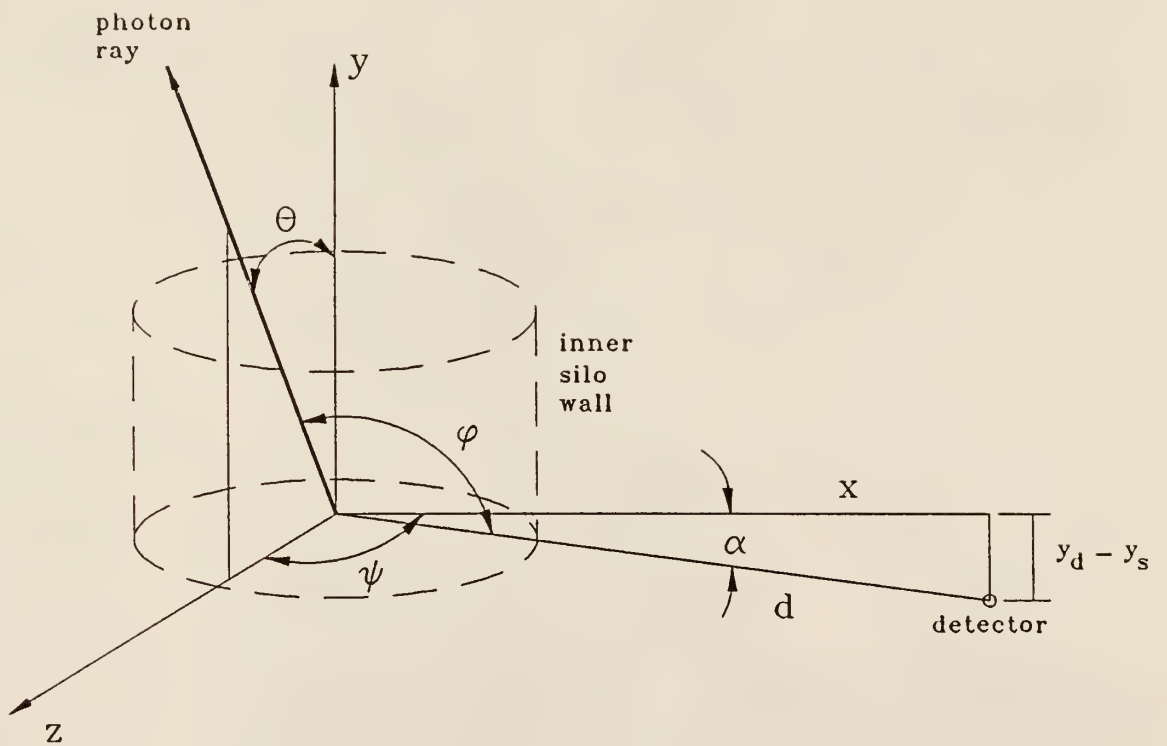


Figure 2.3. Angular coordinate system used to transform the integral equation in MicroSkyshine [Sh87].

2.3.2 Unshielded Silo Calculation

The skyshine dose for an open silo with a point isotropic source is found from Eq. (2.23). For the silo problem the differential solid angle is given by

$$d\Omega = \sin\theta \, d\theta \, d\psi . \quad (2.25)$$

Substitution of Eq. (2.25) into Eq. (2.23) results in the detector response being given by

$$R(d) = \frac{S_p}{4\pi} \int_0^{\theta_{\max}} d\theta \int_0^{2\pi} \sin\theta \, \mathcal{R}(E, \phi, d) \, d\psi . \quad (2.26)$$

In the silo case, the azimuthal contribution is symmetric about the azimuthal reference axis (i.e., the source-to-detector axis). This azimuthal angular symmetry reduces Eq. (2.26) to

$$R(d) = \frac{S_p}{2\pi} \int_0^{\pi} d\psi \int_0^{\theta_{\max}} d\theta \sin\theta \, \mathcal{R}(E, \phi, d) , \quad (2.27)$$

or if one lets $\omega = \cos\theta$ then Eq. (2.27) reduces to

$$R(d) = \frac{S_p}{2\pi} \int_0^{\pi} d\psi \int_{\omega_o}^1 d\omega \, \mathcal{R}(E, \phi, d) . \quad (2.28)$$

Equation (2.28) may be evaluated numerically using a double Gaussian integration scheme [Sh87].

2.3.3 Shielded Silo Dose Calculation

Faw and Shultis [Fa87, Sh87] also accounted for the addition of a horizontal slab shield on top of the silo by using exponential attenuation and a buildup factor along the path through the shielding slab. The path length through the shield is illustrated in Fig. 2.4. The mean-free-path distance along the path through the shield is

$$\lambda = \frac{t}{\omega} \rho_s (\mu/\rho) , \quad (2.29)$$

where t is the shield thickness, ρ_s is the shield's density, (μ/ρ) is the total mass interaction coefficient, and ω is the cosine of the polar angle θ . Inclusion of buildup and exponential attenuation in the shield results in a detector response of

$$R(d) = \frac{S_E}{2\pi} \int_0^\pi d\psi \int_0^{\theta_{\max}} d\omega B(e,\lambda) \mathcal{R}(E,\phi,d) e^{-\lambda} . \quad (2.30)$$

The buildup factor $B(E,\lambda)$ was approximated by a Berger approximation of the form

$$B(E,\lambda) = 1 + a\lambda e^{b\lambda} . \quad (2.31)$$

Values for the mass interaction coefficients (μ/ρ) for air, water, concrete, iron, lead, zirconium, and uranium dioxide were again taken from data by Storm and

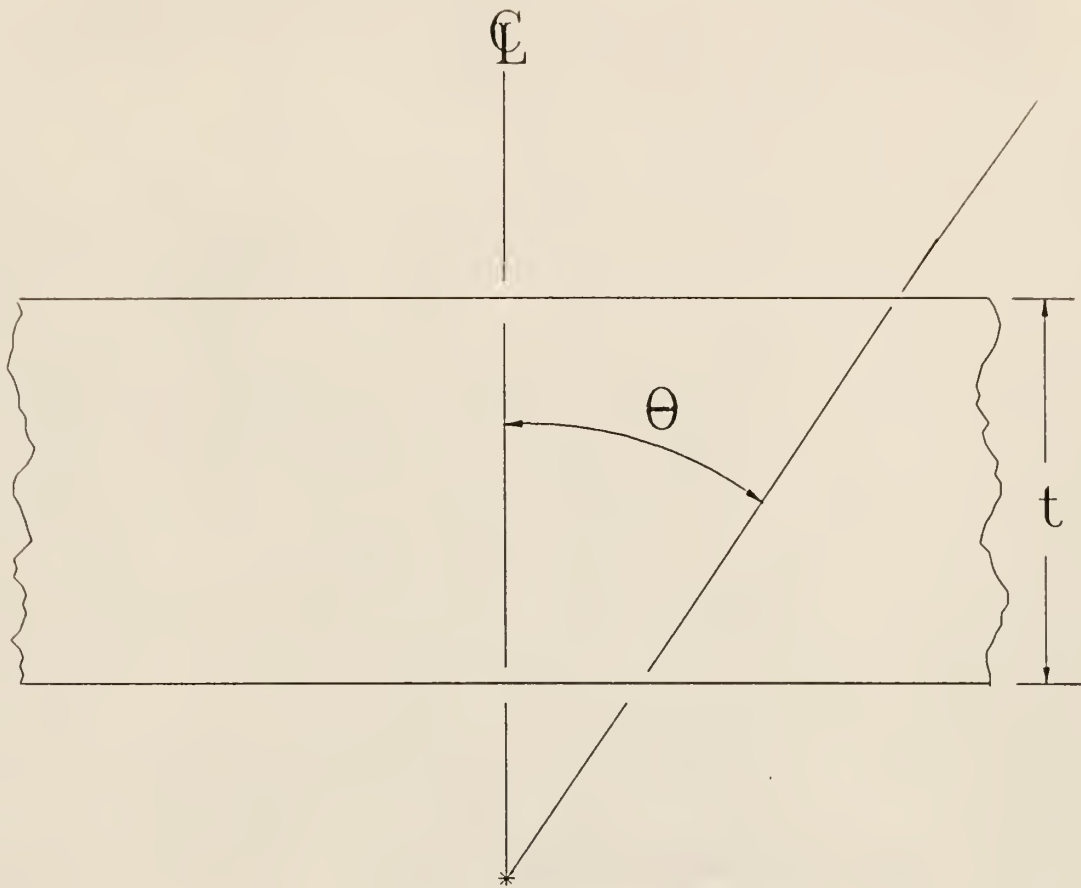


Figure 2.4. Effective slab thickness for a photon penetrating a slab of thickness t at an angle θ .

Israel [St67]. The interpolation in energy of the mass interaction coefficients was performed using a logarithmic fit. The Berger buildup factor $B(E,\lambda)$ [Ch84] is usable for energies between 0.015 MeV and 15 MeV and for shield thicknesses up to 40 mfp. The buildup-factor parameters a and b were interpolated in energy using a linear energy fit.

2.4 Extension to Polyenergetic and Anisotropic Point Sources

The original MicroSkyshine method [Fa87, Sh87] was limited to point, monoenergetic, isotropic sources. To use the MicroSkyshine response functions for cases involving anisotropic point sources with variable source energies, it is necessary to modify the original method. This section presents a modification for calculating the skyshine dose caused by an anisotropic and/or variable energy source.

The skyshine dose for anisotropic point sources with a distribution of source energies is formally given by Eq. (2.21). When an unshielded, anisotropic, polyenergetic, point source is placed on the axis of the cylinder, the detector response thus becomes

$$R(d) = \int_0^{E_{\max}} dE \int_0^{2\pi} d\psi \int_0^{\theta_{\max}} d\theta \sin\theta S(E,\theta,\psi) \mathcal{R}(E,\phi,d) , \quad (2.32)$$

where ϕ is given by Eq. (2.24), d is the source-to-detector distance, and $S(E,\theta,\psi)$ is the energy-direction distribution of source photons emitted with energy E and in

direction defined by θ and ψ . With the definition $\omega = \cos\theta$, Eq. (2.32) reduces to

$$R(d) = \int_0^{E_{\max}} dE \int_0^{2\pi} d\psi \int_{\omega_0}^1 d\omega S(E, \omega, \psi) \mathcal{R}(E, \phi, d) . \quad (2.33)$$

Of particular interest in this study is the case when the source's angular distribution is independent of ψ and when the source's continuous energy distribution is approximated by a multigroup approximation. The multigroup approximation of the source's energy distribution can be incorporated in Eq. (2.33) by replacing the energy integral with a summation over the midpoint energy of each energy group, i.e.,

$$R(d) = \sum_{g=1}^G \int_0^{2\pi} d\psi \int_{\omega_0}^1 d\omega S_g(\omega) \mathcal{R}(E_g, \phi, d) . \quad (2.34)$$

The source's angular independence of ψ allows Eq. (2.34) to be reduced to

$$R(d) = 2 \sum_{g=1}^G \int_0^{\pi} d\psi \int_{\omega_0}^1 d\omega S_g(\omega) \mathcal{R}(E_g, \phi, d) , \quad (2.35)$$

when dealing with an azimuthally symmetric distribution of source photons.

The numerical evaluation of the integrals in Eq. (2.35) can be done using a numerical quadrature method such as Gaussian quadrature. Equation (2.35) can thus be approximated by

$$R(d) = 2 \sum_{g=1}^G \sum_{i=1}^N w_i \sum_{j=1}^N w_j S_g(\omega_j) R(E_g, \phi, d) , \quad (2.36)$$

where w_i and w_j are the Gaussian quadrature weights and ω_i and ω_j are the Gaussian ordinates for ω and ψ integrals, respectively. Implicit in Eq. (2.36) is the implied dependence of ϕ on ω_j and ω_i (recall Eq. (2.24)). The N -th order Gaussian ordinates for the ω integral are [Ho75]

$$\omega_j = \frac{1 - \omega_0}{2} Z_j + \frac{(1 + \omega_0)}{2} \quad (2.37)$$

and for the ψ integral

$$\omega_i = \frac{\pi}{2} Z_i + \frac{\pi}{2} , \quad (2.38)$$

where Z_j and Z_i are the N zeros of the Legendre polynomial $P_N(Z)$. The quadrature weights for the ω integral are given by

$$w_j = \frac{(1 - \omega_0)}{2} W_j , \quad (2.39)$$

and for the ψ integral

$$w_i = \frac{\pi}{2} W_i , \quad (2.40)$$

where z_i and z_j are evaluated using

$$W_i = \frac{2 \left[1 - Z_i^2 \right]}{(N+1)^2 \left[P_{N+1} \left[Z_i \right] \right]^2} . \quad (2.41)$$

3. A COMPOSITE SKYSHINE METHOD

A rigorous treatment of the shielded silo problem requires the solution of a two- or three-dimensional transport equation. Such transport solutions tend to be computationally expensive, thereby limiting the number of different cases which can be explored in design studies. Clearly, there is a need for inexpensive, albeit approximate, methods for estimating the skyshine dose caused by a shielded source. The method used in MicroSkyshine (exponential attenuation with buildup correction for radiation penetrating the shield) is such an approximate method. The validity of the buildup factor method, however, is not well established. Indeed, the inability of the buildup factor method to estimate the emergent energy and angular distribution of photons escaping the shield should call for some caution when using the MicroSkyshine method. This skepticism is especially important for thick shields where most of the photons leaving the shield have undergone interactions in the shield.

In this chapter, a composite method to treat the shielded skyshine problem is developed. The composite method originally proposed by Keck and Herchenroder [Ke82], first uses a one-dimensional transport description to calculate the energy and angular distribution of photons leaving a silo shield. Then the photons leaving the shield are treated as a bare, polyenergetic anisotropic, point source for which the skyshine dose at a given detector location is calculated using the line-beam response functions developed for MicroSkyshine.

With this composite method, the effect of a shielded source, in principle, can be determined more accurately than with the Microskyshine method. The composite method can then be used to assess the accuracy of MicroSkyshine's

approximate treatment of a shielded source. The assessment of the accuracy of the MicroSkyshine method is the central focus of the next chapter. In this chapter, a rigorous description of the composite method along with a test of its validity is presented.

3.1 Decoupling the Shield and Air Transport Calculations

A decoupling of the shielded skyshine source problem can be performed when the number of photons exiting and then reentering the shield after scattering in the air is much smaller than the total number of photons exiting from the shield. When this condition is satisfied, the calculation of the energy and angular distribution of photons penetrating the overhead shield becomes independent of the subsequent transport of photons through the air to the detector. In effect, the source structure and its shield have a negligible effect on the transport of the photons through the air once the photons leave the source structure. This decoupling of a shielded skyshine problem into two separate and independent calculations is the key approximation needed for the composite method.

Before developing the composite skyshine method for the problem of a point source on the axis of a cylindrical silo with an overhead shield, conditions for the validity of decoupling the shield and air transport problems are considered.

3.1.1 Validity of Decoupling for Disk Shields

To determine the validity of decoupling a shielded skyshine problem, a related problem with a point source located at the center of a disk shield is considered. For this problem a point kernel method, similar to Kitazume's [Ki68], will be used to estimate the number of photons reflected by the air back into the shield.

To determine when the number of photons reflecting back from the air into the slab shield is small, a simple point kernel calculation is performed. Figure 3.1 illustrates the geometry used to describe this reflection problem. The reflected flux of single-scattered photons at a point x_p on the shield caused by a point source located on the center of a cylindrical shield emitting photons into the upper hemisphere can be estimated from

$$\Phi(x_p) = \int_{\text{vol air}} dV N Z {}_e\sigma_c(E, \theta_s) \frac{S_p(E_p)}{2\pi} \frac{e^{-\mu_p r_p} e^{-\mu_s r_s}}{r_p^2 r_s^2}, \quad (3.1)$$

where ${}_e\sigma_c(E, \theta_s)$ is the differential scattering cross section, r_p is the source-to-scattering point distance, NZ is the electron density of the air, μ_p is the linear interaction coefficient at the source energy, μ_s is the linear interaction coefficient at the scattered energy, and θ_s is the angle through which the photon scatters.

In spherical coordinates, the differential scattering volume is

$$dV = r_p^2 dr_p \sin\phi d\phi d\beta. \quad (3.2)$$

Using the law of sines with Fig. 3.1 results in the following trigonometric relations

$$r_s/\sin\phi = r_d/\sin\theta_s, \quad (3.3)$$

$$\frac{r_s}{\sin\theta_s} = \frac{r_p}{-\sin(\phi + \theta_s)}, \quad (3.4)$$

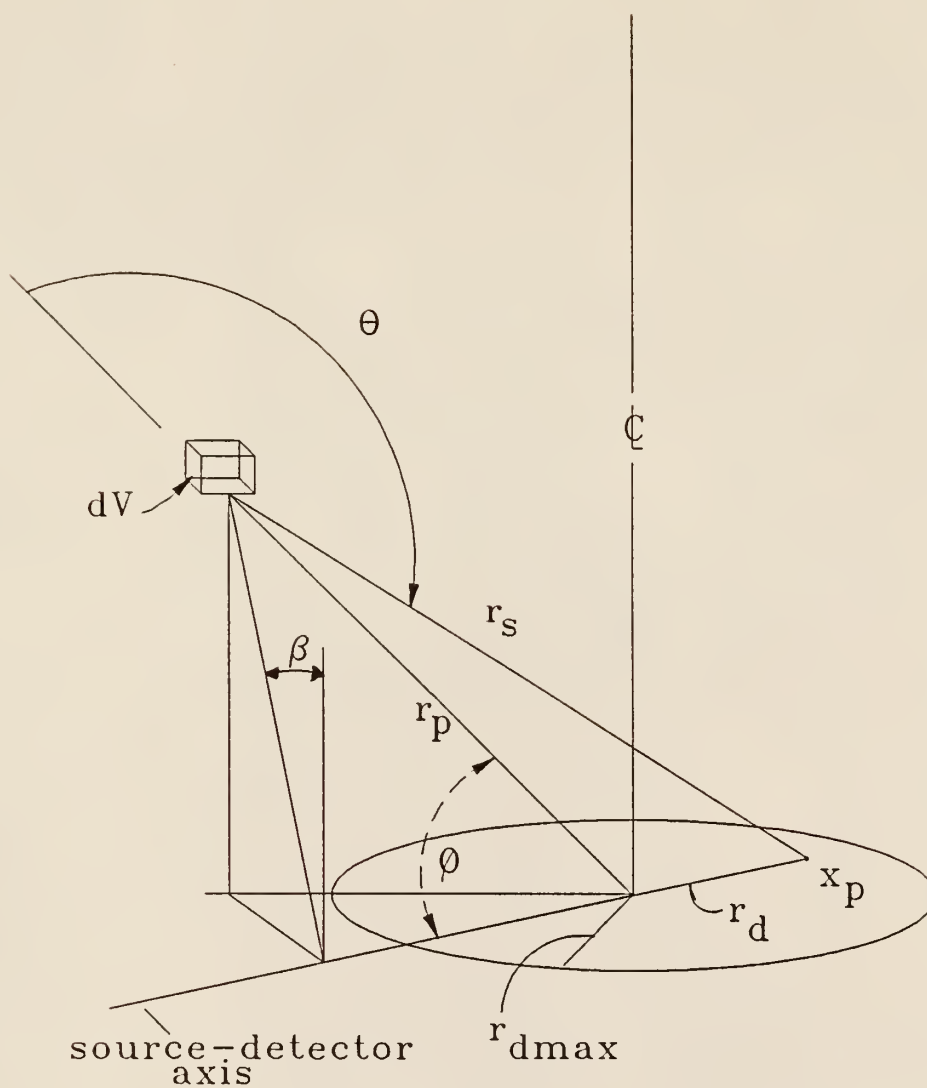


Figure 3.1. Angular and geometrical illustration of the variables with a point source on the axis of a cylindrical shield used to calculate the re-entrant flux into the shield.

and,

$$\frac{r_d}{\sin \theta_s} = \frac{r_p}{-\sin(\phi + \theta_s)} . \quad (3.5)$$

Solving for r_s and r_p in terms of r_d , θ_s , and ϕ results in

$$r_s = \frac{r_d \sin \phi}{\sin \theta_s} , \quad (3.6)$$

and

$$r_p = -r_d \frac{\sin(\phi + \theta_s)}{\sin \theta_s} . \quad (3.7)$$

The derivative dr_p in terms of θ_s after simplifying and substituting for $\sin^2 \theta_s$ is

$$dr_p = \frac{r_s^2}{r_d} \frac{d\theta_s}{\sin \phi} . \quad (3.8)$$

Substituting Eq. (3.8) into Eq. (3.2) results in the differential volume being given by

$$dV = \frac{r_p^2}{r_d} \frac{r_s^2}{\sin \phi} d\theta_s d\phi d\beta . \quad (3.9)$$

Substitution of this expression for dV into Eq. (3.1) then gives the reflected flux at x_p as

$$\Phi(x_p) = \int_{-\pi/2}^{\pi/2} d\beta \int_0^\pi d\phi \int_{\pi-\phi}^\pi d\theta_s N Z e^{\sigma_c(E, \theta_s)} \frac{S_p(E_p)}{2\pi} \quad (3.10)$$

$$\times \frac{r_p^2 r_s^2 e^{-\mu_p r_p} e^{-\mu_s r_s}}{r_d^2 r_p^2 r_s^2},$$

or

$$\Phi(x_p) = \int_{-\pi/2}^{\pi/2} d\beta \int_0^\pi d\phi \int_{\pi-\phi}^\pi d\theta_s N Z e^{\sigma_c(E, \theta_s)} \frac{S_p(E_p)}{2\pi r_d} e^{-\mu_p r_p} e^{-\mu_s r_s}. \quad (3.11)$$

Since, the integrand in Eq. (3.11) is independent of the angle β , Eq. (3.11) can be integrated over $d\beta$ to give

$$\Phi(x_p) = \frac{S_p(E_p)}{2r_d} \int_0^\pi d\phi \int_{\pi-\phi}^\pi d\theta_s N Z e^{\sigma_c(E, \theta_s)} e^{-\mu_p r_p} e^{-\mu_s r_s}. \quad (3.12)$$

The contribution of secondary particles produced along the scattered path to the reflected flux is estimated by including an appropriate exposure buildup factor $B(E, r_s)$ in Eq. (3.12). Thus, the reflected flux of photons at point x_p is

$$\Phi(x_p) = \frac{S_p N Z}{2r_d} \int_0^\pi d\phi \int_{\pi-\phi}^\pi d\theta_s e^{\sigma_c(E, \theta_s)} B(E_s, r_s) e^{-\mu_p r_p} e^{-\mu_s r_s}. \quad (3.13)$$

The fraction F of the photons at the source energy being reflected back to the slab surface can then be estimated by multiplying Eq. (3.13) by the differential slab area dA , integrating overall dA on the shield surface, and dividing by the source strength to obtain

$$F = \frac{\Phi(x_p)}{S_p} = \frac{N}{2} \frac{Z}{2} \int_0^{2\pi} d\psi \int_0^{r_{d\max}} \frac{r_d dr_d}{r_d} \int_0^\pi d\phi \int_{\pi-\phi}^\pi d\theta_s$$

$$\times e\sigma_c(E, \theta_s) B(E, r_s) e^{-\mu_p r_p} e^{-\mu_s r_s} . \quad (3.14)$$

Since all the terms in the integrand are independent of ψ , Eq. (3.14) can be integrated over ψ to obtain

$$F = \frac{N}{2} \frac{Z}{2} \int_0^{r_{d\max}} dr_d \int_0^\pi d\phi \int_{\pi-\phi}^\pi d\theta_s e\sigma_c(E, \theta_s) B(E, r_s) e^{-\mu_p r_p} e^{-\mu_s r_s} . \quad (3.15)$$

Evaluation of Eq. (3.15) was done using the total interaction coefficient data from Hubbell [Hu82]. The total interaction coefficient data was logarithmically interpolated to obtain values at any energy, and the differential scattering cross sections were evaluated using the Klein–Nishina free–electron model given by Eq. (2.2).

The buildup factor $B(E, r_s)$ was approximated by an infinite medium exposure buildup factor for a point isotropic source. The buildup factor used in the numerical evaluation of Eq. (3.15) was taken as the geometric progression model proposed by Harima [Ha83, Ha86] and given by Eq. (2.8). The integral in Eq. (3.15) was evaluated using Gaussian numerical quadrature, [Ho75] and the integral over dr_d was divided as needed until the fractional change in the integrand was less than a small specified value. The inner integrals, those over $d\phi$ and $d\theta_s$, were evaluated using 16–point Gaussian quadrature.

The calculated results obtained from Eq. (3.15) for photon energies of 6.129, 1.25, and 0.5 MeV for different slab radii are plotted in Fig. 3.2. The results shown in Fig. 3.2, indicate that the fraction of source photons reflected back to the slab increases with the slab's radius and decreases with increasing photon energy. For the energies and slab shield sizes considered in this study, the fraction of the particles reentering the slab is very small with the largest F having a value of 4.2%. It is therefore concluded that the reflection of particles from the air back to the shield can be safely ignored for photon energies between 0.5 and 6.2 MeV when the shield radius is less than 7m, and that the problem decoupling used in the composite method is reasonable.

3.2 The Composite Method for a Shielded-Silo Skyshine Problem

Whenever a skyshine problem can be decoupled into two independent transport calculations (transport through the source structure and shielding and the transport through the air), it is always better to take advantage of this decoupling rather than to treat the skyshine problem as a single, more complex, transport calculation.

In this section, the composite method is developed for the particular skyshine source shown in Fig. 3.3. In this skyshine problem, a point monoenergetic source is placed on the axis of a cylindrical silo with very thick walls. The top of the silo has a horizontal slab shield through which most of the radiation that eventually reaches the detector must escape.

In applying the composite method to this problem, first the energy, directional and spatial distribution of the gamma photons leaving the silo structure

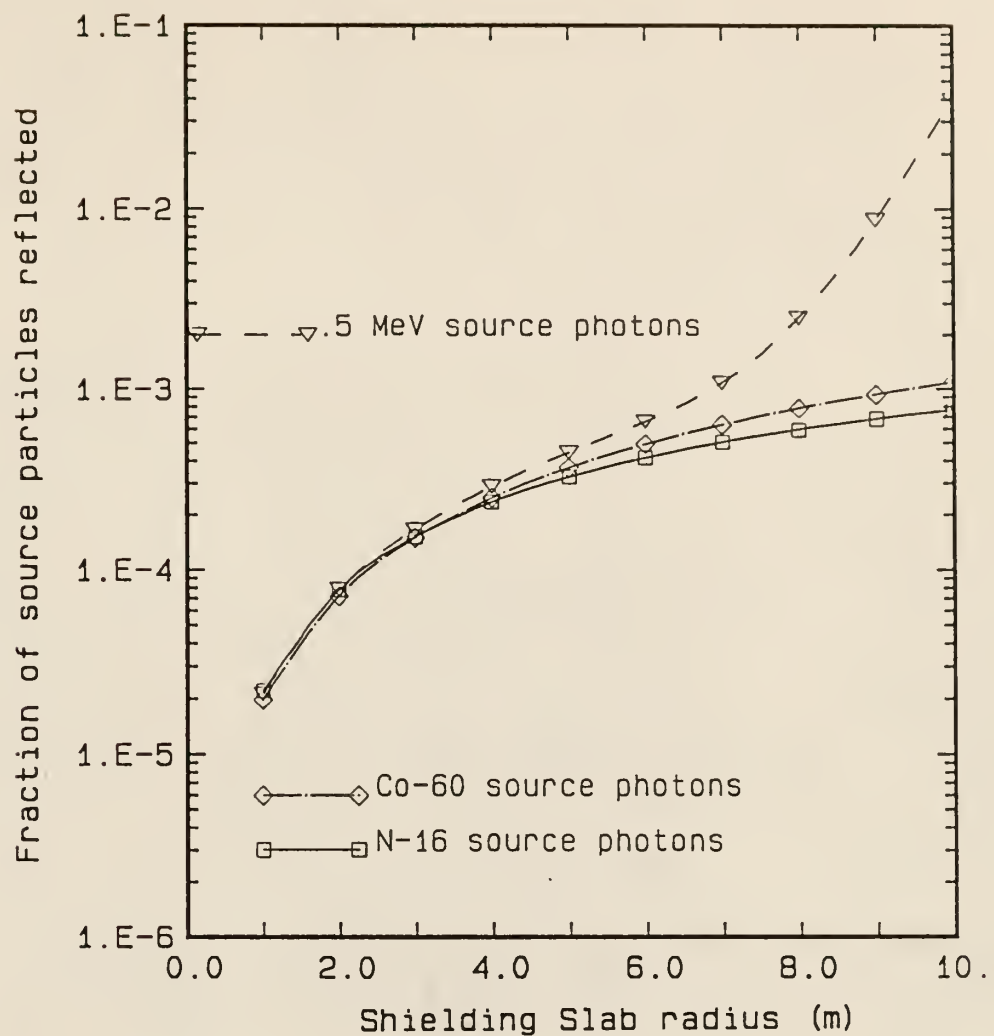


Figure 3.2 Fraction of photons from a point source on the axis of a cylindrical shield reflected back into a cylindrical shield.

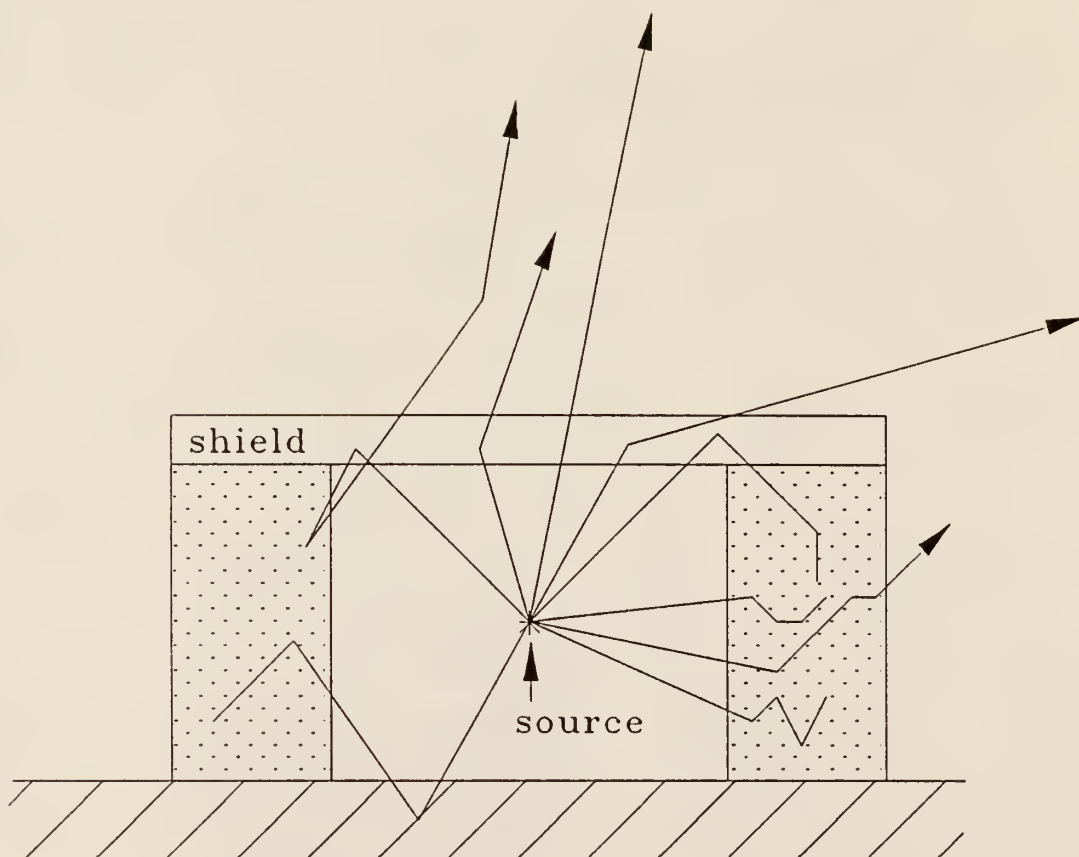


Figure 3.3 Photon scattering paths from a point source into a silo causing a radiation field outside the silo.

are determined. Then this escaping distribution is used as a skyshine source to determine the skyshine dose at locations removed from the silo.

Both the silo leakage problem and the air transport problems are in themselves still formidable transport problems if performed rigorously. However, additional approximations can be made to simplify considerably these two problems. In the sections below, approximations are introduced which allow one to use a simple one-dimensional transport calculation to determine the silo leakage and to use the MicroSkyshine method for the air-transport phase.

3.2.1 Leakage from the Source Silo

The calculation of the energy, direction, and position of photons leaking from the source silo of Fig. 3.3 is a difficult task that requires a two-dimensional transport calculation (after making use of the cylindrical symmetry for this problem). The point source emits (monoenergetic) photons isotropically in all directions, and these photons can travel back and forth in the silo scattering off the silo walls, floor, shield and even the source holder (not shown). Moreover, photons which do escape from the silo can be scattered back to the silo from outside air scatters.

The present silo skyshine problem is modeled after the KSU Benchmark Skyshine Experiment [C178] in which the silo walls were much thicker than the roof shield so that radial photon leakage through the walls was negligible compared to that through the roof shield. Consequently, only photon leakage through the roof shield is considered.

However, even this roof leakage component is complicated by the in-silo scattering which can occur. But, photons which scatter one or more times inside

the silo before reaching the roof shield will have lower energies than photons which reach the roof directly from the source and hence have less chance of escaping through the shield. Moreover, even those few in-silo scattered photons which do escape will have even lower energies and, thus be preferentially absorbed in the air-transport phase. Since skyshine doses are desired only at distances far from the source silo, one may ignore the leakage of source photons which experience in-silo scattering prior to migrating through the roof shield.

Thus if the inside walls, floor, and source equipment are considered black, and if the effect of photon reflection by the air outside the silo is negligible (as required by the composite method), the photon leakage calculation can be modeled by the transport of photons through a finite slab illuminated on the bottom by photons coming directly from the point source and a vacuum boundary condition on the top (i.e., no incident photons). Using the geometry of Fig. 3.4, the angular photon intensity is determined from

$$\vec{\Omega} \cdot \vec{\nabla} \Phi(\vec{r}, E, \vec{\Omega}) + \mu(\vec{r}, E) \Phi(\vec{r}, E, \vec{\Omega}) = S(\vec{r}, E, \vec{\Omega}) + \int_0^\infty dE' \int_{4\pi} d\Omega' \mu_s(\vec{r}, E' \rightarrow E, \vec{\Omega}' \rightarrow \vec{\Omega}) \Phi(\vec{r}', E, \vec{\Omega}') . \quad (3.16)$$

In cartesian coordinate the transport equation is given by

$$\begin{aligned} \vec{\Omega} \cdot \hat{n} \frac{\partial \Phi}{\partial x}(\vec{r}, E, \vec{\Omega}) + \vec{\Omega} \cdot \hat{t}_y \frac{\partial \Phi}{\partial y}(\vec{r}, E, \vec{\Omega}) + \vec{\Omega} \cdot \hat{t}_z \frac{\partial \Phi}{\partial z}(\vec{r}, E, \vec{\Omega}) + \mu(\vec{r}, E) \Phi(\vec{r}, E, \vec{\Omega}) \\ = S_v(\vec{r}, E, \vec{\Omega}) + \int_0^\infty dE' \int_{4\pi} d\Omega' \mu_s(\vec{r}, E' \rightarrow E, \vec{\Omega}' \rightarrow \vec{\Omega}) \Phi(\vec{r}, E', \vec{\Omega}') . \end{aligned} \quad (3.17)$$

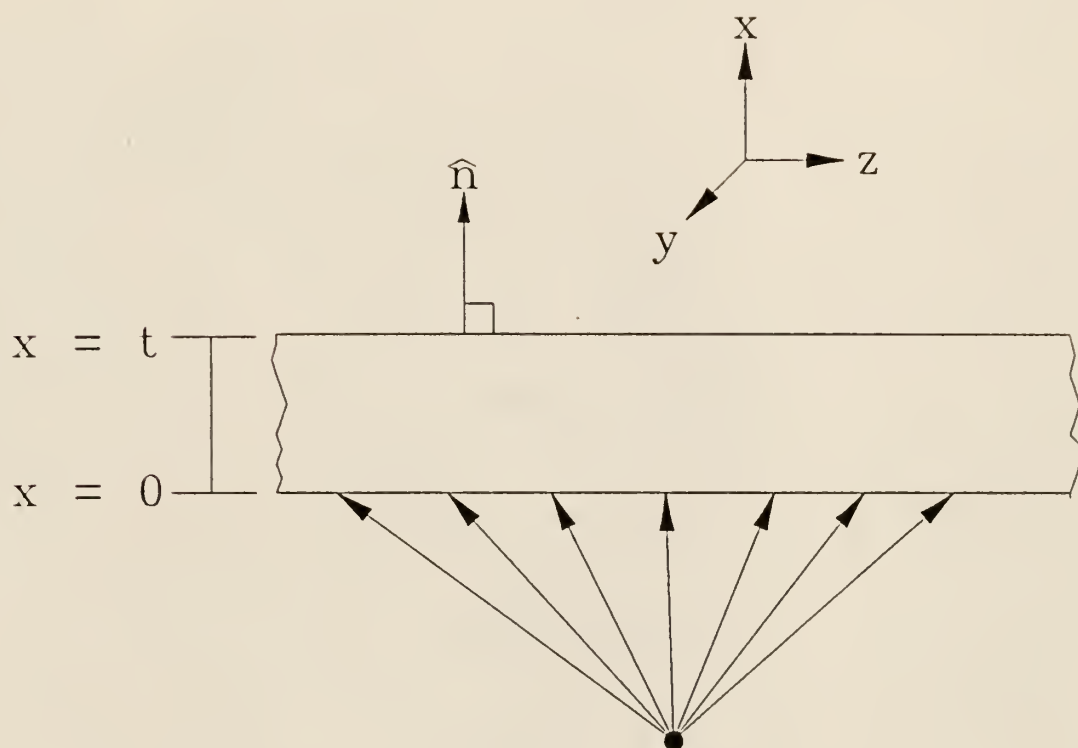


Figure 3.4 Roof-air interface coordinate system used in estimating the source condition on the silo shield's top surface.

With the appropriate boundary conditions, Eq. (3.17) can be solved (at least numerically) for $\Phi(\vec{r}, E, \vec{\Omega})$. From the solution of this transport problem, the leakage distribution of photons from the top of the shield $j_n(\vec{r}_s, E, \vec{\Omega})$ may be found. This distribution, or more precisely, the angular flow rate (per unit area) out of the shield surface is then used as an area or surface source for the air-transport phase of the skyshine calculation. Specifically, the surface source is

$$S_a(\vec{r}_s, E, \vec{\Omega}) = \hat{n} \cdot \vec{\Omega} \Phi(\vec{r}_s, E, \vec{\Omega}) \equiv j_n(\vec{r}_s, E, \vec{\Omega}) \quad (3.18)$$

where \hat{n} is the outward normal on the top shield surface (i.e., unit vector along the x-direction) and \vec{r}_s is a position on the top shield surface.

3.2.2 Approximation of Leakage by an Effective Point Source

The multidimensional transport calculation of the leakage surface source from Eq. (3.17) is still a computationally intensive task. However, if the skyshine dose is to be calculated at a distance far removed from the source silo, the spatial variation of the escaping photons over the upper shield surface is unimportant. In other words, all escaping photons could be considered as coming from the same point on the top of the shield.

Thus, the skyshine source for the air-transport phase of the composite method (for detector locations far from the silo) may be taken as a point, albeit anisotropic, source with strength

$$S_{pt}^{eff}(E, \vec{\Omega}) = \int dA j_n(\vec{r}_s, E, \vec{\Omega}) , \quad (3.19)$$

where the dA integration is performed over that portion of the shield surface from

which photons escape. For an infinite slab shield this gives an infinite integration range; however, in practice only that portion of the shield illuminated directly by the actual source contributes significantly to total leakage, and thus the surface integration is extended only over the silo opening.

This effective skyshine point source thus represents the total (surface integrated) exit current from the top surface of the shield, i.e.,

$$S_{pt}^{eff}(E, \vec{\Omega}) = J_{out}(t, E, \vec{\Omega}) \equiv \int dA j_n(\vec{r}_s, E, \vec{\Omega}) . \quad (3.20)$$

3.2.3 Use of a 1-D Model for Calculating the Effective Skyshine Source

In the composite method, the exact point of emergence of photons from the top shield surface is unimportant. From Eq. (3.20) it is seen that only the total (integrated) exit current J_{out} is needed to find the effective point skyshine source. The importance of this feature is that a comparatively simple one-dimensional (slab geometry) transport model may be used to calculate J_{out} directly for a point source covered by a horizontal slab shield without first having to find $j_n(\vec{r}_s, E, \vec{\Omega})$ (which generally requires a two-dimensional transport calculation). In this section, the procedure is presented for reducing the two-dimensional problem to a one-dimensional one.

For a homogeneous, infinite slab of thickness t , the probability that a particle entering the bottom of the slab shield with energy E and direction of travel $\vec{\Omega}$ will emerge with energies in dE' about E' and directions of travel in $d\Omega'$ about $\vec{\Omega}'$ is denoted by $T(t, E \rightarrow E', \vec{\Omega} \rightarrow \vec{\Omega}') dE' d\vec{\Omega}'$. The *total* flow rates in and out of the slab surfaces caused by an arbitrary point source which illuminates a finite area of the bottom of the slab shield ($z = 0$) are

$$J_{in}^{pt}(0,E,\vec{\Omega}) = \int dA j_{pt}^+(0,x,y,E,\vec{\Omega}) \quad (3.21)$$

$$J_{out}^{pt}(t,E',\vec{\Omega}') = \int dA j_{pt}^-(h,x,y,E',\vec{\Omega}') \quad (3.22)$$

where j_{pt}^{\pm} are the angular flow rates (per unit slab surface area) into and out of the slab and the integration is over all the surface area through which photons pass. Multiplying $T(t,E \rightarrow E', \vec{\Omega} \rightarrow \vec{\Omega}')$ by the total flow rate into the slab will give the total flow rate out of the slab, i.e.,

$$J_{out}^{pt}(t,E',\vec{\Omega}') = J_{in}^{pt}(0,E,\vec{\Omega}) T(t,E \rightarrow E', \vec{\Omega} \rightarrow \vec{\Omega}') . \quad (3.23)$$

It is this total exit current that is sought in order to define the effective skyshine point source as given by Eq. (3.20). However, to use this result to find J_{out}^{pt} , one must first calculate $T(t,E \rightarrow E', \vec{\Omega} \rightarrow \vec{\Omega}')$. Fortunately, this quantity can be obtained by a simple one-dimensional transport calculation.

Consider, the same infinite slab shield uniformly illuminated on the bottom surface, i.e., the angular flow rate $j^+(0,E,\vec{\Omega})$ per unit surface area is independent of position on the slab surface. For this case, the exit angular flow rate per unit area of the top surface, $j^-(t,E'\vec{\Omega}')$, is also independent of the y and z coordinates. Moreover, these two surface flows are again related by

$$j^-(t,E'\vec{\Omega}') = j^+(0,E,\vec{\Omega}) T(t,E \rightarrow E', \vec{\Omega} \rightarrow \vec{\Omega}'). \quad (3.24)$$

Thus T can be found by performing a one-dimensional transport calculation with one slab face uniformly illuminated by $j^+(0,E,\vec{\Omega})$ in which the exit flow $j^-(t,E'\vec{\Omega}')$ is computed.

To calculate $J_{\text{out}}^{\text{pt}}$, however, one can bypass the calculation of T . By comparing Eqs. (3.23) and Eqs. (3.24) it is seen that the exit flow rate for the one-dimensional transport problem becomes $J_{\text{out}}^{\text{pt}}$ if the incident flow rate is simply taken as

$$j^+(0, E, \vec{\Omega}) = J_{\text{in}}^{\text{pt}}(0, E, \vec{\Omega}). \quad (3.25)$$

Thus to find $J_{\text{out}}^{\text{pt}}(0, E, \vec{\Omega})$, perform a one-dimensional transport calculation for the angular flux density $\Phi(z, E, \vec{\Omega})$ in slab geometry subject to the boundary conditions

$$\begin{cases} \Phi(0, E, \vec{\Omega}) \equiv j^+(0, E, \vec{\Omega}) / \hat{n} \cdot \vec{\Omega} = J_{\text{in}}^{\text{pt}}(0, E, \vec{\Omega}) / \hat{n} \cdot \vec{\Omega}, & \vec{n} \cdot \vec{\Omega} > 0 \\ \Phi(t, E, \vec{\Omega}) = 0, & \hat{n} \cdot \vec{\Omega} < 0 \end{cases} \quad (3.26)$$

Then the calculated flow rate out of the top surface, i.e., $j^-(t, E, \vec{\Omega}) \equiv \hat{n} \cdot \vec{\Omega} \Phi(t, E, \vec{\Omega})$, $\hat{n} \cdot \vec{\Omega} > 0$, is the desired total flow rate $J_{\text{out}}^{\text{pt}}$ and, thus, the effective point skyshine source of Eq. (3.20) given by

$$S_{\text{pt}}^{\text{eff}}(E, \vec{\Omega}) = j^-(t, E, \vec{\Omega}) = \hat{n} \cdot \vec{\Omega} \Phi(t, E, \vec{\Omega}), \quad \hat{n} \cdot \vec{\Omega} > 0. \quad (3.27)$$

3.2.4 1-D Boundary Condition for a Point Collimated Source

Figure 3.3 shows a cylindrical silo with a cylindrical concrete shield placed over a point source located on the center line of the cylinder. A point source emits particles isotropically, so that the energy-angular dependence of photons leaving the source is

$$S(E, \vec{\Omega}) = \frac{S_P(E)}{4\pi}. \quad (3.28)$$

It is also assumed that there are negligible interactions in the air as photons travel from the source to a point (x,y) on the bottom of the slab shield. Thus the angular flux density at the bottom of the shield ($z = 0$) is

$$\Phi(x,y,0,\vec{\Omega}) = \frac{S_p}{4\pi d^2} \delta(\vec{\Omega} - \vec{\Omega}'(x,y)) , \quad (3.29)$$

where $\vec{\Omega}'$ is the unit vector in the direction of the ray from the source to the position (x,y) on the bottom surface, and d is the distance from the point source to the point (x,y). Integration over the slab surface then gives

$$\Phi_{\text{tot}}(0,\vec{\Omega}) = \int \frac{S_p}{4\pi d^2} \delta(\vec{\Omega} - \vec{\Omega}') dA \equiv \int dA \Phi(x,y,0,\vec{\Omega}) . \quad (3.30)$$

A explicit form of Eq. (3.30) can be obtained by using a polar coordinate system (origin at the source) rather than the Cartesian (x,y) system. Let h be the perpendicular distance from the source to the slab (polar axis), (θ, ψ) be the polar and azimuthal angles to the point (x,y), and r be the perpendicular distance from the polar axis to the point (x,y). For this coordinate system one has

$$d = h / \cos \theta , \quad (3.31)$$

$$dA = r dr d\psi , \quad (3.32)$$

$$r = h \tan \theta , \quad (3.33)$$

and

$$dr = h \sec^2 \theta d\theta . \quad (3.34)$$

Substitution of these relations into Eq. (3.30) yields

$$\Phi(0, \vec{\Omega}) = \int_0^R r \, dr \int_0^{2\pi} \frac{S_P}{4\pi h^2} \cos^2 \theta' \, \delta(\vec{\Omega} - \vec{\Omega}') \, d\psi. \quad (3.35)$$

Because the point source is on the axis of the cylinder, the problem is azimuthally symmetric and Eq. (3.35) reduces to

$$\Phi(0, \cos \theta) = \int_0^R \frac{S_P}{2h^2} r \cos^2 \theta' \, \delta(\cos \theta - \cos \theta') \, dr. \quad (3.36)$$

Let $\omega' = \cos \theta'$ and $\omega = \cos \theta$ and substitute into Eq. (3.36) to get

$$\Phi(0, \omega) = \int_0^R \frac{S_P}{2h^2} \omega'^2 \, \delta(\omega - \omega') \, r \, dr. \quad (3.37)$$

Next, substitute $r = h \tan \theta'$ and $dr = h \sec^2 \theta' \, d\theta'$ into Eq. (3.37) and simplify to obtain

$$\Phi(0, \omega) = \int_0^{\theta_0} \frac{S_P}{2h^2} \omega'^2 \, \delta(\omega - \omega') \, h \tan \theta' \, \frac{h}{\omega'^2} \, d\theta'. \quad (3.38)$$

Simplification and use of $-d\omega' = \sin \theta' \, d\theta'$ reduces Eq. (3.38) to

$$\Phi(0, \omega) = \int_{\omega_0}^1 \frac{S_P}{2} \frac{\delta(\omega - \omega')}{\omega'} \, d\omega' \quad (3.39)$$

or after integration

$$\Phi(0,\omega) = \begin{cases} \frac{S_p}{2\omega} , & 1 \geq \omega \geq \omega_0 , \\ 0 , & \omega < \omega_0 . \end{cases} \quad (3.40)$$

To relate the total angular flux (i.e. the angular flux density integrated over the finite slab area) to the total flow rate into the slab recall that

$$\hat{\mathbf{n}} \cdot \vec{\Omega} \Phi_{\text{in}}(0, \vec{\Omega}) = J_{\text{in}}^+(0, \vec{\Omega}) . \quad (3.41)$$

With azimuthal symmetry Eq. (3.41) reduces to

$$J_{\text{in}}^+(0, \omega) = \omega \Phi_{\text{in}}(0, \omega) . \quad (3.42)$$

The one-dimensional transport boundary condition in terms of the total angular flow rate is found by substituting Eq. (3.40) into Eq. (3.42) to obtain

$$J_{\text{in}}^+(0, \omega) = \begin{cases} \frac{S_p}{2} , & 1 \geq \omega \geq \omega_0 , \\ 0 , & \omega < \omega_0 . \end{cases} \quad (3.43)$$

3.3 Transport Calculation of the Effective Point Skyshine Source

In this section, the calculational procedure used to find the emergent photon energy and angular distribution on the shield's top surface will be examined.

3.3.1 Use of KSLAB for Shield Penetration Calculations

The one-dimensional, azimuthally symmetric, time-independent transport equation for an inhomogeneous medium can be written as [Ry79]

$$\omega \frac{\partial \Phi}{\partial x}(z, E, \omega) + \mu(z, E) \Phi(z, E, \omega) = Q(z, E, \omega) + \int_0^\infty dE' \int_{-1}^{+1} d\omega' \mu_s(z, E' \rightarrow E, \omega' \rightarrow \omega) \Phi(z, E', \omega') \quad (3.44)$$

where $\Phi(z, E, \omega)$ is the angular flux density (integrated over azimuth) and the flux independent source is $Q(x, E, \omega)$. The total macroscopic cross section is $\mu(z, E)$. The azimuthally averaged macroscopic scattering cross section is defined such that $\mu_s(z, E' \rightarrow E, \omega' \rightarrow \omega) dE' d\omega$ is the probability a photon of energy E' and direction of travel ω' will scatter into energies dE about E , and directions of travel $d\omega$ about ω . Following steps outlined by Ryman [Ry79], this one-dimensional transport equation can be reduced with the multigroup and finite-difference approximations to a form suitable for a numerical solution. The finite difference form of the multi-group discrete ordinates transport equation is

$$\begin{aligned} \frac{\omega_i}{\Delta_{k+\frac{1}{2}}} \left[\Phi_g(z_{k+1}, \omega_i) - \Phi_g(z_k, \omega_i) \right] + \mu_g(z_{k+\frac{1}{2}}) \Phi_g(z_{k+\frac{1}{2}}, \omega_i) \\ = Q_g(z_{k+\frac{1}{2}}, \omega_i) + S_g(z_{k+\frac{1}{2}}, \omega_i), \end{aligned} \quad (3.45)$$

where the subscripts have the ranges

$$k = 1, 2, \dots, K, \quad i = 1, 2, \dots, N, \quad g = 1, 2, \dots, G,$$

and where $\Phi_g(z_k, \omega_i)$ are the angular flux densities in energy group g and $Q_g(z_{k+\frac{1}{2}}, \omega_i)$ is the flux-independent source in energy group g . The modal positions x_k inside the slab are shown in Fig. 3.5, and the position $x_{k+\frac{1}{2}}$ is defined by

$$z_{k+\frac{1}{2}} = \frac{(z_k + z_{k+1})}{2}, \quad (3.46)$$

and the internode spacing by

$$\Delta_{k+\frac{1}{2}} = z_{k+1} - z_k. \quad (3.47)$$

The cell-centered angular flux is calculated from the cell-edge values using [Ry79]

$$\Phi_g(z_{k+\frac{1}{2}}, \omega_i) = \frac{\Phi_g(z_k, \omega_i) + \Phi_g(z_{k+1}, \omega_i)}{2}. \quad (3.48)$$

The final term in Eq. (3.45) is the scatter source and is given by [Ry79]

$$S_g(x_{k+\frac{1}{2}}, \omega_i) = \sum_{g'=1}^g \sum_{j=1}^N w_j \mu_{g' \rightarrow g}(z, \omega_j \rightarrow \omega_i) \Phi_{g'}(z, \omega_j). \quad (3.49)$$

The sum over energy proceeds from the highest energy group (1) to the energy group g . The inner sum calculates the scatter source into energy group g and angular direction ω_i from energy group g' and directions ω_j .

The quadrature set which defines the angular directions can be broken into several subregions symmetric about the angular direction $\omega = 0$. In Fig. 3.6 an example is shown that breaks the direction cosines into a region composed of 6

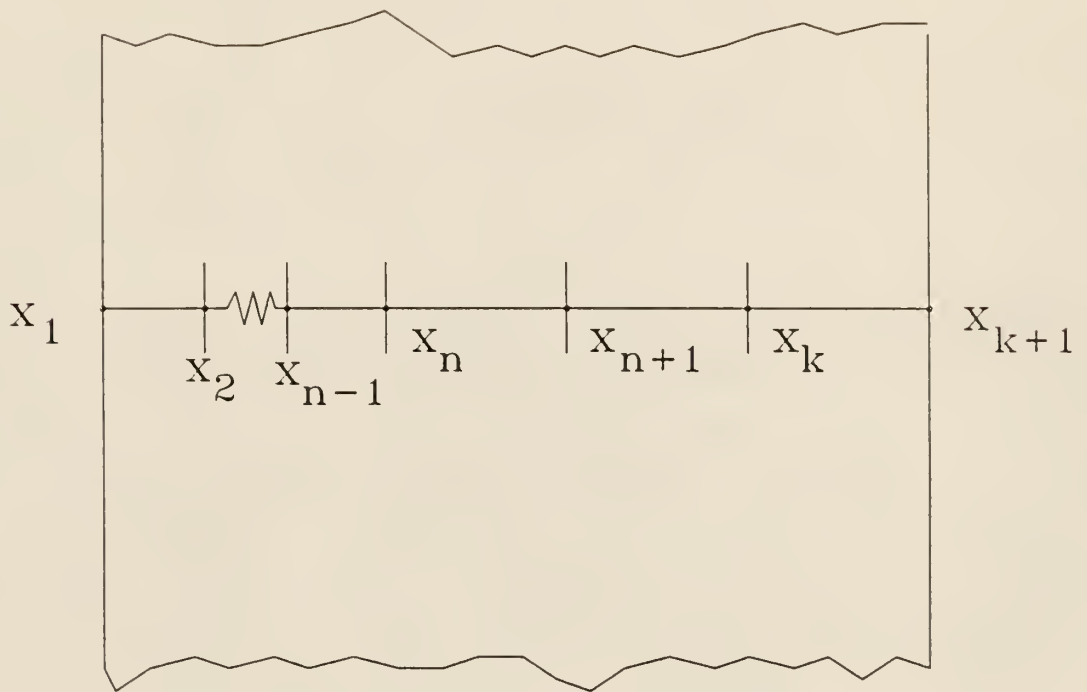


Figure 3.5 Discrete ordinates coordinate system defined inside a slab shield as used in the one-dimensional transport code KSLAB [Ry79].

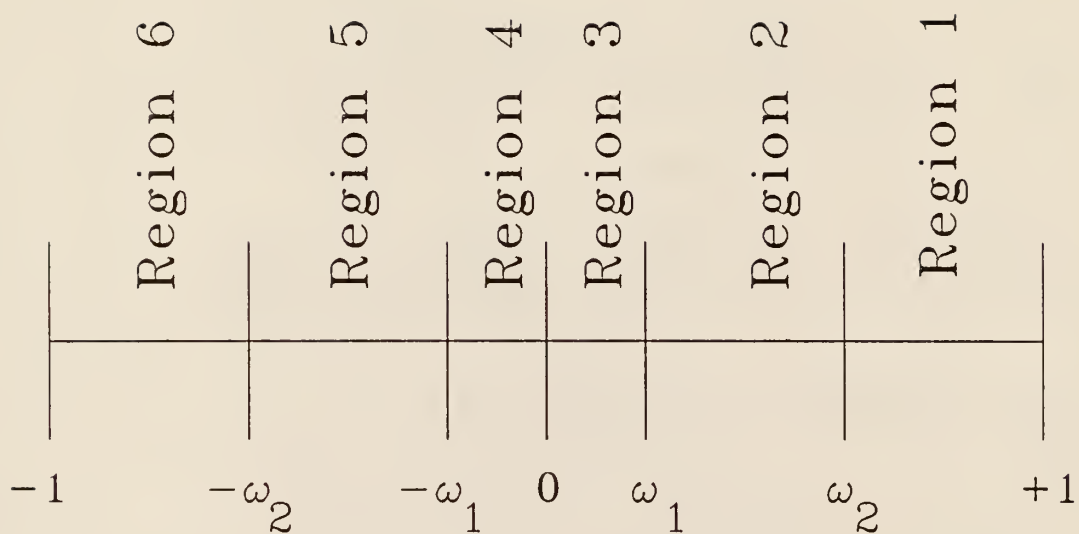


Figure 3.6. Example breaking apart the angular coordinate system into six distinct regions which will allow different source collimation angles.

parts. The points ω_1 and ω_2 are angular break points. The reason the direction cosines are broken into smaller subregions is the need to treat a source which contains a sharp angular cutoff (i.e. a collimated source). As an example, a monoenergetic source incident on an infinite slab with source strength given by S/ω , for $\omega_c \leq \omega < 1$, and 0 for $\omega < \omega_c$ would be modeled using a cross section set with interval regions $-1 < \omega < \omega_c$, $-\omega_c < \omega < \omega_c$, and $\omega_c < \omega < 1$.

The angular direction cosines in each region are generated using

$$\tilde{\omega}_j = \frac{b-a}{2} \omega_j + \frac{b+a}{2}, \quad (3.50)$$

and the angular weights using

$$\tilde{w}_j = \frac{b-a}{2} w_j, \quad (3.51)$$

where $\{\omega_j\}$ are the standard Gaussian ordinates with associated weights $\{w_j\}$, b is the direction cosine for the top of the interval, and a is the direction cosine for the bottom of the interval. The only restrictions for the subinterval regions are the avoidance of a direction cosine at zero (where the discrete ordinates equations becomes indeterminate) and the production of a sufficiently fine angular mesh so that there is at least one nonzero exact kernel cross section $\mu_{g' \rightarrow g}(z, \omega_j \rightarrow \omega_i)$, $g' = 1, \dots, g$, $\{\omega_j \neq \omega_i\}$ for each possible group-to-group cross section [Ry79].

The group-to-group cross sections $\mu(E_{g'}, \rightarrow E_g, \omega_i \rightarrow \omega_j)$ are evaluated using an exact kernel representation [Mi77]. To evaluate the multigroup cross sections, the angular flux density is assumed to be separable in energy and direction, [Ry79], i.e.

$$\Phi(z, \omega, E) \cong \Psi(z, \omega) M(E) . \quad (3.52)$$

The exact-kernel multigroup cross sections are evaluated using [Ry79]

$$\mu_{g' \rightarrow g}(z, \omega' \rightarrow \omega) \equiv \frac{1}{M_{g'}} \int_{E_{g+1}}^{E_g} dE \int_{E_{g'+1}}^{E_{g'}} dE' M(E') \mu_s(z, E' \rightarrow E, \omega' \rightarrow \omega) , \quad (3.53)$$

where

$$M_{g'} = \int_{E_{g'+1}}^{E_{g'}} dE' M(E') . \quad (3.54)$$

The exact kernel cross sections were evaluated in this study for each allowed energy group-to-energy group transfer for all the direction cosines in the angular quadrature set using the code PHOGROUP [Ry79]. The energy group structures used in evaluating the cross sections in this work were chosen so that the skyshine dose caused by each energy group were relatively equal. The energy group structure causing each energy group to contribute equally occurred when the energy structure was spaced equally. After selecting the energy group structure, the angular group structure was selected to insure angular coverage.

3.3.2 Effective Skyshine Source for Shielded Silo Problem

The use of KSLAB [Ry79] to solve the one-dimensional discrete ordinates transport equation required a multi-group approximation for the energy dependence of the photons emerging from the shield. To use MicroSkyshine's beam response functions with the energy group structure from KSLAB, the photon

energies were taken as the midpoint energy of each energy group used in the KSLAB calculations. The midpoint energy for each energy group was calculated by the cross section preparation code PHOGROUP [Ry79].

A change made in the output from KSLAB was to remove the unscattered source photons from the calculated angular flux density $\Phi_g(z, \omega_i)$ which contains both scattered and unscattered photons. In this way, the contribution of the unscattered and scattered photons could be calculated separately. The unscattered flux component penetrating the shield is readily calculated using exponential attenuation and the incident angular flux on the bottom surface in direction ω_i . The scattered angular flux density in direction ω_i at the top shield surface is then calculated as

$$\Phi_g^{\text{scat}}(t, \omega_i) = \Phi_g(t, \omega_i) - \frac{S_p(E_g)}{2\omega_i} e^{-\mu_g t / \omega_i}, \quad \omega_i > 0 \quad (3.55)$$

where t is the thickness of the slab and μ_g is the total macroscopic cross section for energy group g .

Finally, the effective point skyshine source $S_{\text{pt}}^{\text{eff}}(E_g, \omega)$ needed for the composite skyshine method is obtained from the KSLAB calculated scattered angular flux densities that exit from the top shield surface (i.e., from $\Phi_g^{\text{scat}}(t, \omega)$, $\omega > 0$) by using Eq. (3.27), namely

$$S_{\text{pt}}^{\text{eff}}(E_g, \omega) = \omega_i \Phi_g^{\text{scat}}(t, \omega), \quad \omega > 0 \quad (3.56)$$

The effective point source for uncollided photons penetrating the shield is thus

$$S_{\text{pt}}^{\text{eff}}(E_g, \omega) = \frac{S_p(E_g)}{2} e^{-\mu_g t / \omega}, \quad 0 < \omega < \omega_0. \quad (3.57)$$

In the composite method, these two effective skyshine sources are treated separately since they generally have different ranges of angular support. The uncollided photons are collimated by the silo walls and emerge only in the directions $\omega_0 < \omega \leq 1$, while the scattered photons emerge in all directions.

An interpolation in the angular flux density was required to link the air transport and slab transport problems together. The interpolation was required because, in general, the direction cosines used by KSLAB will not correspond to the Gaussian direction cosines used to integrate Eq. (2.34). To estimate $S_{pt}^{eff}(E_g, \omega_i)$ from $\Phi_g(\omega_j)$ it was necessary to interpolate the emergent angular flux densities (calculated at discrete ω_j values). A cubic spline interpolation method was used to perform this interpolation.

A problem arose when the spline fitting procedure was done over the entire outward angular range ($0 < \omega < 1$). A spline fit to the angular flux densities from KSLAB for unscattered and scattered components of the flux are shown in Figs. 3.7 and 3.8, respectively. The scattered angular flux in Fig. 3.7 appears to be adequately represented by the spline fit through the data points. The unscattered flux fit (Fig. 3.8) however, contains spurious oscillations especially in the region below the source's collimation angle. These oscillations are due to the sharp cutoff in the angular source at the source's collimation angle.

A better fit of the unscattered flux component is obtained by breaking the region into two parts with the breakpoint for the two regions being the source collimation angle. The spline fitting procedure was then applied to the region above and below the breakpoint. The results, shown in Fig. 3.9, no longer contain spurious oscillations in the angular flux density and thus, more accurately represent the angular flux.

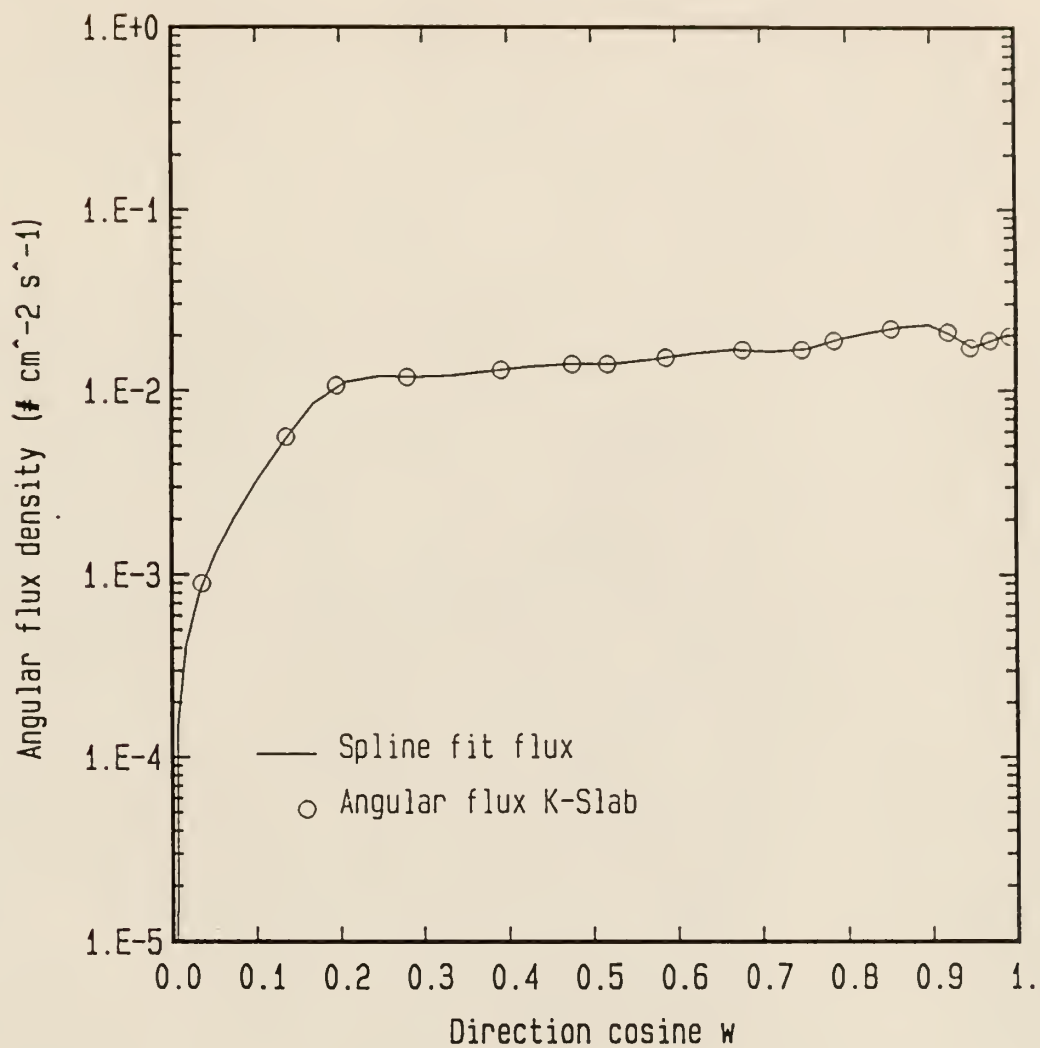


Figure 3.7. Emergent angular flux densities spline fit for the eighth energy group of the N-16 source for a source collimation angle of 120°.

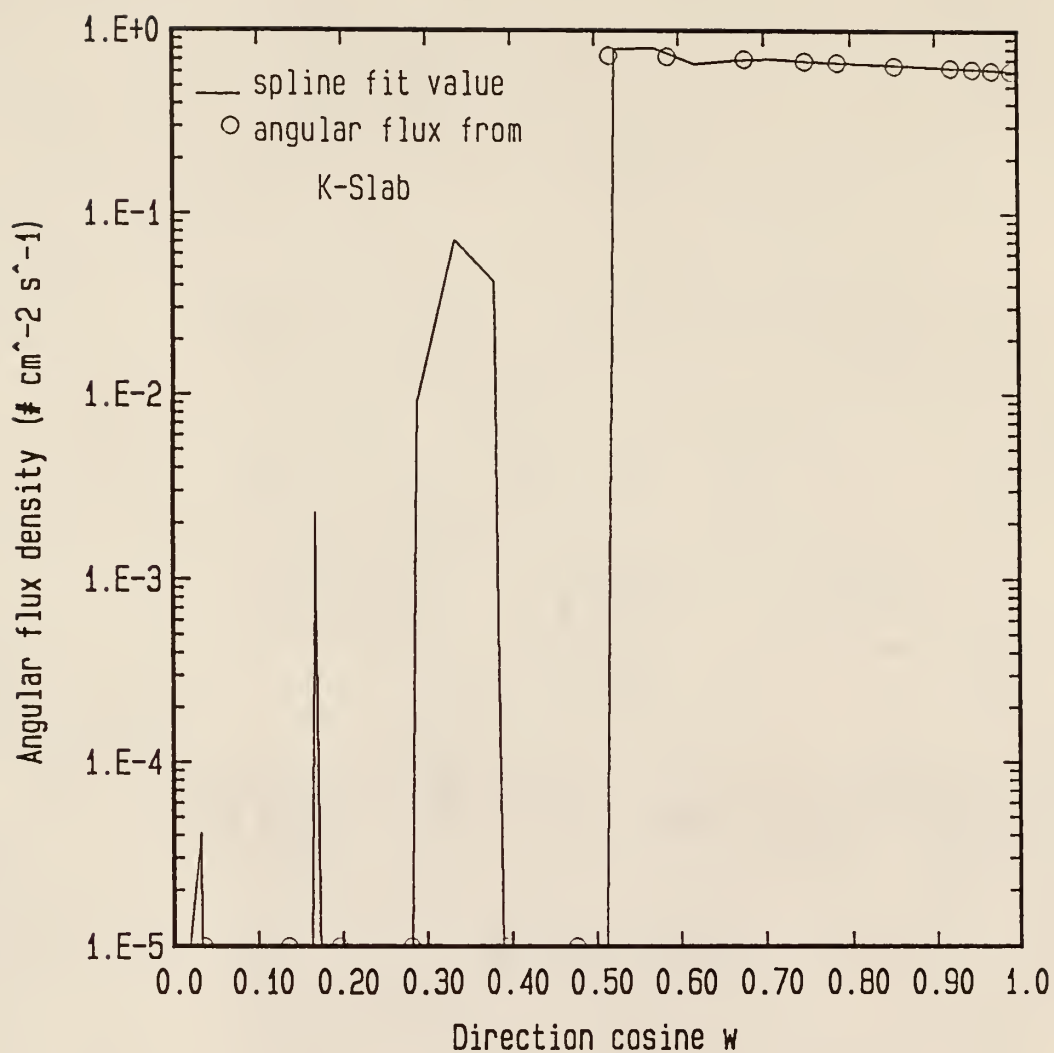


Figure 3.8. Emergent angular flux densities for the source energy group spline fit at intermediate points (i.e. between the KSLAB values) over the outward angular directions (i.e. out of the slab face) for the N-16 source collimated at 120° .

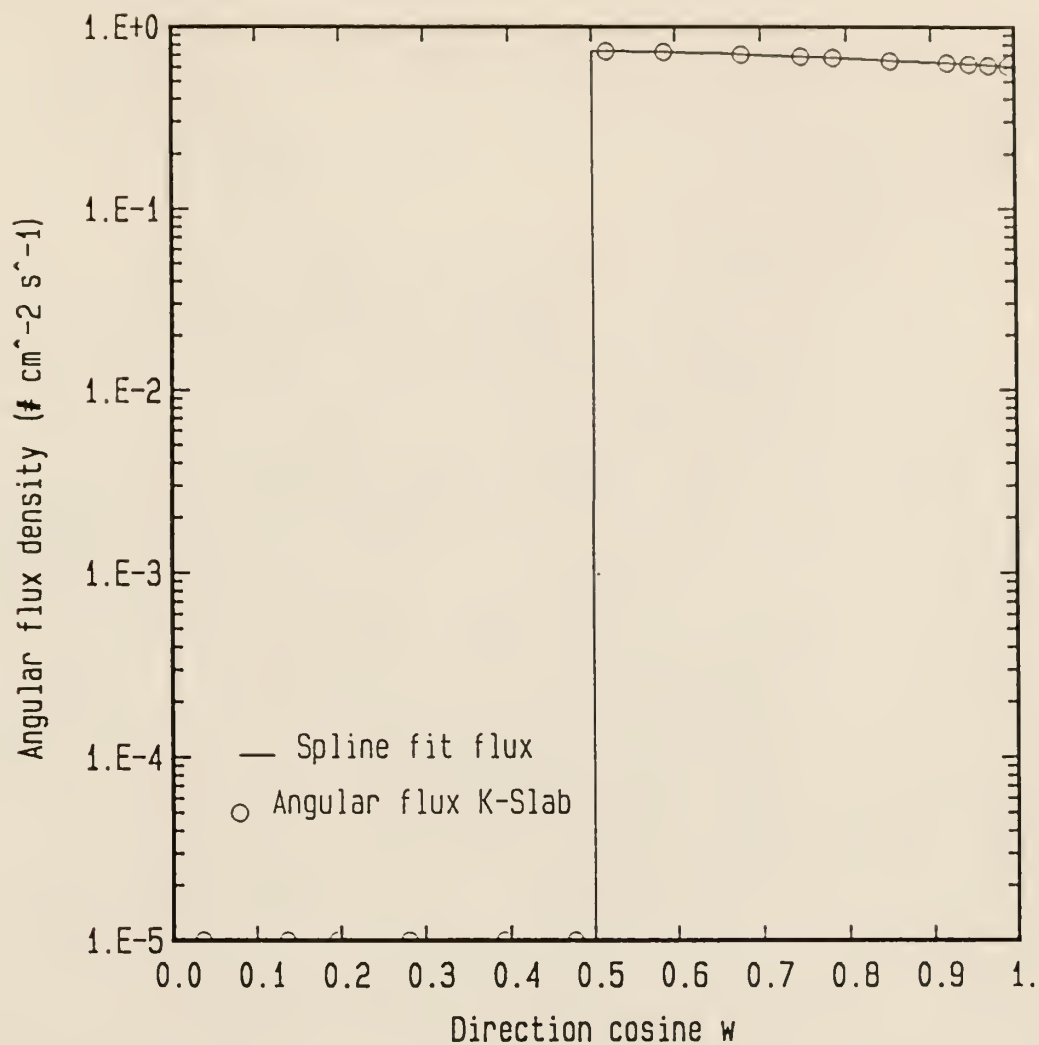


Figure 3.9. Emergent angular flux densities for the source energy group spline fit in two regions (one above the source collimation angle and the other below it) for the N-16 source collimated at 120° .

3.4 Validation of the Composite Dose Calculation Method

The composite method developed above is similar to a two-step method used by Keck and Herchenroder [Ke82] to obtain results which they compared to the experimental results from K-State's benchmark skyshine experiment. Keck and Herchenroder used a hybrid method composed of an one-dimensional discrete ordinates code ANISN to estimate the effective point source used by SKYSHINE-II. ANISN used 18 energy groups and a P-3 Legendre cross section representation [Ke82]. The hybrid method gave excellent agreement with the K-State Benchmark experiment despite the known tendency of SKYSHINE-II to over predict the skyshine dose and the questionable representation of the photon scattering cross sections resulting from a low-order Legendre expansion.

The composite method, as developed in this chapter, uses a similar procedure (i.e. one-dimensional discrete ordinates code and an approximate method to estimate the skyshine dose) to calculate the skyshine dose. The main differences are in the detailed theoretical background used, the improved representation of the photon cross sections afforded by the exact kernel representation, and the use of the improved skyshine response functions developed for MicroSkyshine.

3.4.1 Benchmark Experimental Calculations

The group-to-group cross sections for Co-60 gamma rays were calculated using the photon data base developed by Biggs and Lighthill [Bi72, Bg68, Bg72]. The group-to-group cross section types considered were the incoherent component of the Compton scatter, the production of annihilation photons, and the photoelectric effect. The group-to-group cross sections were developed for a concrete shield of density 2.13 g/cm³, for the concrete composition shown in Table

Table 3.1. Material composition of the concrete used in preparing the group-to-group cross sections used in K-SLAB [Ch87].

| Element | Mass Fraction | Element | Mass Fraction |
|---------|---------------|---------|---------------|
| H | 5.558(-03)* | Si | 3.151(-01) |
| O | 4.981(-01) | S | 1.283(-02) |
| Na | 1.710(-02) | K | 1.924(-02) |
| Mg | 2.565(-03) | Ca | 8.294(-02) |
| Al | 4.575(-02) | Fe | 1.240(-02) |

*read as 5.558×10^{-3}

Table 3.2. Angular directions and angular weights used in calculating the exact kernel cross sections for the Co-60 benchmark calculations. This quadrature set is designed for a source collimation angle of 150.5 degrees.

| direction cosines (\pm) | angular weights |
|--------------------------------|-----------------|
| 0.9958127475 | 0.01048910703 |
| 0.9800979934 | 0.01966458257 |
| 0.9595946276 | 0.01966458257 |
| 0.9438798735 | 0.01048910703 |
| 0.9165603678 | 0.05868640587 |
| 0.8236414762 | 0.1235771943 |
| 0.6788851739 | 0.1602817361 |
| 0.5154093952 | 0.1602817361 |
| 0.3706530928 | 0.1235771943 |
| 0.2777342012 | 0.05868640587 |
| 0.2259078846 | 0.07072276339 |
| 0.1273009741 | 0.1131564214 |
| 0.02869406358 | 0.07072276339 |

Table 3.3. Energy group ranges and average energies used in the Co-60 benchmark calculations. The average energies were generated by PHOGROUP [Ry79] and were used by SKYCALC [Ba88].

| Group No. | Energy Group Ranges (MeV) | Average Group Energies (MeV) |
|-----------|------------------------------|---------------------------------|
| 1 | 1.33 – 1.17 | 1.249135 |
| 2 | 1.17 – 1.00 | 1.083897 |
| 3 | 1.00 – 0.89 | 0.944484 |
| 4 | 0.89 – 0.78 | 0.834432 |
| 5 | 0.78 – 0.67 | 0.724365 |
| 6 | 0.67 – 0.57 | 0.619407 |
| 7 | 0.57 – 0.46 | 0.514170 |
| 8 | 0.46 – 0.35 | 0.403997 |
| 9 | 0.35 – 0.24 | 0.293706 |
| 10 | 0.24 – 0.15 | 0.193723 |
| 11 | 0.15 – 0.05 | 0.093052 |

3.1, and for the average energy of the Co-60 gamma photons (1.33 and 1.17 MeV). Eleven energy groups and 26 direction cosines in 6 subregions were used in the benchmark group-to-group cross section calculations (see Table 3.2 and 3.3). Output from PHOGROUP [Ry79] gave the group-to-group scattering cross sections, the total group cross sections, and the average photon energy in each energy group.

With the calculated cross sections, a plane one-dimensional transport code, KSLAB [Ry79], was used for the benchmark shield thicknesses of 21 and 42.8 cm. The boundary condition used in the discrete-ordinates transport code was determined using Eq. (3.43). The mesh spacing used in the discrete-ordinates calculation was chosen to guarantee the convergence of the angular flux densities. The maximum mesh size allowable is calculated using [Ch87]

$$\Delta x_{\max} = \frac{2 \omega_{\min}}{\mu_g}, \quad (3.58)$$

where ω_{\min} is the direction cosine closest to the origin and μ_g is the total group cross section with the largest value. The inner iteration scheme used in KSLAB was considered converged when the absolute fractional difference between the previous angular fluxes and the newly calculated angular fluxes was less than 5×10^{-6} ("point-wise" convergence).

With the transmitted angular fluxes calculated by KSLAB, the skyshine doses were then calculated using the code SKYCALC written by the author (see Appendix A). The calculated skyshine doses were divided by the source strength to express the doses in units of rad/photon. Also, to plot the SKYCALC results against the benchmark experimental data, the source-to-detector distance d was

expressed in units of mass thickness and the dose in units of normalized exposure ($R \cdot m^2/Sr$). The mass thickness source detector distance in g/cm^2 was calculated with

$$\tilde{d} = d \rho , \quad (3.59)$$

where ρ was the density of the air in g/cm^3 used by SKYCALC in it's calculation of the skyshine doses. The normalized exposure is calculated using [Ch84]

$$R_x(d) = 1.154 R_d(d) d^2/\Delta\Omega_o , \quad (3.60)$$

where 1.154 is the conversion factor between dose and exposure, d is the source-to-detector distance in m, and $\Delta\Omega_o$ is the source's solid angle of collimation given by

$$\Delta\Omega_o = 2\pi (1-\cos\theta_o) . \quad (3.61)$$

The normalized composite results are shown in Fig. 3.10 along with results obtained with a 10-group DOT calculation [Fa87], results from the MicroSkyshine method [Fa87, Sh87], and the experimental results from the K-State benchmark experiment [Fa87]. The worst agreement between the composite method and the benchmark experimental data occurs for small air mass-thickness distances (i.e., close to the source). The composite method using 11 energy groups calculated the skyshine dose as well or better than, the more sophisticated DOT procedure using 10 energy groups. The composite method was mostly conservative (i.e., over predictive) in its estimation of the skyshine dose while the 10 group DOT calculations were always underpredictive. As might be expected, the

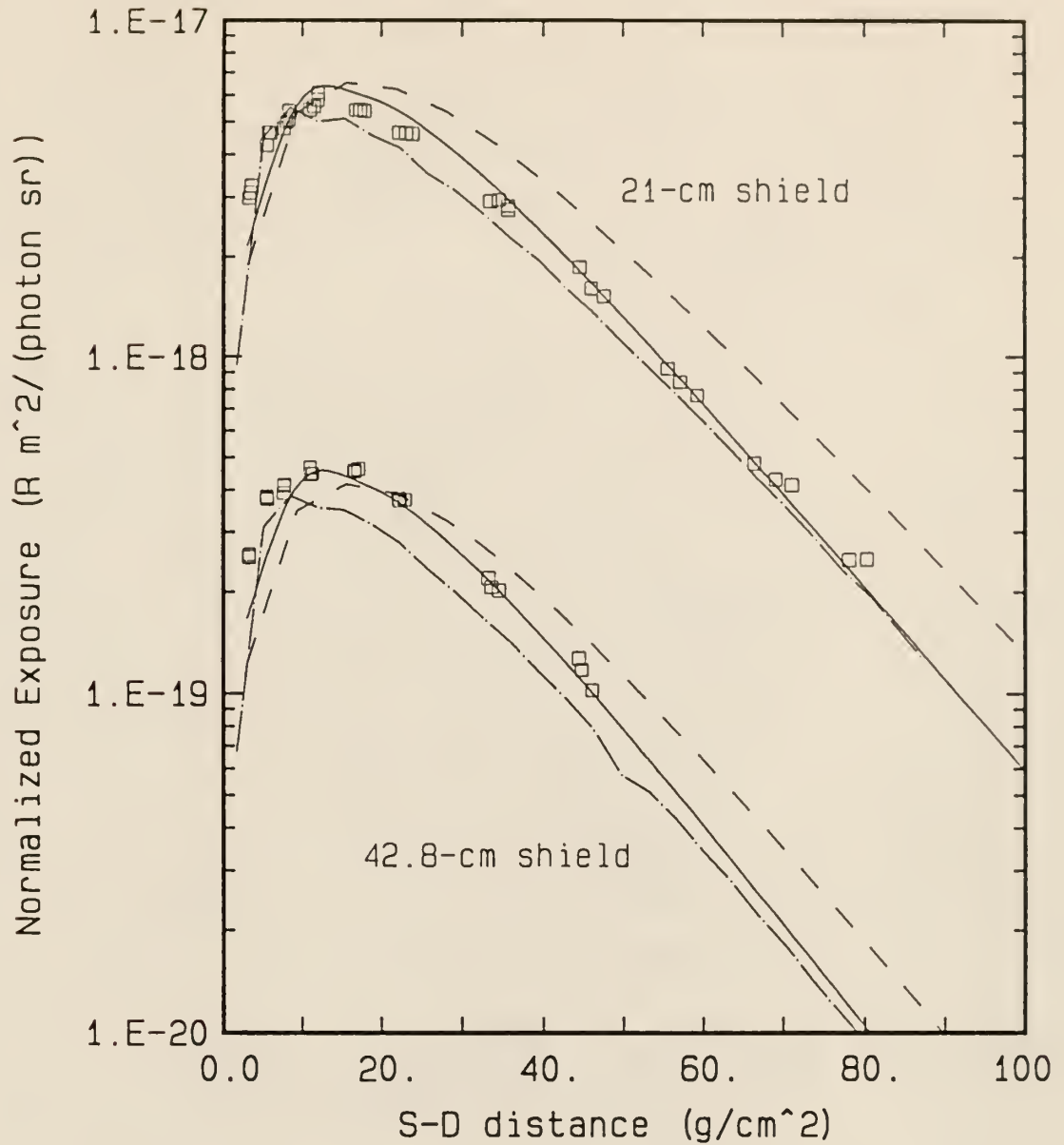


Figure 3.10. MicroSkyshine results (---), Composite Method results (—), and DOT results (-·-·-) compared to the experimental data from the K-State benchmark experiment [C178] for shield thicknesses of 21 and 42.8 cms.

MicroSkyshine results do not agree with experimental values as well as either the DOT or the composite method skyshine dose calculations, although given the simplicity of the MicroSkyshine method, the results are remarkably good.

The hybrid method of Keck and Herchenroder [Ke82] along with the experimental data and the composite method is shown in Fig. 3.11. Figure 3.11 indicates that the composite method and the hybrid method results are very similar over the entire range plotted. Both the hybrid method and the composite method agree closely with the measured experimental results.

The fraction of the total dose that each group of photons leaving the source shield contributes to the total dose in the composite method is shown in Table 3.4. As expected, the lower energy groups contribute less to the total dose as the source-to-detector distance increases, indicating that the lower energy photons are being preferentially attenuated. Table 3.4 and Fig. 3.11 indicate that the greater errors in the composite method occur when the lower energy groups, as calculated at the shield-air interface, contribute larger portions of the total dose. To check the adequacy of the energy group and angular structures used, the 21-cm benchmark problem was rerun using a 16-group energy structure and a 32-group angular structure. The results for the new 21-cm benchmark case were within 3% of the 11-group composite method results indicating that the group structure used in the 11-group energy structure was adequate.

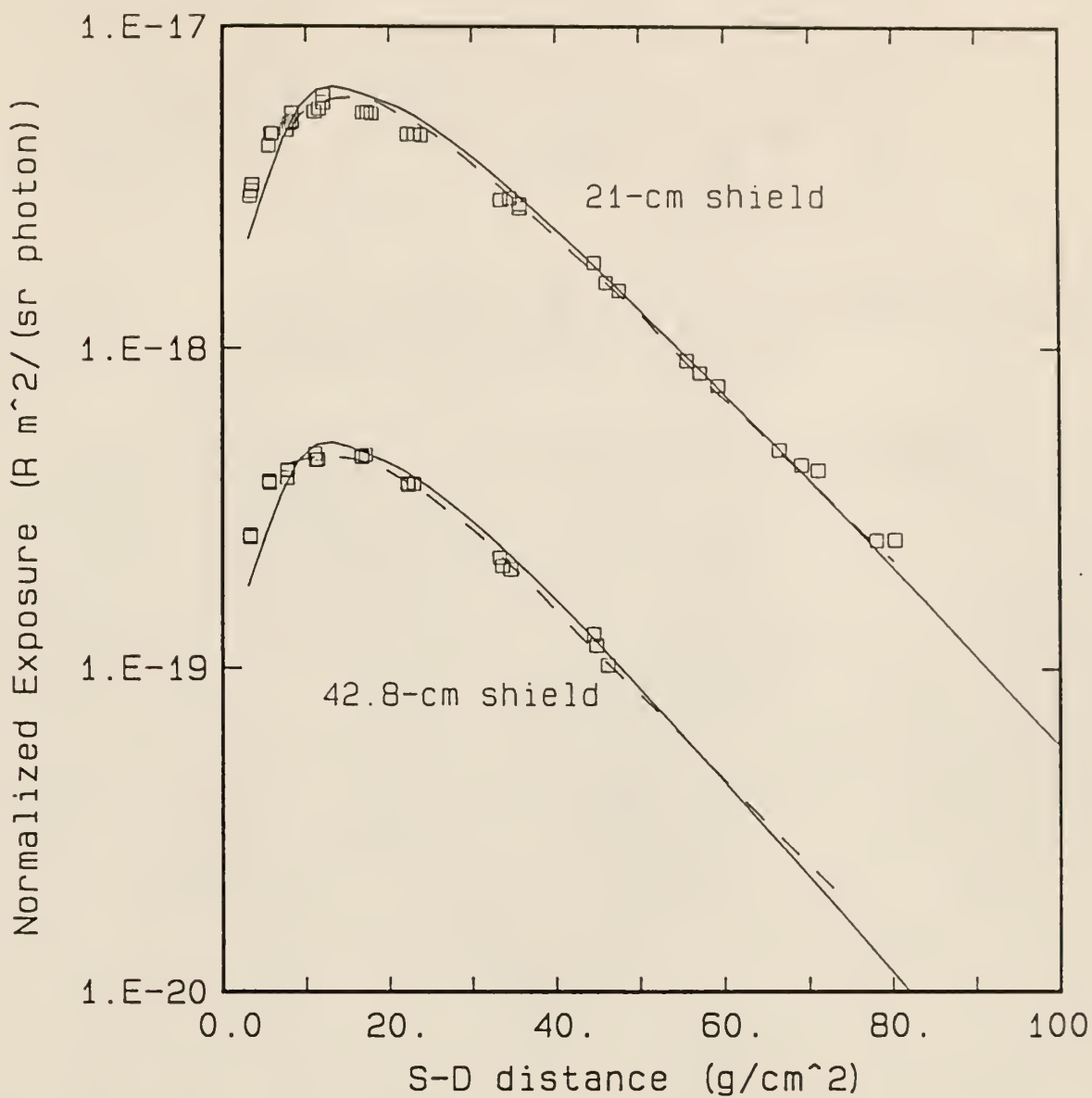


Figure 3.11. Comparison using Koch and Herchenroder's data [Ke82] (---) with the composite method results (—) and the K-State benchmark experimental results [C178].

Table 3.4. Fraction of the total dose each energy group contributes to the skyshine dose for source-to-detector mass thickness for the 21 cm and 42.8 Benchmark cases.

| Energy Group | Source Detector Mass Thickness (g/cm ²) | | | | |
|-----------------------|---|----------|----------|----------|----------|
| | 3.125 | 21.875 | 40.625 | 59.375 | 78.125 |
| A 21 cm slab shield | | | | | |
| 1 | 1.08E-01 | 1.50E-01 | 1.84E-01 | 2.11E-01 | 2.33E-01 |
| 2 | 2.74E-02 | 3.94E-02 | 5.03E-02 | 6.03E-02 | 7.00E-02 |
| 3 | 6.34E-02 | 8.84E-02 | 1.08E-01 | 1.25E-01 | 1.39E-01 |
| 4 | 4.48E-02 | 6.16E-02 | 7.41E-02 | 8.34E-02 | 9.05E-02 |
| 5 | 4.84E-02 | 6.62E-02 | 7.88E-02 | 8.76E-02 | 9.31E-02 |
| 6 | 5.44E-02 | 7.14E-02 | 8.22E-02 | 8.84E-02 | 9.11E-02 |
| 7 | 6.48E-02 | 7.62E-02 | 7.94E-02 | 7.85E-02 | 7.58E-02 |
| 8 | 8.57E-02 | 9.45E-02 | 9.14E-02 | 8.36E-02 | 7.48E-02 |
| 9 | 9.73E-02 | 1.03E-01 | 9.34E-02 | 7.86E-02 | 6.37E-02 |
| 10 | 1.24E-01 | 1.05E-01 | 8.40E-02 | 6.36E-02 | 4.59E-02 |
| 11 | 1.64E-01 | 9.22E-02 | 5.34E-02 | 3.24E-02 | 2.05E-02 |
| 12 | 1.18E-01 | 5.17E-02 | 2.06E-02 | 7.50E-02 | 2.54E-03 |
| B 42.8 cm slab shield | | | | | |
| 1 | 6.23E-02 | 8.68E-02 | 1.08E-01 | 1.25E-01 | 1.38E-01 |
| 2 | 5.97E-03 | 8.88E-03 | 1.16E-02 | 1.41E-02 | 1.66E-02 |
| 3 | 5.21E-02 | 7.45E-02 | 9.26E-02 | 1.07E-01 | 1.19E-01 |
| 4 | 3.99E-02 | 5.67E-02 | 7.01E-02 | 8.06E-02 | 8.91E-02 |
| 5 | 4.54E-02 | 6.50E-02 | 8.05E-02 | 9.27E-02 | 1.03E-01 |
| 6 | 5.46E-02 | 7.57E-02 | 9.16E-02 | 1.04E-01 | 1.13E-01 |
| 7 | 6.83E-02 | 8.57E-02 | 9.51E-02 | 1.00E-02 | 1.04E-02 |
| 8 | 9.38E-02 | 1.11E-01 | 1.16E-01 | 1.14E-01 | 1.10E-01 |
| 9 | 1.08E-01 | 1.24E-01 | 1.21E-01 | 1.11E-01 | 9.78E-02 |
| 10 | 1.41E-01 | 1.29E-01 | 1.11E-01 | 9.15E-02 | 7.21E-02 |
| 11 | 1.91E-01 | 1.16E-01 | 7.30E-02 | 4.83E-02 | 3.35E-02 |
| 12 | 1.40E-01 | 6.65E-02 | 2.89E-02 | 1.15E-02 | 4.28E-03 |

4. ASSESSMENT OF THE MICROSKYSHINE METHOD

The MicroSkyshine [Sh87] method for calculating the skyshine dose from a shielded skyshine source had only the K-State benchmark experimental data for verification of the accuracy of the shield treatment. Accounting for the shield above the source with exponential attenuation and an infinite-medium, isotropic-source, buildup factor is an unverified approximation. One of this report's objectives is to assess the accuracy of the MicroSkyshine method.

In this chapter, the exponential-attenuation, buildup-factor approach MicroSkyshine uses when a slab shield is placed above a point source will be investigated for its accuracy. The accuracy of the MicroSkyshine method will be determined using the more accurate composite method as a benchmark. The difference between the two methods will be expressed as

$$\text{Fraction Difference} = \frac{R_{\text{micro}}(d) - R_{\text{comp}}(d)}{R_{\text{comp}}(d)} \quad (4.1)$$

where $R_{\text{micro}}(d)$ is the skyshine dose calculated by MicroSkyshine at a source-to-detector distance d and $R_{\text{comp}}(d)$ is the skyshine dose calculated by the composite method for the same source-to-detector distance.

In the investigation of MicroSkyshine, three different primary photon energies were used. The photon energies were the 6.129 MeV photon from N16, the two primary photons from Co-60, and a 0.5 MeV photon. In addition to the three photon energies used, four conical source collimation angles were used, namely, 160, 120, 80, and 40 degrees.

4.1 Nitrogen-16 Photon Test Case

The Nitrogen-16 exact-kernel cross sections [Ry79] for concrete and iron were generated using 12 energy groups and 32 angular directions (see Tables 4.1 and 4.2). The material composition and the density (2.13 g/cm^3) of concrete was the same as that used for the benchmark case (see Table 3.1). The iron cross sections generated for the 6.129 MeV photon used a material density of 7.86 g/cm^3 . The exact kernel cross sections generated using PHOGROUP [Ry79] contained angular break points to represent source collimation angles of 160, 120, 80, and 40 degrees.

One-dimensional solutions of the transport equation using KSLAB [Ry79] were run for various iron and concrete shield thicknesses between 0.01 and 6 mean free path (mfp) thicknesses. The spatial mesh spacing, chosen to guarantee the convergence of the numerical solutions, was ($\Delta x_m = 0.25 \text{ cm}$). The point convergence criteria set for the Nitrogen-16 test cases was 1×10^{-4} (i.e., maximum fraction difference between old and new angular fluxes.)

4.1.1 Nitrogen-16 Results for Concrete Shields

The fraction difference between the composite and MicroSkyshine results for N-16 photons for a concrete shield with 160-degree source collimation angle is shown in Fig. 4.1. This figure shows that the MicroSkyshine method underestimates the skyshine dose at the detector for source-to-detector distances less than 500 m and for shield thicknesses greater than 4 mfp. The maximum dose underestimation by MicroSkyshine occurs at a source detector distance of 250 m (the minimum source-to-detector distance considered) and is approximately 2.5 times too low. The maximum overestimation by the MicroSkyshine method

Table 4.1. Energy group structure and average group energies used with the 6.129 MeV n-16 photon in generating the exact kernel group-to-group cross sections for iron and concrete. The generated cross sections will support source collimation angles of 160, 120, 80, and 40 degrees.

| Energy Group Range (MeV) | Average Group Energy (MeV) |
|-----------------------------|-------------------------------|
| 6.129 - 5.5 | 5.812401 |
| 5.5 - 5.0 | 5.248438 |
| 5.0 - 4.5 | 4.748177 |
| 4.5 - 4.0 | 4.247850 |
| 4.0 - 3.5 | 3.747436 |
| 3.5 - 3.0 | 3.246904 |
| 3.0 - 2.5 | 2.746203 |
| 2.5 - 2.0 | 2.245244 |
| 2.0 - 1.5 | 1.743843 |
| 1.5 - 1.0 | 1.241495 |
| 1.0 - 0.5 | 0.736987 |
| 0.5 - 0.05 | 0.239269 |

Table 4.2. Angular direction cosines and Gaussian Weights used in generating the exact kernel group-to-group cross sections for the N-16 photon energy 6.129 MeV in iron and concrete. The direction cosines and Gaussian weights will allow angular source collimation angles of 160, 120, 80, and 40 degrees.

| Angular Direction Cosines | Angular Weights |
|---------------------------|-----------------|
| 0.99320326 | 0.016752050 |
| 0.96984631 | 0.026803280 |
| 0.94648936 | 0.016752050 |
| 0.92012218 | 0.048235605 |
| 0.85286853 | 0.077176968 |
| 0.78561488 | 0.048235605 |
| 0.74757249 | 0.046272424 |
| 0.67824725 | 0.086749797 |
| 0.58779719 | 0.086749797 |
| 0.51847196 | 0.046272424 |
| 0.47734079 | 0.056761531 |
| 0.39230081 | 0.10641438 |
| 0.28134737 | 0.10641438 |
| 0.19630739 | 0.056761531 |
| 0.13695200 | 0.086824089 |
| 0.036696178 | 0.086824089 |

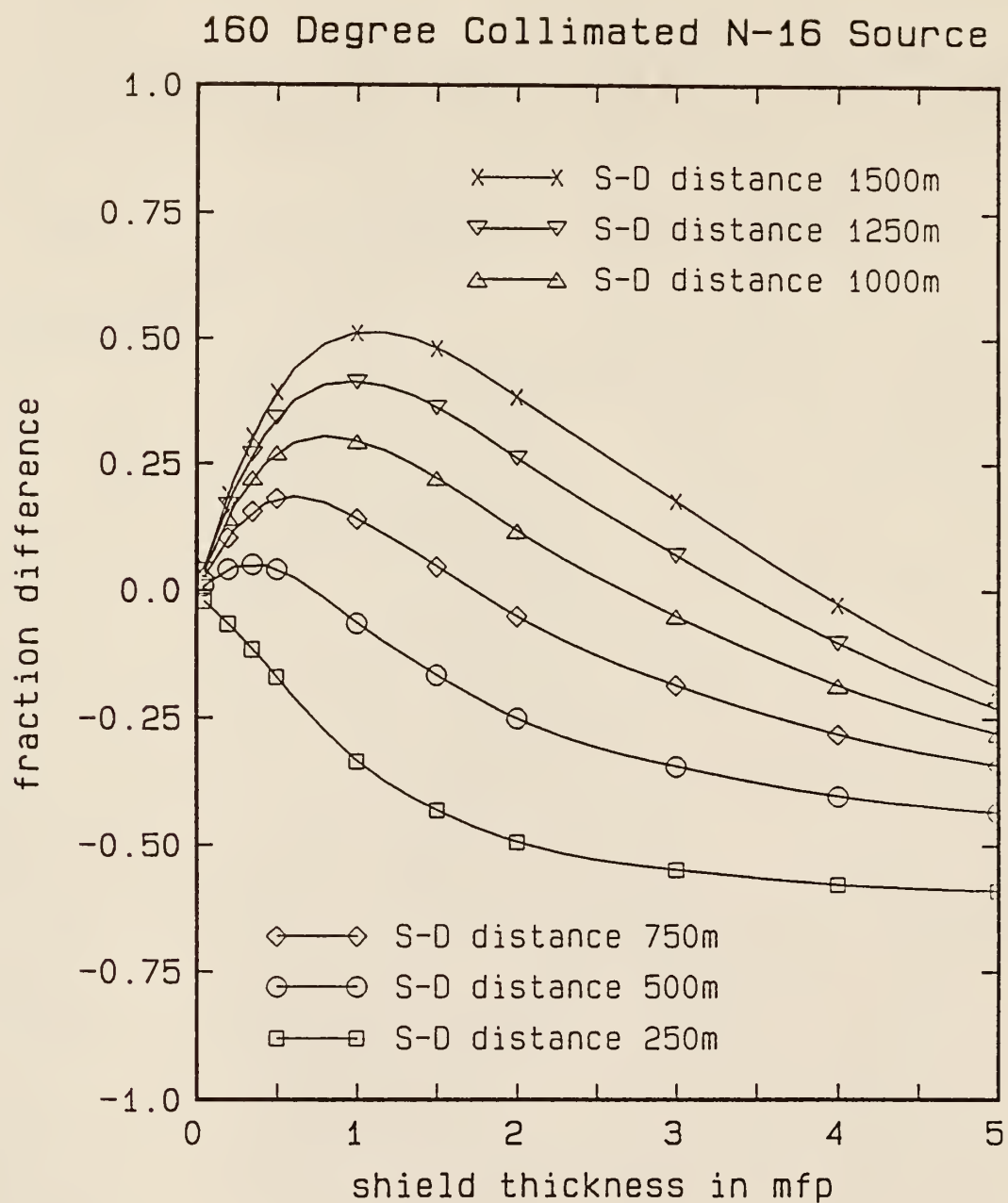


Figure 4.1. Fractional difference between the MicroSkyshine method with the composite method for concrete shields of various mfp thicknesses using a N-16 source collimated at 160°.

occurs at a shield mfp thickness of 1 mfp at the source-to-detector distance of 1500 m and was approximately 1.5 times greater than the composite method dose.

The fractional difference results for a 120-degree source collimation angle are shown in Fig. 4.2. The plotted results show that the MicroSkyshine method always underestimates the skyshine dose. The worst agreement occurs at the smaller source-to-detector distances where the MicroSkyshine method underestimates by a factor of 2.3. When the shield thicknesses are greater than 1 mfp, the MicroSkyshine method was never closer than a factor of 1.2 times too low.

The fractional difference results for the 80 and 40 degree source collimation angle cases are shown in Fig. 4.3 and in Fig. 4.4, respectively. The plotted results show that the MicroSkyshine method consistently underestimates the response at both source collimation angles, for all source detector distances and for all mfp shield thicknesses. The MicroSkyshine method's results fall in a band between 1.7 times and 2.5 times too low for shield thicknesses greater than 1 mfp at source collimation angle of 80 degrees. For the 40 degree source collimation angle the MicroSkyshine method's results fall in a band between 1.7 times and 5.5 times too low for shields with thicknesses greater than 1 mfp.

The effect of shield thickness on the detector response is shown in Fig. 4.5. The 160 and 120 degree source collimation angle cases indicate that the agreement between the MicroSkyshine method and the composite method was reasonably good for large source collimation angles. At the narrower source collimation angles, the MicroSkyshine method and the composite method disagree (see Fig. 4.5). As shown in Fig. 4.5, the composite method's skyshine dose increases with increasing shield mfp thickness out to approximately 1 mfp. The increase in the

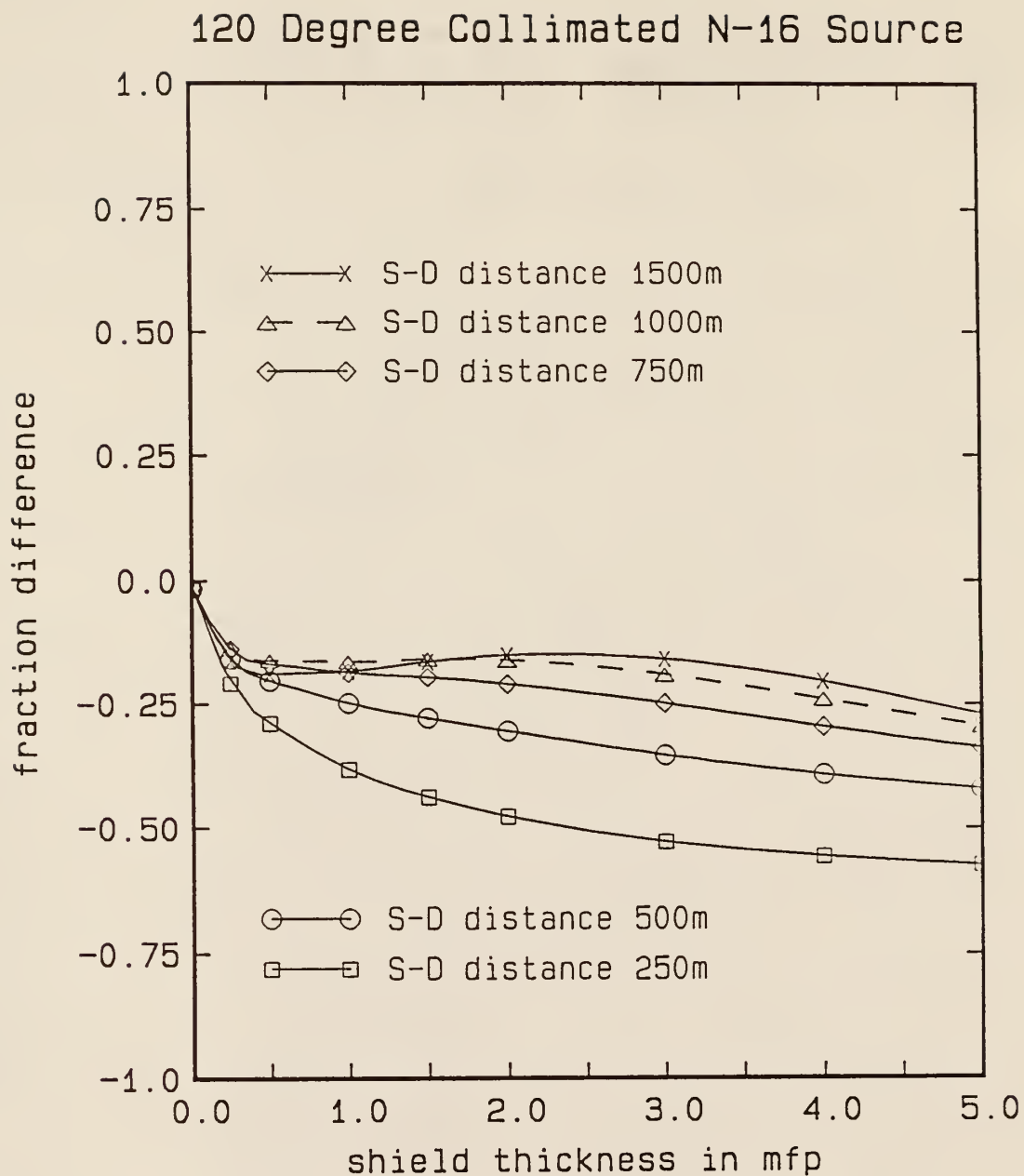


Figure 4.2. Fractional difference results comparing the MicroSkyshine method with the composite method for concrete shields of various mfp thicknesses using a N-16 source collimated at 120°.

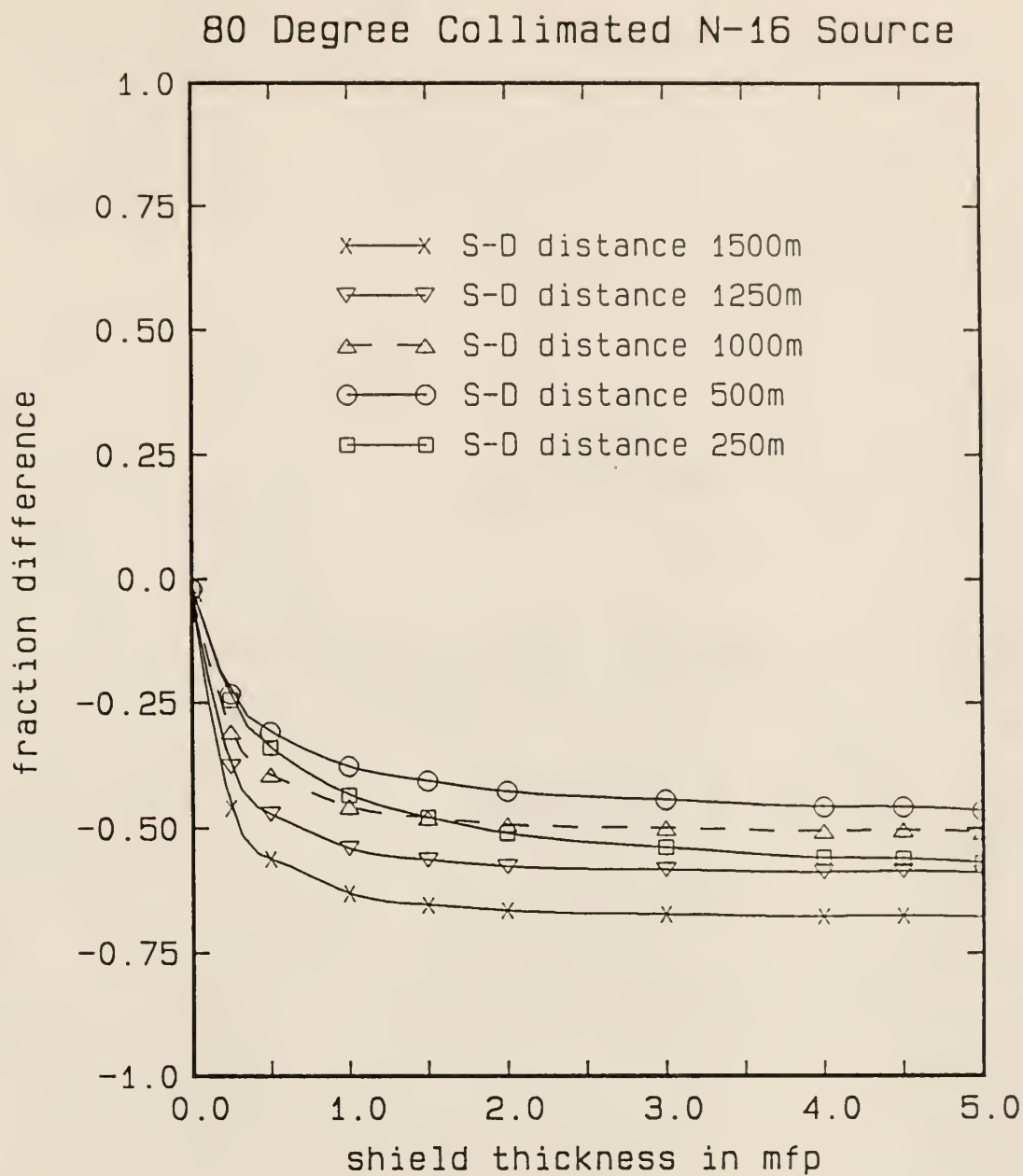


Figure 4.3. Fractional difference results comparing the MicroSkyshine method with the composite method for concrete shields of various mfp thicknesses using a N-16 source collimated at 80°.

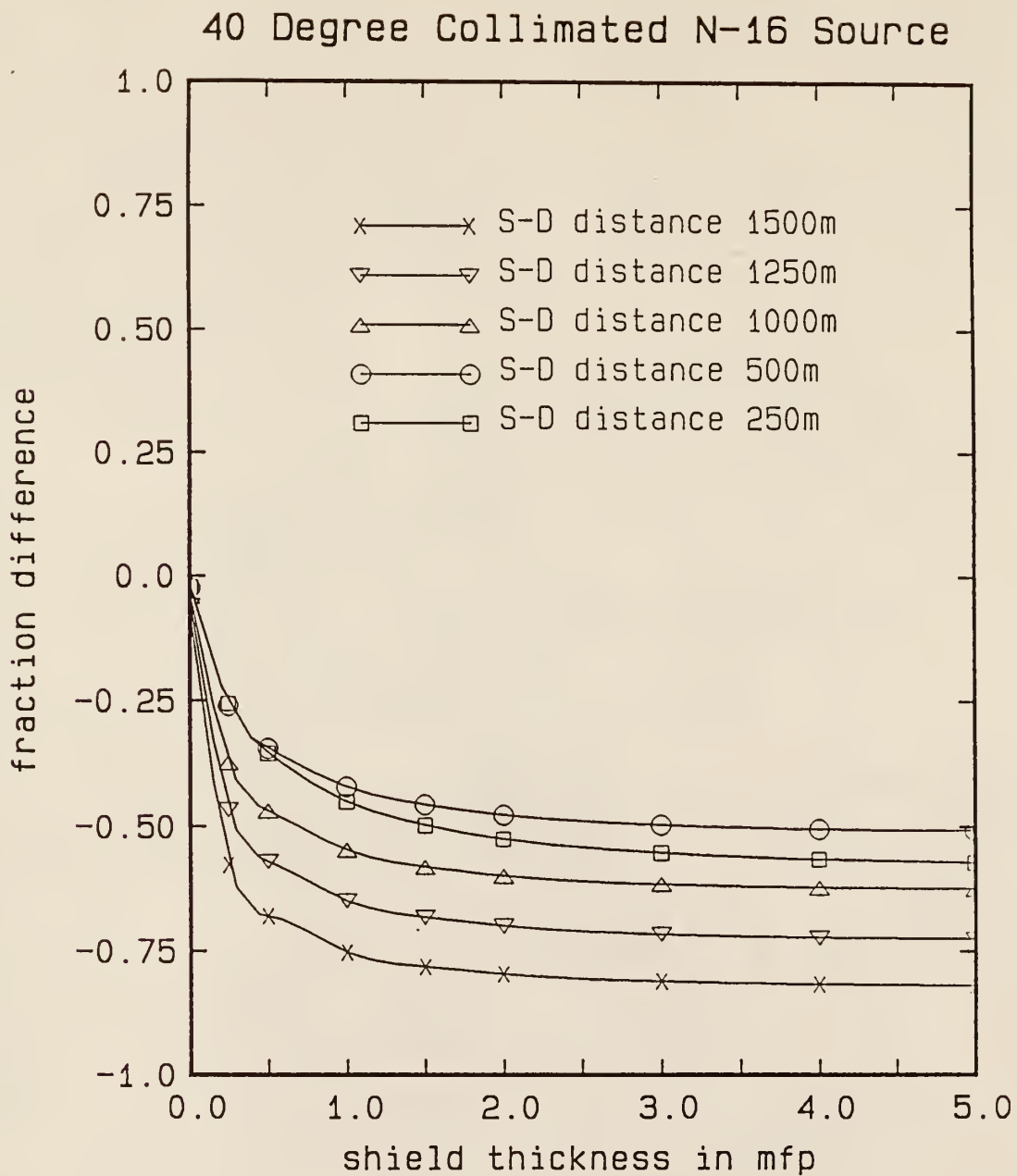


Figure 4.4. Fractional difference results comparing the MicroSkyshine method with the composite method for concrete shields of various mfp thicknesses using a N-16 source collimated at 40°.

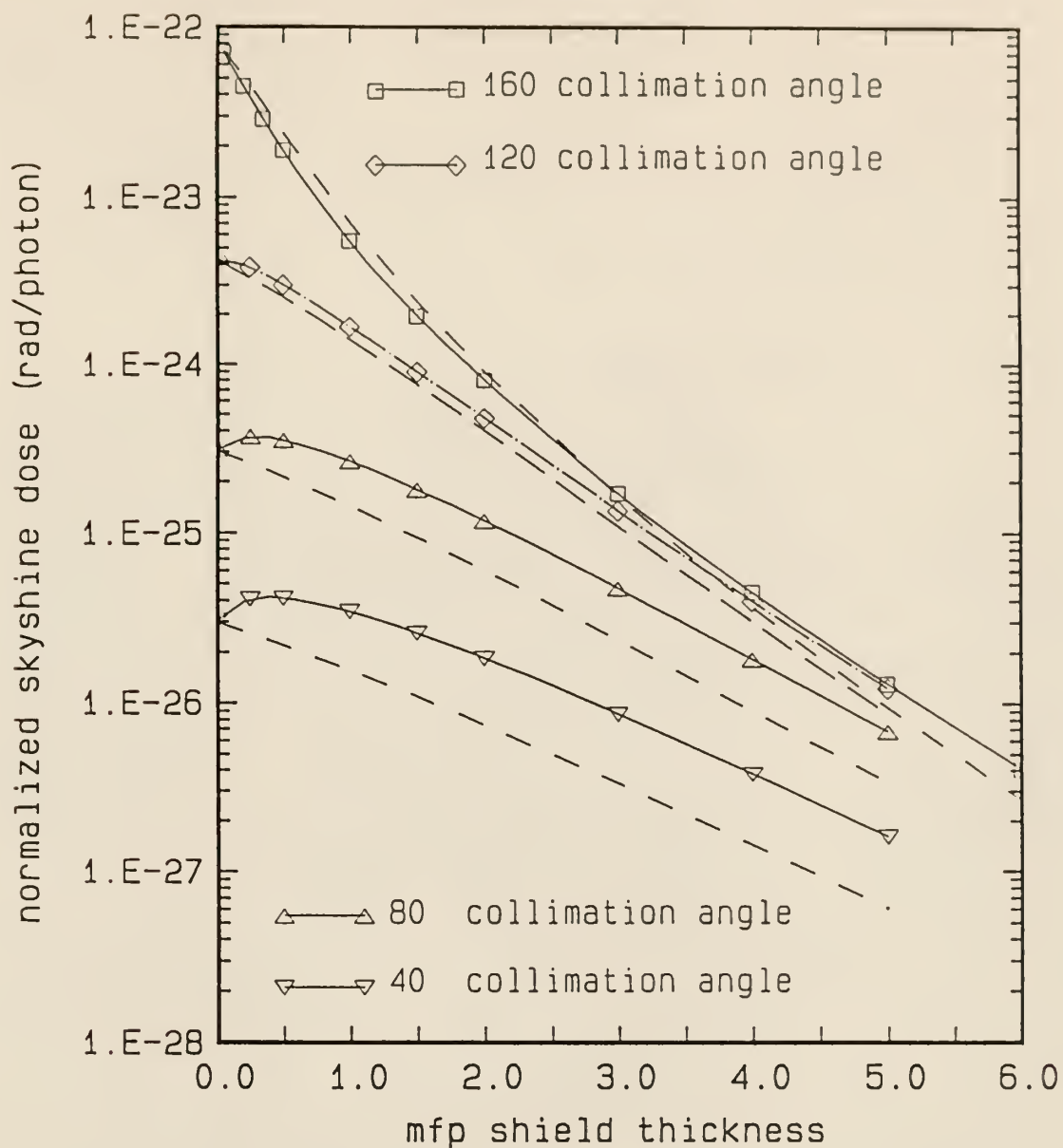


Figure 4.5. Plot of the skyshine dose rate at 1000 m for various mfp concrete shields illuminated by N-16 gamma photons. The solid line (—) is the composite method and the dashed line (---) is the MicroSkyshine method.

skyshine dose predicted by the composite method caused the major difference between the two methods, as both methods have approximately the same asymptotic slope.

The increase in the skyshine dose observed for the composite method was caused by the slab shield redistributing the photons to lower energies and into new directions of travel, effects the MicroSkyshine method ignores. In particular, photons are redistributed into lower energies with directions of travel that would bring them closer to the detector. This change in photon direction was the important mechanism leading to the increased skyshine dose, especially for small source collimation angles. The decrease in photon energies has a smaller effect; a change from 6.129 MeV to 1 MeV was shown to cause only a small change in the detector response functions [Sh87].

The MicroSkyshine method showed no similar increase in the skyshine dose as the collimation angle decreases, since this method is incapable of accounting for the redirection of photons into new directions of travel that come closer to the detector. It is possible that the MicroSkyshine method could be improved by using a semi-empirical correction to the buildup factor in the shield which depends on the source's collimation angle.

4.1.2. Results for Nitrogen-16 Shielded by Iron

To test the effect of shield material on the calculated skyshine doses, an iron test case was run for a source collimation angle of 160 degrees. Fractional difference results between the two methods are plotted in Fig. 4.6 and show the same trends as were evident in the concrete shield for a source collimation angle of 160 degrees. These trends were observed despite the fact that the calculated skyshine doses were different (see Table 4.3). The fact that the shape of the

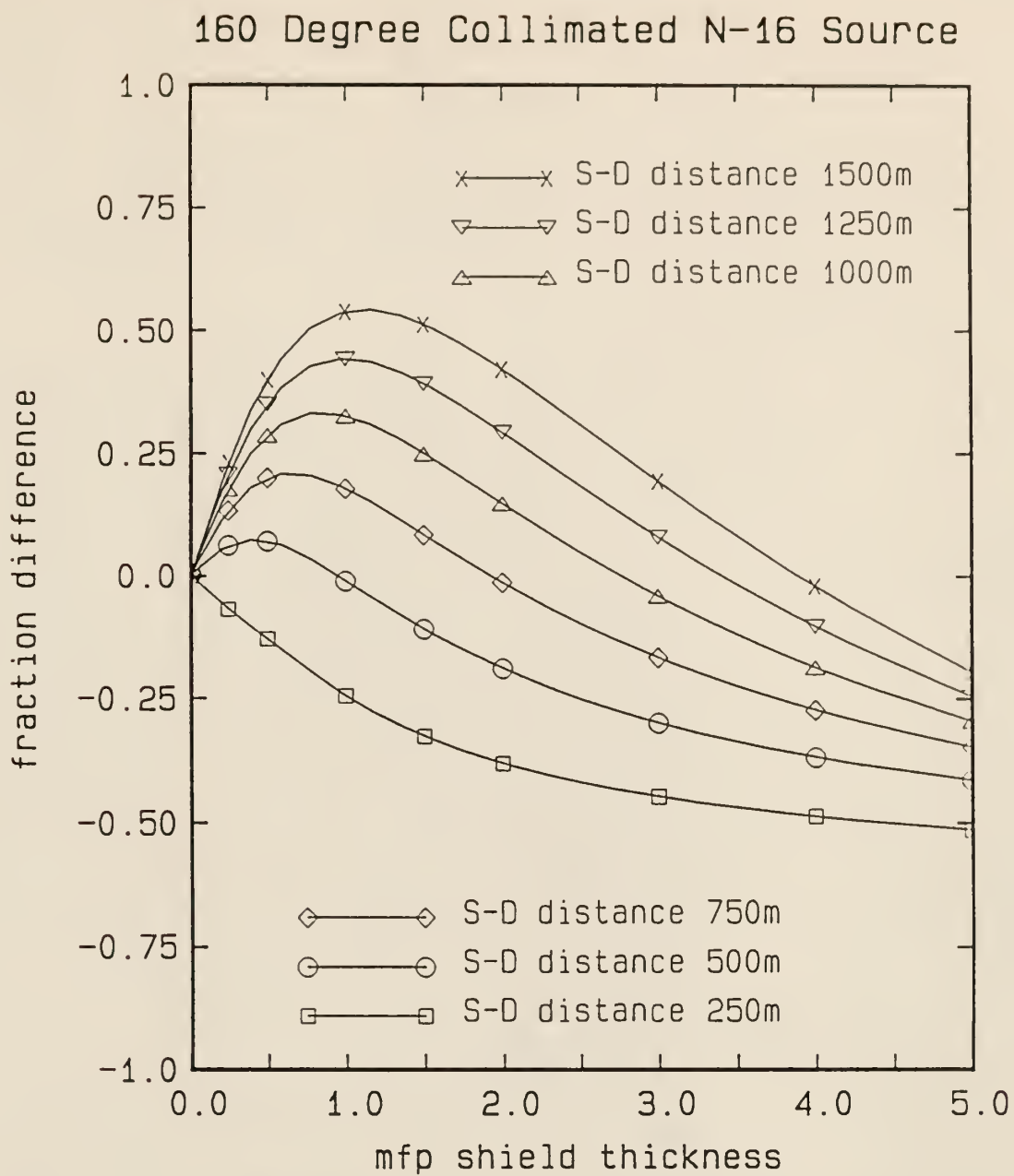


Figure 4.6. Fractional difference results comparing the MicroSkyshine method with the composite method for iron shields of various mfp thicknesses using a N-16 source collimated at 160°.

Table 4.3 Comparison of the normalized SkyShine dose caculated with the composite method for an iron and a concrete shield of 1 mfp thickness. The fraction Difference is calculated using (iron-dose - concrete-dose)/concrete-dose.

| Areal Density (g/cm ²) | Iron SkyShine Dose (rad/photon) | Concrete SkyShine Dose (rad/photon) | Fraction Difference |
|--|---------------------------------------|---|------------------------|
| 6.250 | 2.60E-20 | 3.66E-20 | -0.2896 |
| 12.500 | 1.05E-20 | 1.38E-20 | -0.2391 |
| 18.750 | 5.12E-21 | 6.40E-21 | -0.2000 |
| 25.000 | 2.74E-21 | 3.29E-21 | -0.1672 |
| 31.250 | 1.55E-21 | 1.81E-21 | -0.1436 |
| 37.500 | 9.17E-22 | 1.05E-21 | -0.1267 |
| 43.750 | 5.62E-22 | 6.32E-22 | -0.1108 |
| 50.000 | 3.54E-22 | 3.93E-22 | -0.0992 |
| 56.250 | 2.29E-22 | 2.52E-22 | -0.0913 |
| 62.500 | 1.51E-22 | 1.65E-22 | -0.0848 |
| 68.750 | 1.02E-22 | 1.10E-22 | -0.0727 |
| 75.000 | 6.96E-23 | 7.51E-23 | -0.0732 |
| 81.250 | 4.84E-23 | 5.20E-23 | -0.0692 |
| 87.500 | 3.41E-23 | 3.65E-23 | -0.0658 |
| 93.750 | 2.43E-23 | 2.60E-23 | -0.0654 |
| 100.000 | 1.76E-23 | 1.87E-23 | -0.0588 |
| 106.250 | 1.28E-23 | 1.36E-23 | -0.0588 |
| 112.500 | 9.41E-24 | 9.98E-24 | -0.0571 |
| 118.750 | 6.97E-24 | 7.39E-24 | -0.0568 |
| 125.000 | 5.20E-24 | 5.51E-24 | -0.0563 |
| 131.250 | 3.90E-24 | 4.10E-24 | -0.0488 |
| 137.500 | 3.00E-24 | 3.10E-24 | -0.0323 |
| 143.750 | 2.20E-24 | 2.40E-24 | -0.0833 |
| 150.000 | 1.70E-24 | 1.80E-24 | -0.0556 |

fraction difference curves are the same despite the different skyshine doses suggests that the fraction difference curves generated for concrete can be used for other materials.

4.2. Cobalt-60 Photon Test Cases in Concrete

The Co-60 cross sections for concrete were generated using 12 energy groups and 28 angular directions (see Tables 4.4 and 4.5). The concrete composition was the same as that used in the benchmark case (see Table 3.1). The concrete cross sections were generated with a density of 2.13 g/cm³. The cross sections generated for concrete allowed source collimation angles of 160, 120, 80, and 40 degrees.

The energy-angle distribution of photons emerging from the concrete shield was calculated for the different collimation angles and different shield thicknesses using K-SLAB. The convergence criteria used on all the runs with Co-60 photons was 5×10^{-5} . The input source for KSLAB used two energy groups to represent separately the 1.33 and 1.17 MeV photons emitted by Co-60 decay.

4.2.1 Results for Co-60 Photons and Concrete Shields

The fractional differences versus shield thickness are plotted in Fig. 4.7 and 4.8 for Co-60 calculations using 160 and 120 degree source collimation angles, respectively. From these results it is seen that increasing the source-to-detector distance increases the amount by which the MicroSkyshine method overpredicts skyshine doses. Figures 4.7 and 4.8 also show that, as shield thickness increases above 1 mfp, the amount of the overestimation or underestimation by MicroSkyshine decreases. The MicroSkyshine error for a source collimation angle of 160 degrees ranges from a 2.5 overestimation factor to an underestimation by a

Table 4.4 Energy group sturcture and anverage group energies used with the two Co-60 photons to generate the exact kernel group-to-group cross sections for iron and concrete. The generated cross sections will support source collimation angles of 160, 120, 80, and 40 degrees.

| Energy Group Range (MeV) | Average Group Energy (MeV) |
|-----------------------------|-------------------------------|
| 1.33 - 1.25 | 1.289790 |
| 1.25 - 1.00 | 1.122683 |
| 1.00 - 0.90 | 0.949576 |
| 0.90 - 0.80 | 0.849537 |
| 0.80 - 0.72 | 0.759677 |
| 0.72 - 0.63 | 0.674551 |
| 0.63 - 0.54 | 0.584498 |
| 0.54 - 0.45 | 0.494427 |
| 0.45 - 0.36 | 0.404329 |
| 0.36 - 0.27 | 0.314181 |
| 0.27 - 0.18 | 0.223901 |
| 0.18 - 0.09 | 0.132712 |

Table 4.5 Angular direction cosines and Gaussian weights used to generate the exact kernel group-to-group cross sections for the Co-60 photon energies of 1.33 and 1.17 Mev in concrete. The direction cosines and Gaussian weights will allow angular source collimation angles of 160, 120, 80, and 40 degrees.

| Angular Direction Cosines | Angular Weights |
|---------------------------|-----------------|
| 0.9932032580 | 0.01675204978 |
| 0.9698463105 | 0.02680327964 |
| 0.9464893630 | 0.01675204978 |
| 0.9201221820 | 0.04823560492 |
| 0.8528685320 | 0.07717696787 |
| 0.7856148820 | 0.04823560492 |
| 0.7360607943 | 0.07390123423 |
| 0.6330222215 | 0.1182419748 |
| 0.5299836517 | 0.07390123423 |
| 0.4632196062 | 0.09065328401 |
| 0.3368240889 | 0.1450452544 |
| 0.2104285716 | 0.09065328401 |
| 0.1369519990 | 0.08682408885 |
| 0.0366961778 | 0.08682408885 |

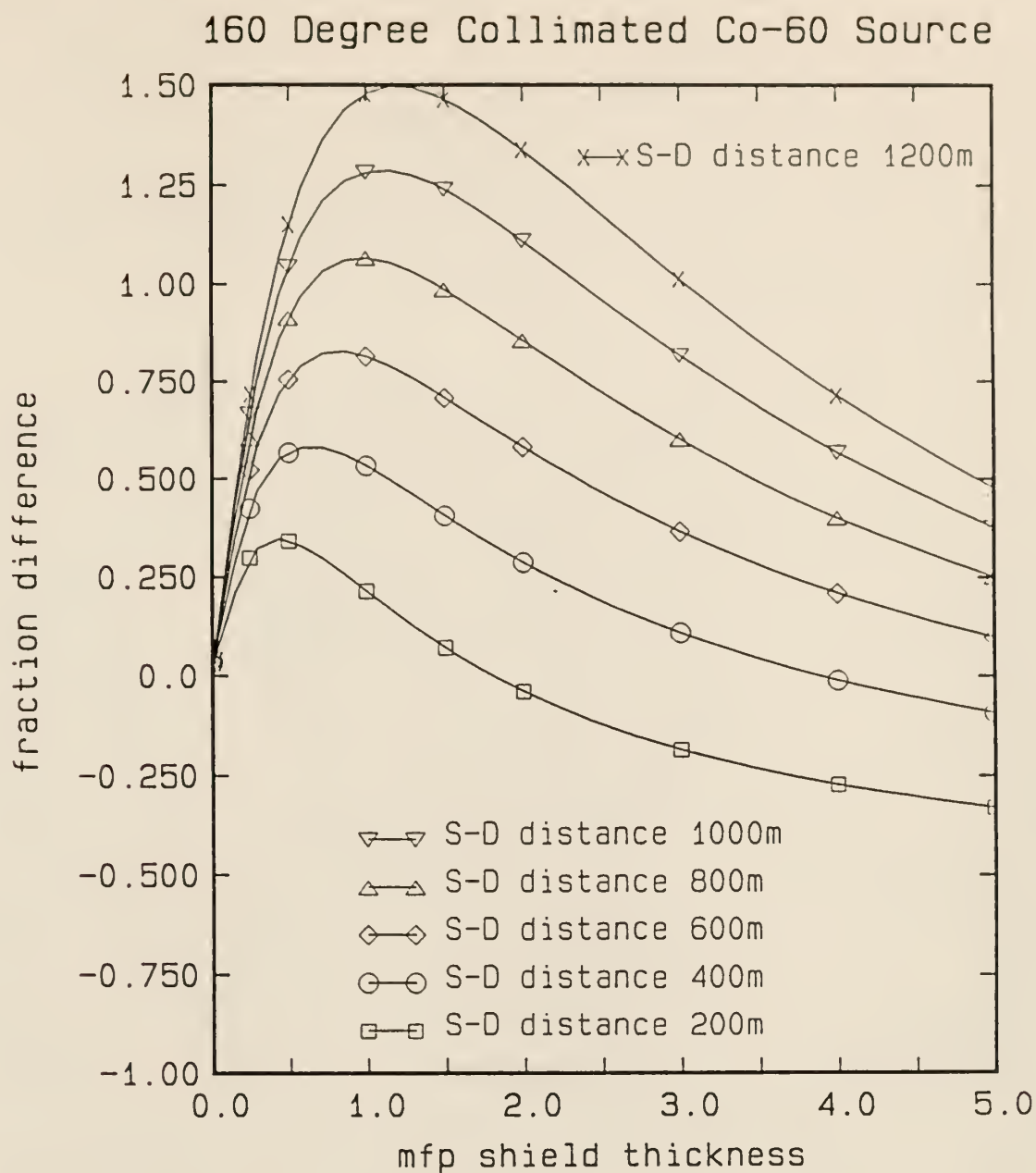


Figure 4.7. Fractional difference results comparing the MicroSkyshine method with the composite method for concrete shields of various mfp thicknesses using a Co-60 point source collimated at 160°.

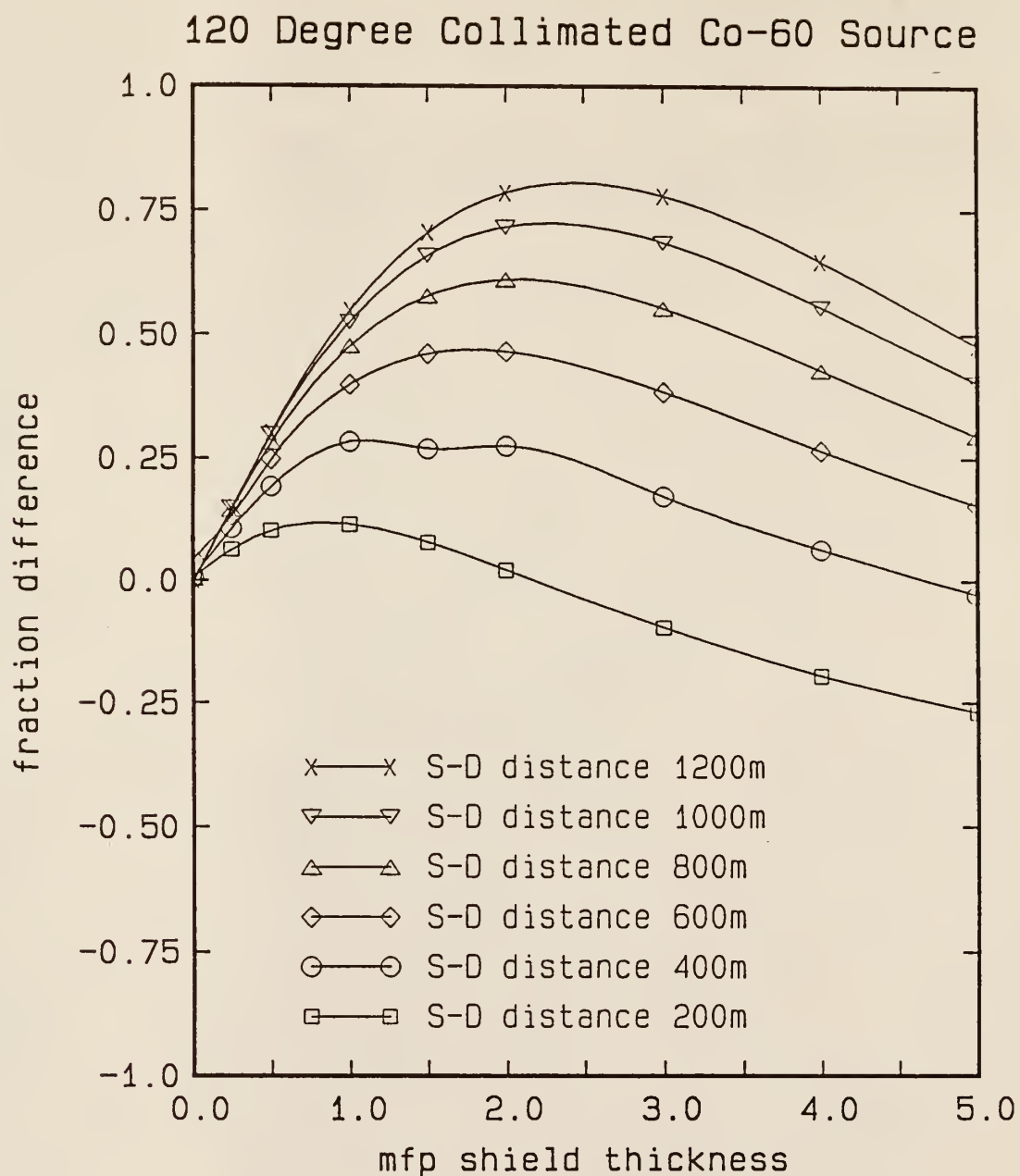


Figure 4.8. Fractional difference results comparing the MicroSkyshine method with the composite method for concrete shields of various mfp thicknesses using a Co-60 point source collimated at 120°.

factor of 1.5 times. The fraction error for the 120 degree source collimation angle ranges from an overestimation by 1.8 times to an underestimation by 1.4 times.

The fractional differences for the 80 degree source collimation angle are shown in Fig. 4.9. This figure indicates that the MicroSkyshine method results and the composite method results agree reasonably well with each other (within 25%) at all source-to-detector distances and at all mfp shield thicknesses.

The fractional differences for a 40 degree source collimation angle are shown in Fig. 4.10 and it is seen that the MicroSkyshine results are within a factor of 2 for all source-to-detector distances and for all the shield thicknesses investigated. In general, as the source-to-detector distance increases, the amount by which the MicroSkyshine method underpredicts increases. The worst agreement between the MicroSkyshine method and the composite method at the 40 degree source collimation angle occurs at source-to-detector distance of 1200 m and the agreement was no worse than a 1.8 factor underestimation.

The 40 and 80 degree source collimation angle cases show an increase in the skyshine dose as the mfp shield thickness increased. The detector response at 600 m for all four source collimations is shown in Fig. 4.11. The increase in the skyshine dose as the shield thickness increases is much less pronounced for the Co-60 photons than for the N-16 photons. The smaller increase in the skyshine dose indicates that significant preferential attenuation of the low energy photons that emerge from the shield is occurring before the photons reach the detector.

The MicroSkyshine doses for source collimation angles of 160 and 120 degrees decrease more slowly than the composite method results as the source-to-detector distance is increased. The slower decrease in the skyshine dose for the 160 and 120 degree source collimation angles is caused by the MicroSkyshine method using the

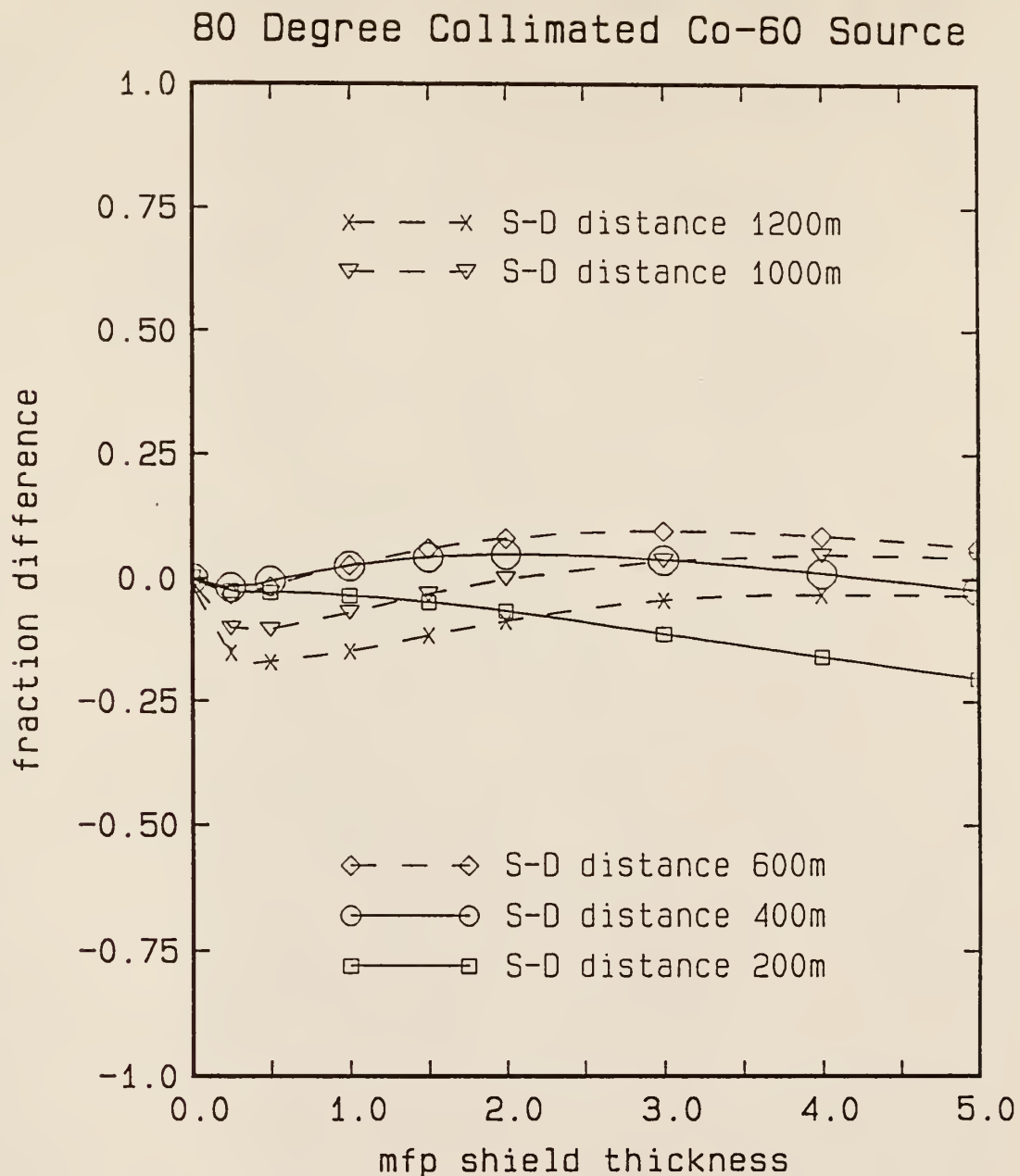


Figure 4.9.

Fractional differences between MicroSkyshine and the composite method results for concrete shields of various mfp thicknesses using a Co-60 point source collimated at 80°.

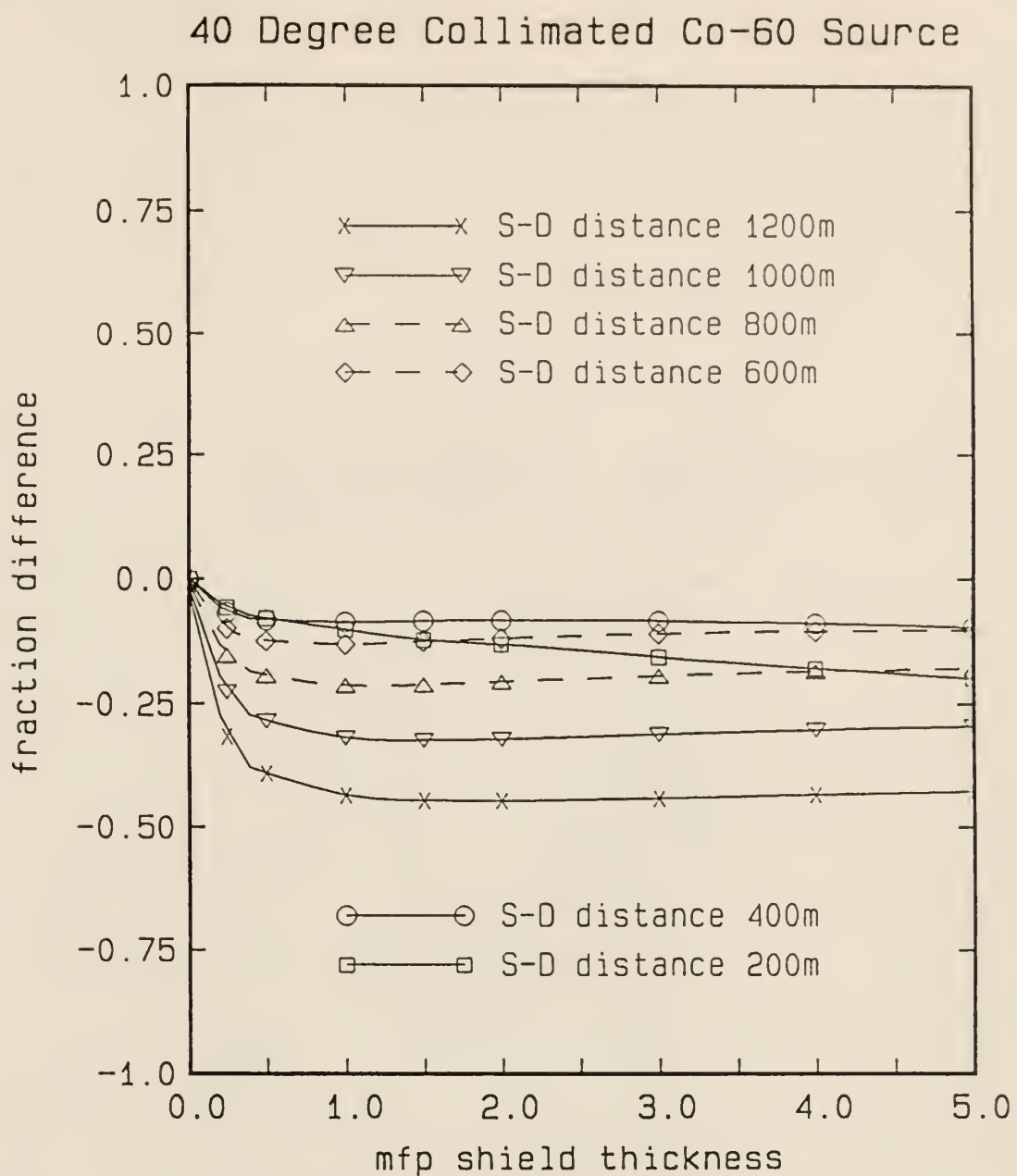


Figure 4.10. Fractional differences between MicroSkyshine composite method results for concrete shields of various mfp thicknesses using a point Co-60 source collimated at 40°.

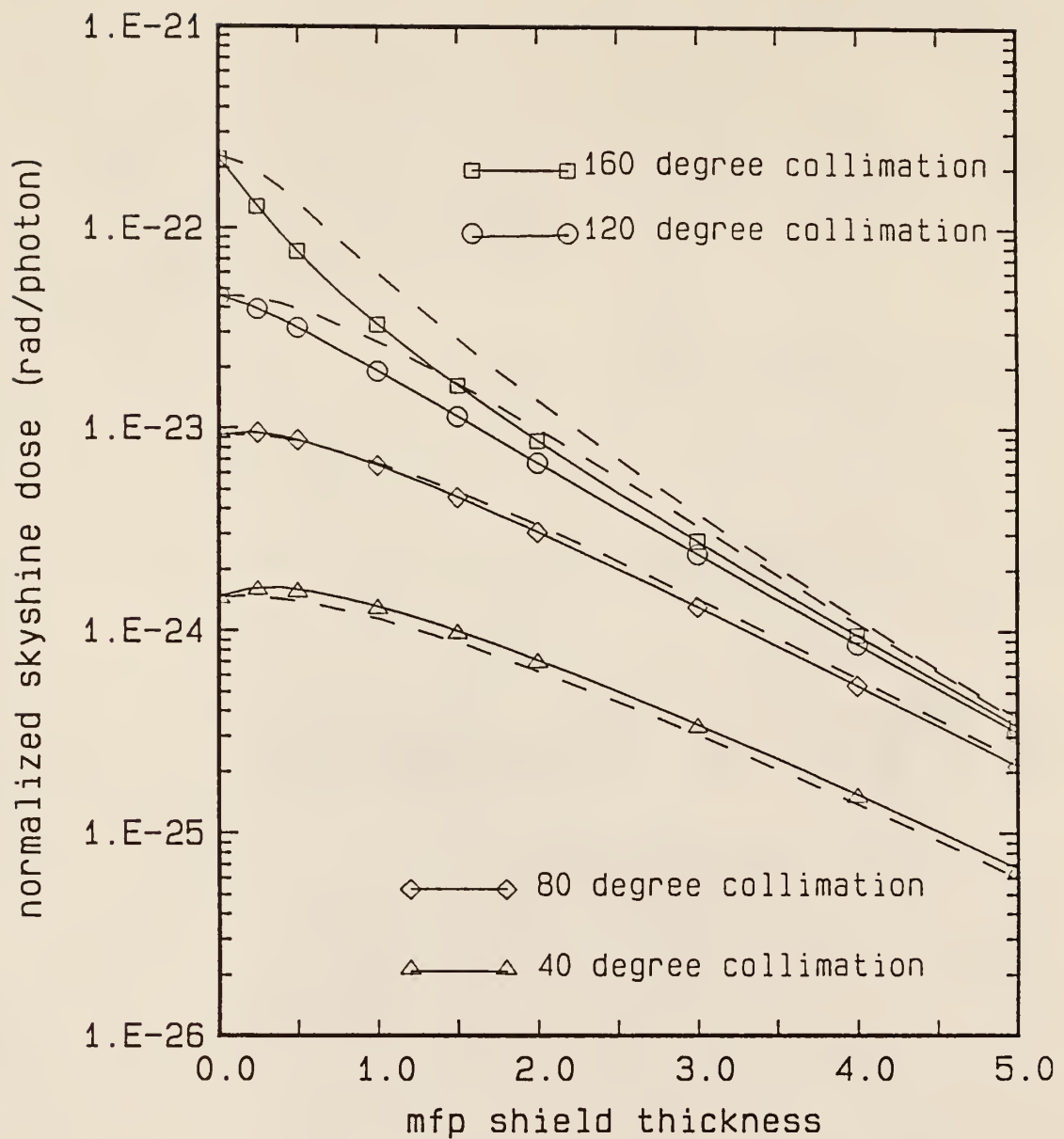


Figure 4.11. Plot of the skyshine dose rate at 600 m for various concrete shield thicknesses illuminated by Co-60 gamma photons. The solid line (—) is the composite method and the dashed line (---) is the MicroSkyshine method.

original energy of the photons in the buildup factor approach instead of the correct lower energy as is used in the composite method. The less pronounced increase in the skyshine doses is caused by the change in the energy spectrum of the photons. Faw and Shultis showed [Sh87] that below 1 MeV, the response functions became dependent upon the photons energy especially at the longer source-to-detector distances.

4.3. 0.5 MeV Photon Test Cases in Concrete

Cross sections generated for 0.5 MeV photons used 9 energy groups and 20 angular groups. The energy and angular group structures used are shown in Tables 4.6 and 4.7. The material composition of the concrete remained the same as that used for the Benchmark Co-60 calculations (see Table 3.1). The 0.5 MeV cross sections were generated for a concrete density of 2.13 g/cm³. The 0.5 MeV cross sections were generated for source collimation angles of 160, 120, 80, and 40 degrees.

The 0.5 MeV cases were calculated by MicroSkyshine and the composite method for shield thicknesses between 0.01 mfp and 5 mfp. The KSLAB criterion used for ending the iteration scheme in the transport equation was 1×10^{-4} fractional difference between the old angular fluxes and the new angular flux values.

4.3.1 Results for 0.5 MeV Photons in Concrete

The 0.5 MeV fractional differences between the MicroSkyshine and the composite method results are shown in Figs. 4.12 and 4.13 for source collimation angles of 160 and 120 degrees, respectively. These figures show that the amount by which MicroSkyshine overestimates increases with increasing source-to-detector

Table 4.6. Energy group structure and average group energies used with the 0.5 MeV photons to generate the exact kernel group-to-group cross sections for iron and concrete. The generated cross sections will support source collimation angles of 160, 120, 80, and 40 degrees.

| Energy Group Range (MeV) | Average Group Energy (MeV) |
|-----------------------------|-------------------------------|
| 0.50 - 0.45 | 0.4748176 |
| 0.45 - 0.40 | 0.4248010 |
| 0.40 - 0.35 | 0.3747805 |
| 0.35 - 0.30 | 0.3247541 |
| 0.30 - 0.25 | 0.2747182 |
| 0.25 - 0.20 | 0.2246636 |
| 0.20 - 0.15 | 0.1745596 |
| 0.15 - 0.10 | 0.1242421 |
| 0.10 - 0.05 | 0.0719813 |

Table 4.7. Angular direction cosines and Gaussian weights used to generate the exact kernel group-to-group cross sections for the 0.5 MeV photons in concrete. The direction cosines and Gaussian weights will allow angular source collimation angles of 160, 120, 80, and 40 degrees.

| Angular Direction Cosines | Angular Weights |
|---------------------------|-----------------|
| 0.987255551 | 0.030153690 |
| 0.952437070 | 0.030153690 |
| 0.902997311 | 0.086824089 |
| 0.802739753 | 0.086824089 |
| 0.709823967 | 0.133022222 |
| 0.556220476 | 0.133022222 |
| 0.431035377 | 0.163175911 |
| 0.242612801 | 0.163175911 |
| 0.136952868 | 0.086824089 |
| 0.036695310 | 0.086824089 |

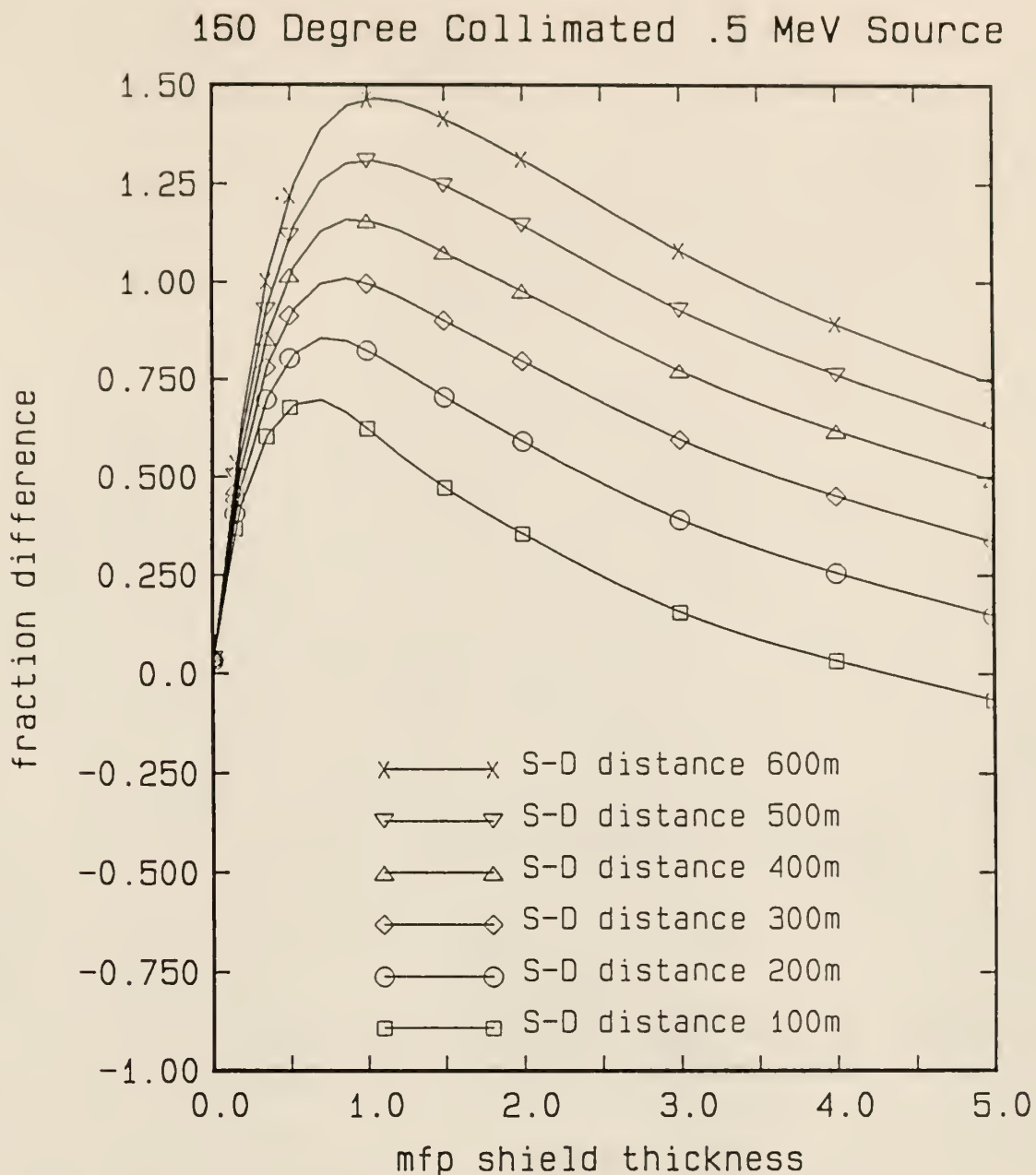


Figure 4.12. Fractional differences between MicroSkyshine and the composite method results for concrete shields of various thicknesses using a point .5 MeV source collimated at 160°.

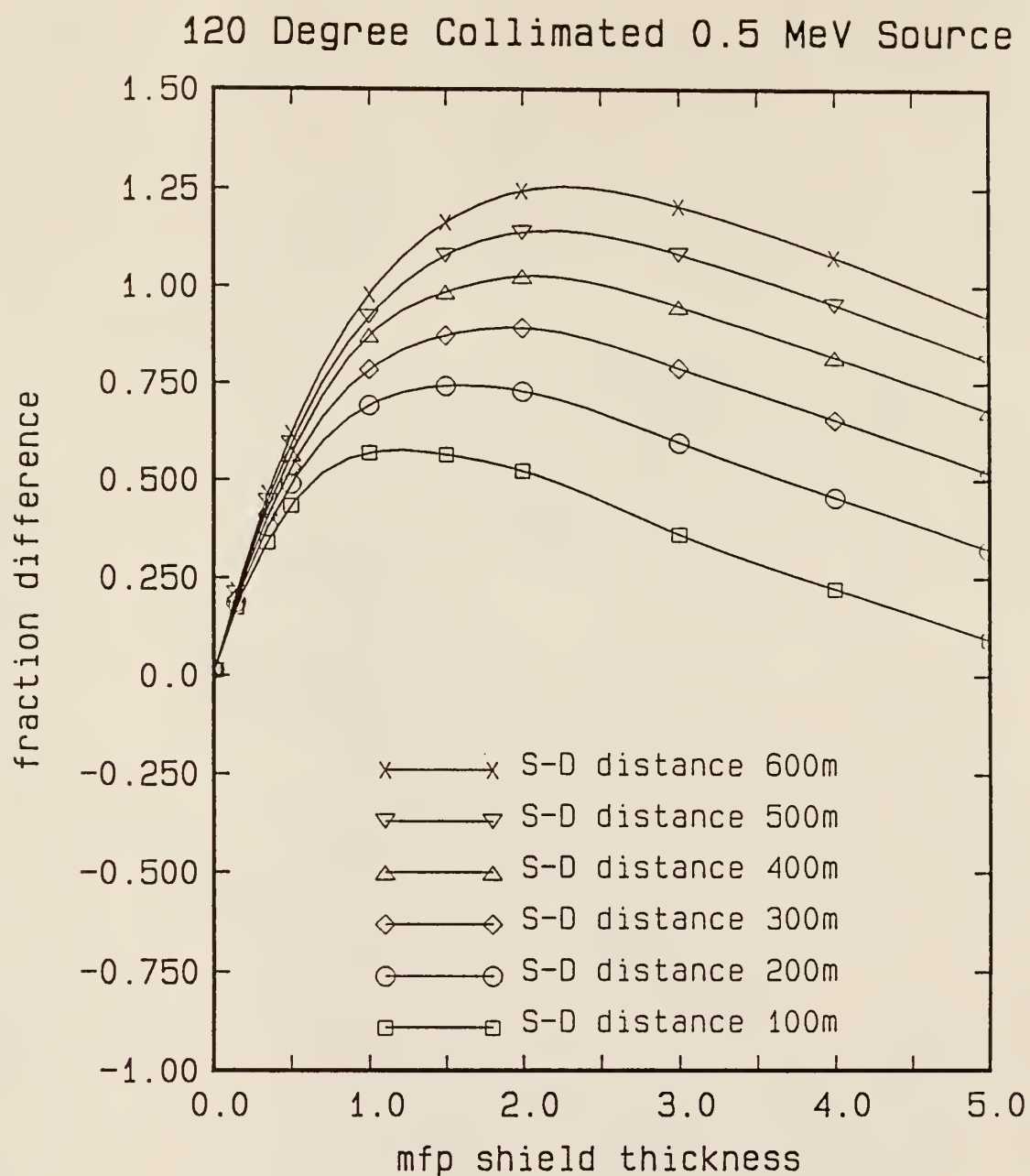


Figure 4.13. Fractional difference results comparing the MicroSkyshine method with the composite method for concrete shields of various mfp thicknesses using a .5 MeV source collimated at 120°.

distance. The effect of the shield thickness is more complicated; the fractional difference goes through a local maximum and then decreases with increasing shield thickness. The MicroSkyshine method's maximum overestimation is 2.46 times the composite doses for 160-degree source collimation and is 2.25 times greater for 120-degree collimation.

The fractional differences for 80 and 40 degree source collimation angles are shown in Figs. 4.14 and 4.15, respectively. Fractional difference plots for 80 and 40 degree collimation show that increasing the source-to-detector distance increases the amount by which the MicroSkyshine method will overestimate the detector response. In the 80 degree collimation case, the increase in shield thickness initially causes the fractional difference to increase until, at various distances depending on the source-to-detector distance, the fractional difference slowly begins to decrease. In the 40 degree collimation case, the fractional difference increases with increasing source-to-detector distance. The MicroSkyshine method's maximum overestimation for 80 degree collimation is 1.9 times the composite result, and, for the 40 degree collimation, the maximum overestimation was 1.7 times the composite method result.

Plotting the shield thickness against the detector response at 300m results in Fig. 4.16. For the composite method, the increase in the skyshine dose with increasing shield thicknesses has virtually disappeared. The MicroSkyshine calculated doses for all source collimation angles now show an increase with increasing shield thicknesses for thin shields. The MicroSkyshine method overpredicts the skyshine dose because the buildup factor approach with the original source energy does not take into account the large energy variation in the response functions for low-energy photons.

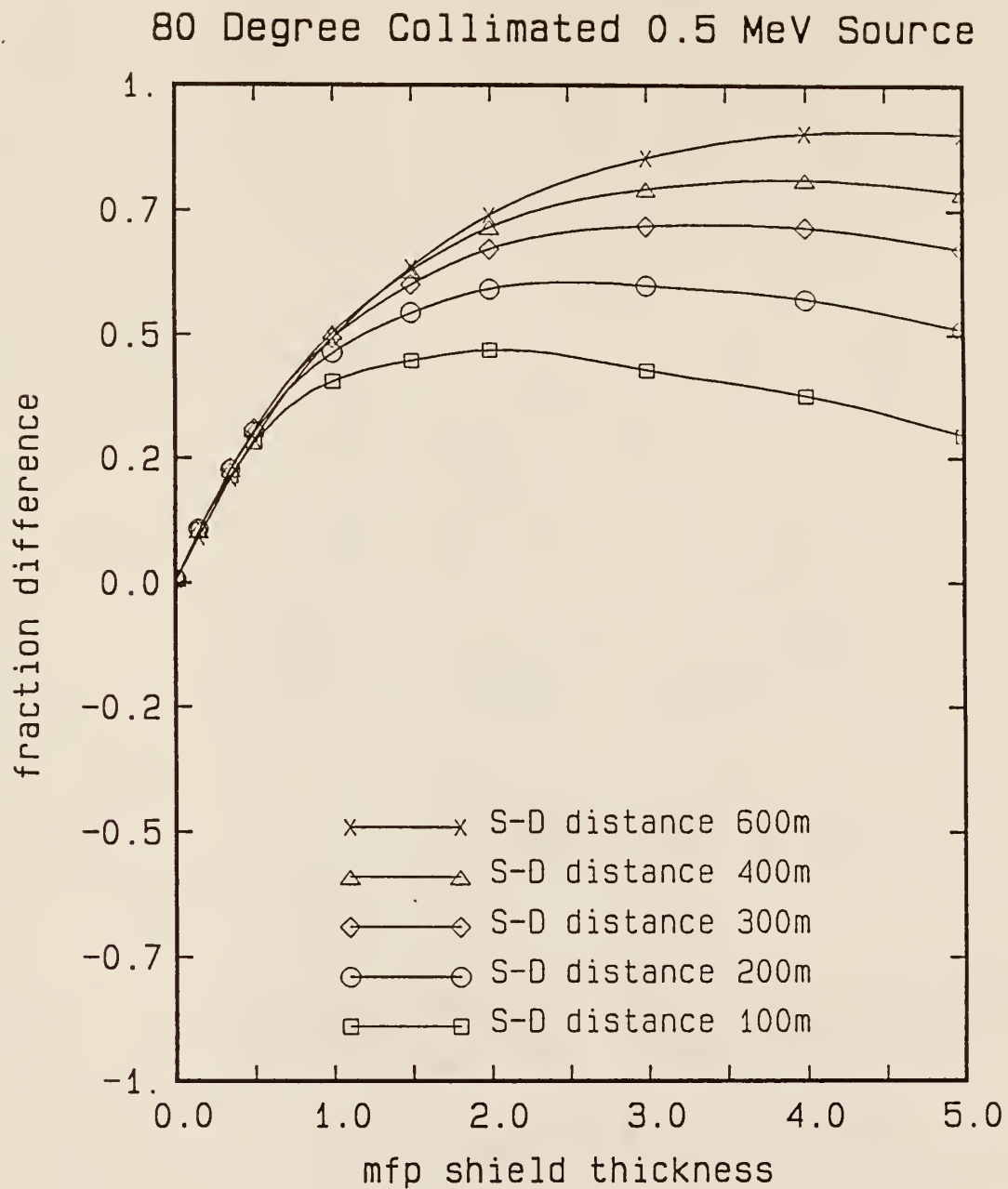


Figure 4.14. Fractional differences between MicroSkyshine and the composite method results for concrete shields of various mfp thicknesses using a point .5 MeV source collimated at 80°.

40 Degree Collimated 0.5 MeV Source

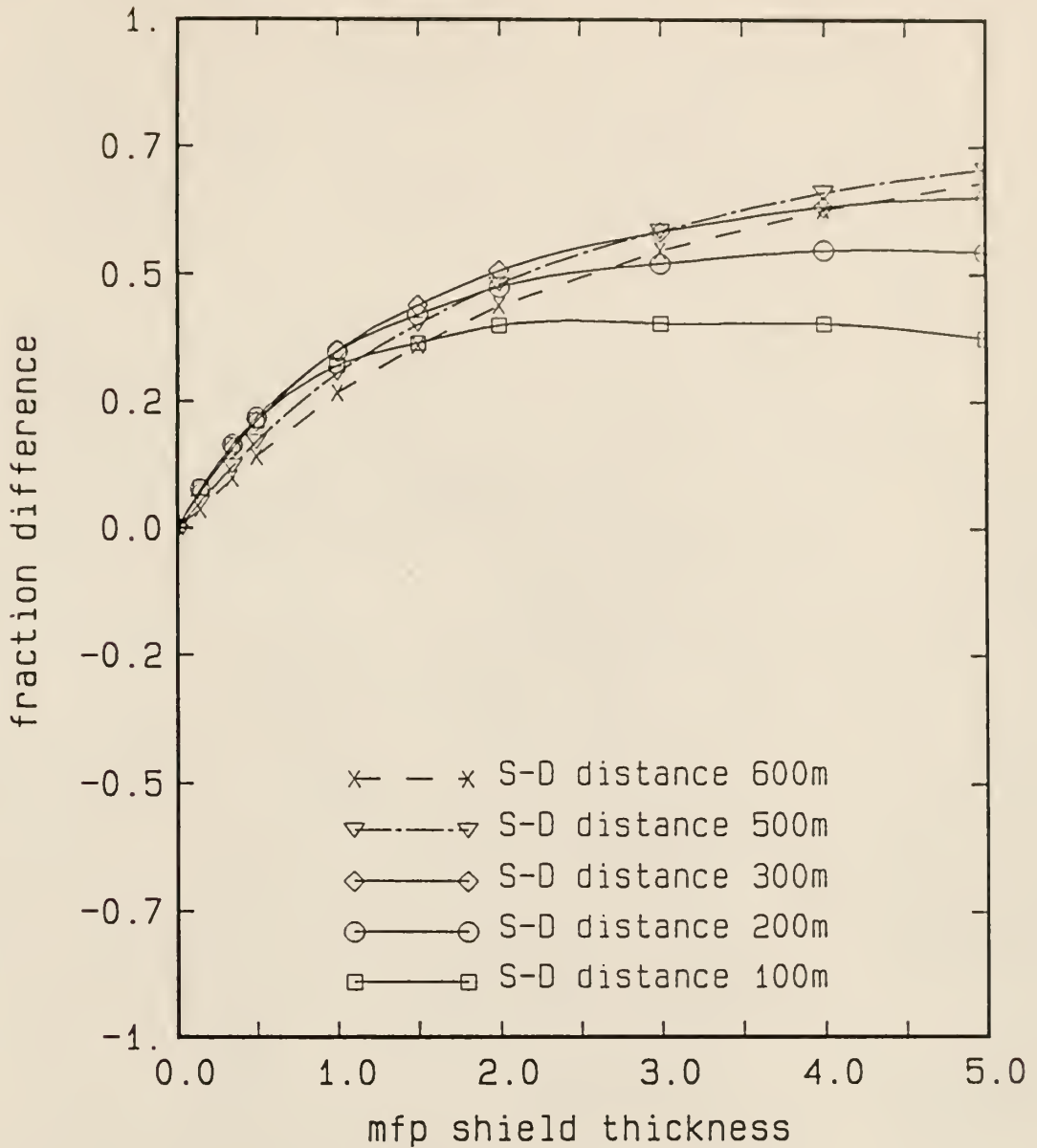


Figure 4.15. Fractional differences between MicroSkyshine and the composite method results for concrete shields of various mfp thicknesses using a point .5 MeV source collimated at 40°.

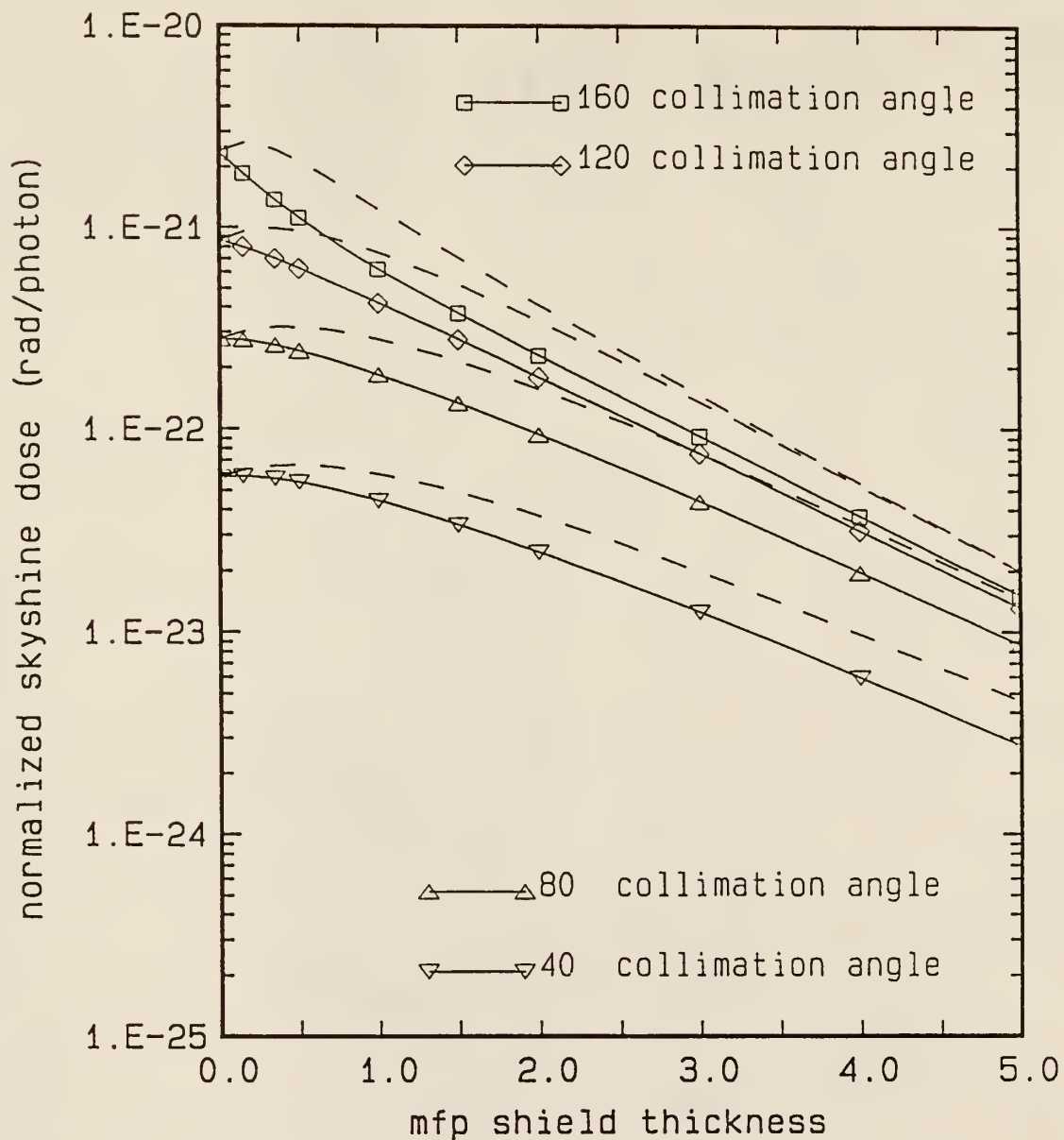


Figure 4.16. Plot of the skyshine doses at 300 m for various thicknesses of concrete shields illuminated by .5 MeV gamma photons. The solid line (—) is for the composite method and the dashed line (--) is for the MicroSkyshine method.

4.4. Composite Skyshine Results.

The composite method results display two interesting characteristics. The first feature of interest is the energy dependence of the skyshine dose in the composite method. The second result of interest for the calculated skyshine dose is the variation shown by the dose for different shield thicknesses at different source collimation angles.

The primary result observed from examining the skyshine dose's variation with energy is that the energy dependence of the skyshine dose is different for two ranges of source-to-detector distance. The first range is for small source-to-detector distances less than 250 to 300 m. In this range, the skyshine dose is relatively insensitive to the energy of the primary photon (see Fig. 4.17) for all the different shield thicknesses examined for both concrete and iron shields.

The second range is for source-to-detector distances greater than 250 to 300 m. In this range, the skyshine dose becomes dependent on the initial photon energy. A sample case (see Fig. 4.17), chosen as representative, shows that the skyshine dose for the far range increases with increasing source photon energy.

The second feature of interest observed with the composite method is how the skyshine dose varies with different shield thicknesses. Figures 4.18, 4.19, and 4.20 are representative of the variation in the skyshine dose for the N-16 source, the Co-60 source, and the 0.5 MeV source, respectively. The three different sources show the same basic trends in their response to different shield thicknesses and different source collimation angles. The skyshine dose, in all cases, decreases below that for the unshielded case when the shield thickness is greater than 1 mfp. When the shield is less than 1 mfp thick, the skyshine dose can increase with

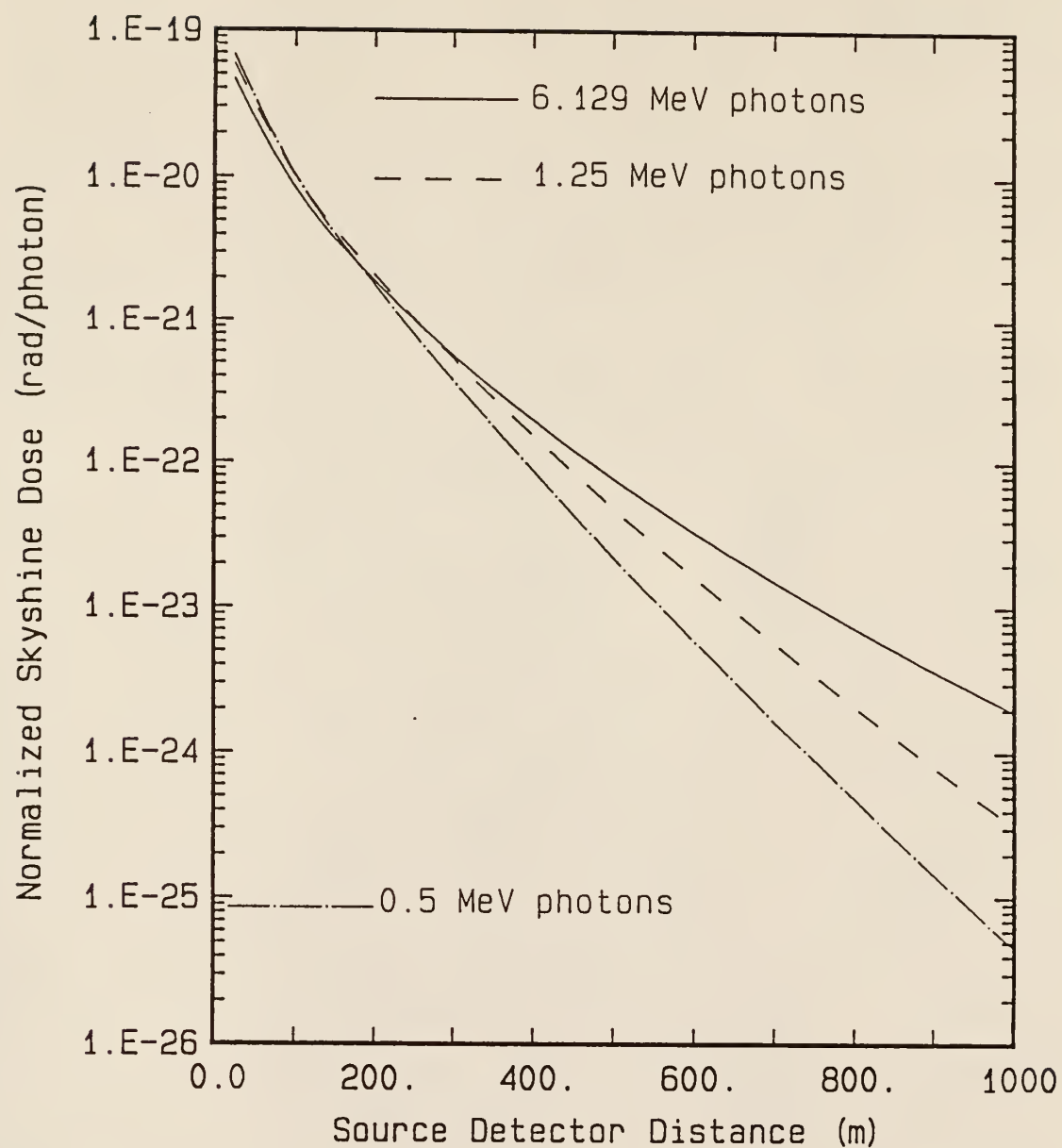


Figure 4.17. Example plot showing the source-energy dependence of the composite skyshine dose with source-to-detector distance for the sources collimated at 160° and covered by a 1.5 mfp shield (with respect to each of the source energies).

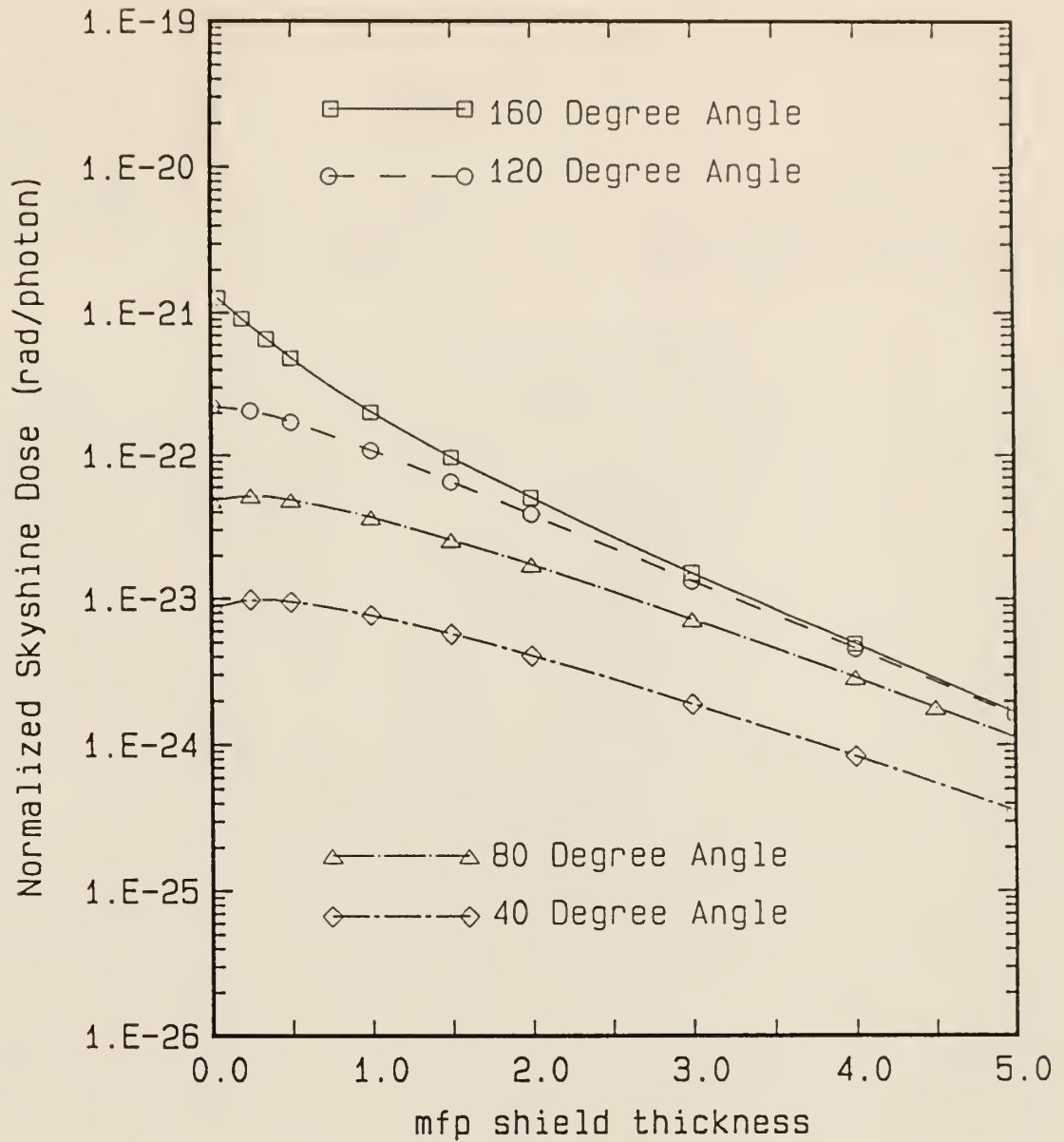


Figure 4.18. Example plot showing the variation of the composite skyshine dose with various degrees of source collimation for a N-16 point source at a source-to-detector distance of 475 m.

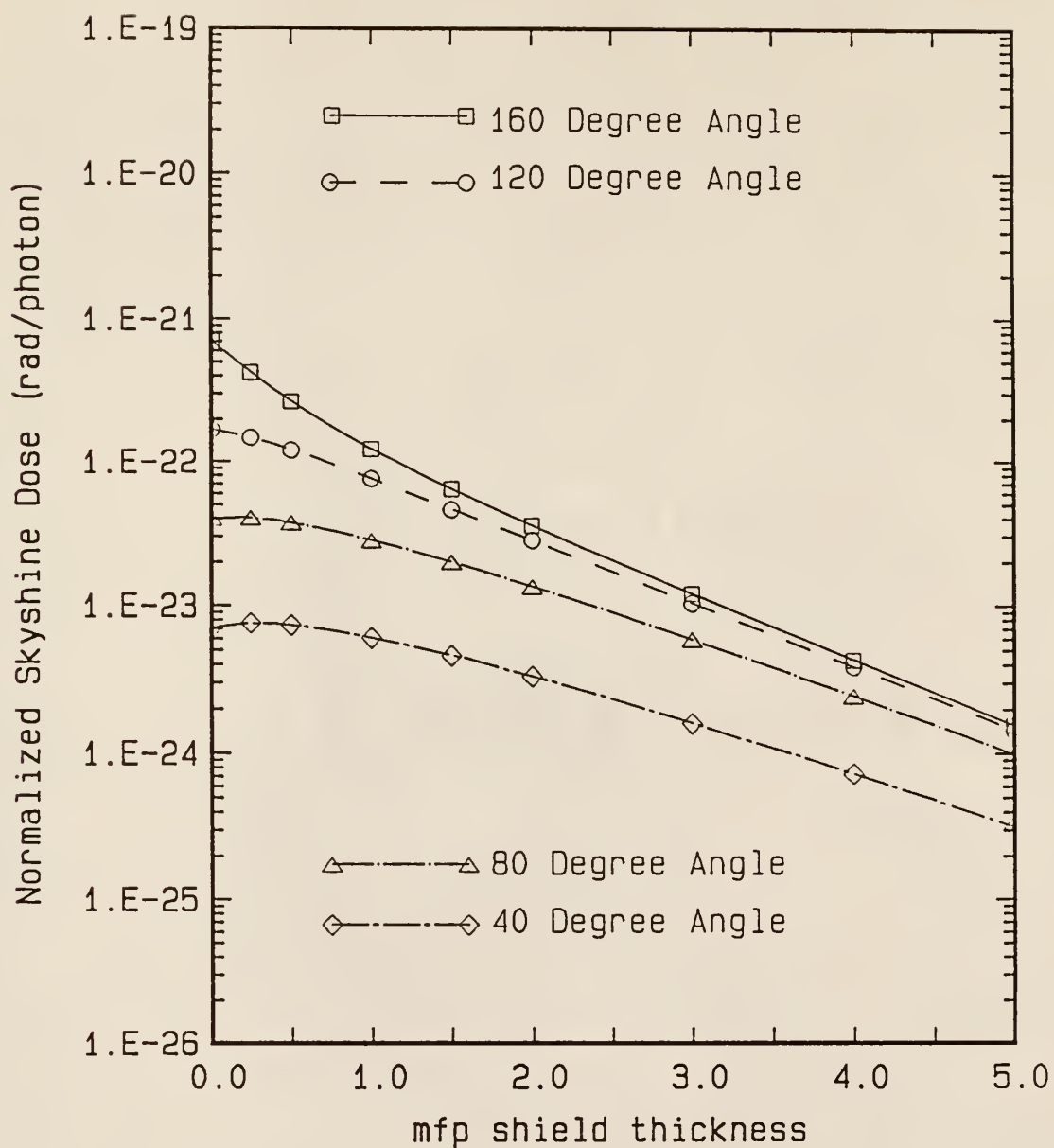


Figure 4.19. Example plot showing the variation of the skyshine dose with various source collimation angles in the Co-60 source with a source-to-detector distance of 475 m.

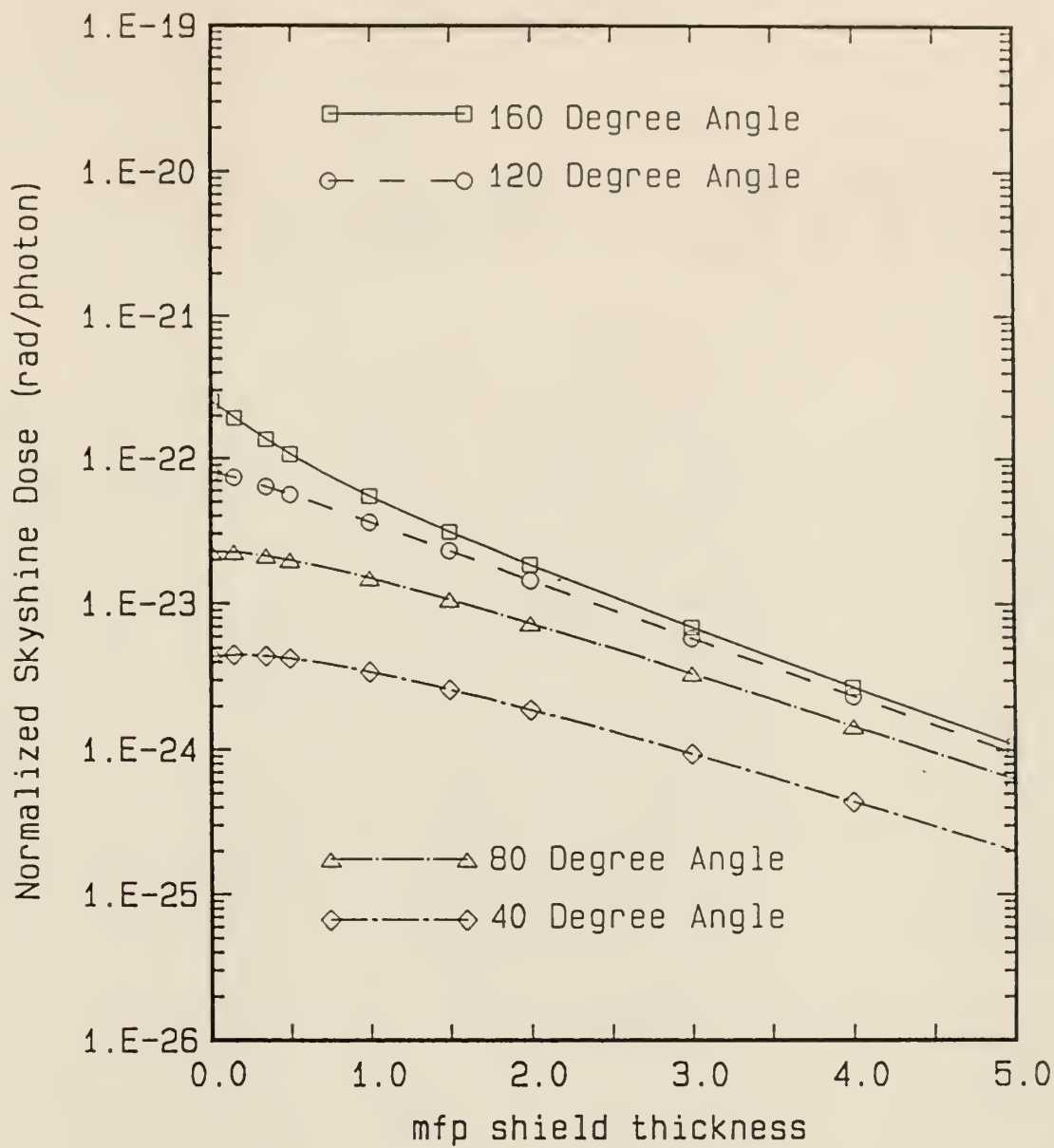


Figure 4.20. Example plot showing the variation of the composite skyshine dose with various source collimation angles for the .5 MeV source with a source-to-detector distance of 475 m.

increasing shield thickness. The skyshine dose was found to increase for all cases when the source collimation angle is 80 or 40 degrees. By contrast the skyshine dose was found to decrease with increasing shield thickness for the 120 and 160 degree source collimation angles.

5 CONCLUSIONS

In this study, an approximate method has been studied for calculating the skyshine dose caused by a point gamma-photon source inside a shielded silo. The approximate method, known as the composite method, uses a one-dimensional, discrete-ordinates transport equation to estimate the angular source leaving the top of the cylindrical shielding slab. The angular source is then used with beam response functions from MicroSkyshine [Sh87] to calculate the skyshine dose at the desired points of interest.

The objectives in developing the composite method were to achieve better accuracy than was achieved using a conventional exponential attenuation buildup factor approach to overhead shielded sources and to explore the accuracy of the conventional technique for different energy photons, different shield thicknesses, and different source collimation angles.

The composite method was capable of very accurately estimating the skyshine dose measured in the K-State benchmark experiment. The only regions where caution may be needed is for source-to-detector mass thicknesses less than 8 g/cm² and greater than 100 g/cm². Near the silo, photons scattering inside the silo are of importance causing the composite method, which neglects in-silo scattered photons, to underpredict the skyshine dose. At far distances from the silo, the composite method's slope was slightly more negative value than was the DOT method's slope. Thus, for far distances the composite method could underestimate the actual skyshine dose.

The complexity of the composite method and its limited ability to deal with geometries other than a source on the axis of a silo will limit its usefulness in many

practical applications. The composite method, unlike the MicroSkyshine method, requires considerable computer resources for generating the photon group-to-group cross sections and then for solving the one-dimensional transport equation. The calculation of the skyshine dose, once the angular source is known, is fairly easy and can be done using a microcomputer.

The second objective of this study, namely, the evaluation of MicroSkyshine's method of approximating a shield, yielded complex results and two interesting observations. When the source is shielded by 1 mfp or thicker shield, MicroSkyshine can underestimate the skyshine dose. The underestimation was largest for the 6.129 MeV gamma source with the source collimated tightly at 40 degrees. In general, the smaller the source collimation angle the more likely it is for MicroSkyshine to underestimate the skyshine dose. On the other hand, when gamma ray energies are lower and the source collimation angles wider, the buildup-factor method used in MicroSkyshine overpredicts the skyshine dose.

The actual amount by which the buildup factor method in MicroSkyshine overestimates or underestimates the skyshine dose is dependent upon the photon energy, the source detector distance, and the source's angle of collimation. The maximum underprediction observed with the MicroSkyshine method was a factor of 5.5 times lower than the composite method result at a source-to-detector distance of 1500m for a N-16 source collimated at 40 degrees. The maximum overprediction observed with the MicroSkyshine method was a factor of 2.5 times higher than the composite method result at a source-to-detector distance of 600m for the 0.5 MeV source collimated at 160 degrees.

The primary photons of interest when calculating practical skyshine doses are the high energy N-16 photons. The results of this study for N-16 photons

show that, for broadly collimated sources and source detector distances greater than 200 m, the MicroSkyshine method is within a factor of 2 for shield thicknesses up to 6 mfps.

Two interesting observations were made during the course of this study. First, the skyshine dose near the source can increase with increasing shield thickness for some source collimation angles. Second, the skyshine dose is relatively insensitive to the energy of the source photons for source-to-detector distances less than 300m.

The skyshine dose, for all photon energies investigated, increases with shield thicknesses up to approximately 1 mfp for the 80 and 40 degree source-collimation angles. The overhead shield increases the skyshine dose by redirecting photons into directions toward to the detector. In the narrower collimation cases no uncollided photons are heading in these directions and, as a result, the shield-scattered photons increase the skyshine dose. The increase in the skyshine dose with increasing shield thickness is more noticeable for N-16 photons than it is for Co-60 and 0.5 MeV photons.

The composite method results showed that, for source-to-detector distances less than 250 m to 300 m, the skyshine dose is relatively insensitive to the primary photon energy. The range for which the primary photon energy becomes important is dependent upon the shield thickness and the source collimation angle. When the distance is greater than 250 m to 300 m the skyshine dose becomes very dependent upon the initial photon energy. At a source-to-detector distance of 1000m the skyshine dose varies by an order of magnitude between each of the three source photons studied.

5.1 Suggestions For Further Study

The most interesting area for further research is the correction of the MicroSkyshine method for the shielded source cases. The MicroSkyshine method could be corrected by calculating empirical correction factors for different energies, collimation angles, and shield thicknesses using the composite method results and the MicroSkyshine results. The correction of the MicroSkyshine calculations, by such empirical factors, would apply rigorously only for the cylindrical silo case since the present composite method is limited to this relatively simple geometry.

Another recommendation for further study is to extend the composite method to different geometries. This extension will require the calculation of the total emergent angular current from the source shield. Symmetry about the source axis would still be required for the use of a one-dimensional, azimuthally-symmetric transport code when calculating the effective skyshine point source on the top of a slab shield. For more general geometry, multi-dimensional, azimuthally-dependent transport codes would be required to calculate the energy-direction distribution of photons escaping from the source shield.

Finally, the number of lower energy groups in the MicroSkyshine response function set should be expanded, if composite techniques are to be applied to problems involving low energy photon sources. As Faw and Shultis [Sh87] showed, the normalized skyshine dose varied the most rapidly in the lower energy ranges (energies below 1 MeV.). These energies were shown to be of importance in this study especially for small source-to-detector distances. An increased number of lower energy groups may reduce the errors observed at the small source-to-detector distances in this study.

6. ACKNOWLEDGEMENTS

The author wishes to thank J. K. Shultis for his guidance and suggestions during the course of this research and report preparation. The financial support given by INPO and the KSU Nuclear Engineering Department is also deeply appreciated. Additionally, this author is thankful for the support and assistance given by the Nuclear Engineering graduate students. Lastly, the author wishes to express his deepest appreciation to his family for their support and understanding during my college education.

BIBLIOGRAPHY

- An87 ANSI/ANS-6.6.1-1987, "American National Standard for Calculation and Measurement of Direct and Scattered Gamma Radiation from LWR Nuclear Power Plants," American Nuclear Society, La Grange Park, Illinois, 1987.
- Bi72 Biggs, F. and R. Lighthill, "Analytical Approximations for Total and Energy Absorption Cross Sections for Photon-Atom Scattering," SC-RR-720685, Sandia Laboratories (Dec. 1972).
- Bg68 Biggs, F. and R. Lighthill, "Analytical Approximation for Total Pair Production Cross Sections," SC-RR-710507, Sandia Laboratories (Sep. 1971).
- Bg72 Biggs, F. and R. Lighthill, "Analytical Approximation for Photon Differential Scattering Cross Sections Including Electron Binding Effects," SC-RR-720659, Sandia Laboratories, (Oct. 1972).
- Ch84 Chilton, A. B., J. K. Shultis, and R. E. Faw, *Principles of Radiation Shielding*, Prentice-Hall, Inc., Englewood Cliffs, NJ., 1984.
- Cl78 Clifford, C. E., W. Y. Yoon, and R. E. Faw, "Skyshine Benchmark Experiment," RRA-T 78802, Vols. 1 and 2, Radiation Research Associates, (1978).
- En67 Engle, W. W., Jr., "A User's Manual for the ANISN Code," USAEC K-1963, U.S. Atomic Energy Commission, 1967.
- Fa87 Faw, R. E. and J. K. Shultis, "The MicroSkyshine Method For Gamma-ray Skyshine Analysis," Report 188, (Engineering Experiment Station, Kansas State University Manhattan, KS,) 1987.
- Gr87 "MicroSkyshine Users Manual," Grove Engineering, Inc., 15215 Shady Grove Rd., Rockville, MD 20950, 1987.
- Ha83 Harima, Y., "An Approximation of Gamma-Ray Buildup Factors by Modified Geometric Progression," Nuclear Science and Engineering, 83, 299-309 (1983).
- Ha86 Harima, Y., Y. Sakamoto, S. Tanaka, and M. Kawai, "Validity of the Geometric-Progression Formula in Approximating Gamma-Ray Buildup Factors," Nuclear Science and Engineering, 94, 24-35 (1986).
- Ho75 Hornbeck, R. W., *Numerical Methods*, (Quantum Publishers, Inc., New York, New York, 1975).
- Hu82 Hubbell, J.H., *Int. J. Appl. Radiat. Isot.*, 33, 1269-1290 (1982).

- Ke82 Keck, B., and P. Herchenroder, "Nachrechnen eines Gamma- Skyshine-Benchmark experiments," *Atomwirtschaft* (1982).
- Ki68 Kitazume, Mitsuhuki, "A Simple Calculation for Air-Scattered Gamma-rays," *Journal of Nuclear Science and Technology*, 5, 464-471 (1968).
- La79 Lampley, C. M., "The SKYSHINE II Procedure: Calculation of the Effects of Structure Design on Neutron, Primary Gamma-Ray, and Secondary Gamma-ray Dose Rates in Air," Report RRA-T7901 (NUREG/CR-0791), Radiation Research Associates, Fort Worth, Texas, 1979.
- La88 Lampley, C. M., M. C. Andrews, and M. B. Wells, "The SKYSHINE-III Procedure: Calculation of the Effects of Structure Design on Neutron, Primary Gamma-Ray and Secondary Gamma-Ray Dose Rates in Air," RRA-T8209A, (RSIC Code Collection CCC-289), Radiation Research Associates, Fort Worth, Texas, 1988.
- Ly58 Lynch, et al., "A Monte Carlo Calculation of Air-Scattered Gamma-rays," Report ORNL 2292, Oak Ridge National Laboratory, Oak Ridge Tennessee, 1958.
- Ma73 Malefent, R. E., "G³: A General Purpose Gamma-ray Scattering Program," Report La-5176, Los Alamos Scientific Laboratory, Los Alamos, New Mexico, 1973.
- Mi77 Mikols, W. J. and J. K. Shultis, "Selection of Angular Quadrature for Anisotropic Transport Computations," *Nuclear Science and Engineering* 63, 91 (1977).
- My73 Mynatt, F. R., et al., "The DOT II Two-Dimensional Discrete-Ordinates Transport Code," Report ORNL-TM-4280, Oak Ridge National Laboratory, Oak Ridge, Tennessee (1973).
- Na81 Nason, R. R., et al., "A Benchmark Skyshine Experiment," *Nuclear Science and Engineering*, 79, 404 (1981).
- Pe84 Peng, Wu-Heng, "Skyshine Radiation from a PWR containment Dome," *Trans. Am. Nucl. Soc.*, 47, 373-375 (1984).
- Pe65 Penny, S. K., D. K. Trubey, and M. B. Emmett, "OGRE, A Monte Carlo System for Gamma-ray Transport Studies, Including an Example (OGRE-P1) for Transmission Through Laminated Slabs," Oak Ridge National Laboratory Report ORNL-3905 (1965).
- Pr76 Price, J. H., D. G. Collins, and M. B. Wells, Utilization Instructions for SKYSHINE," Radiation Research Associates, Inc. Research Note RRA-N7608, 1976.
- Ro80 Roseberry, M. L., "Benchmark Skyshine Exposure Rates." M.S. Thesis. Nuclear Engineering Department, KSU (1980).

- Ro82 Roseberry, M. L. and J. K. Shultis, "Point-Kernel Calculations of Skyshine Exposure Rates," *Nuclear Science and Engineering*, **80**, 334-338, 1982.
- Rs86 "Documentation for CCC-49313/QAD-CGCP Code Package," Report CCC-493, Radiation Shielding Information Center, Oak Ridge National Laboratory, Oak Ridge, Tennessee, 1986.
- Sh87 Shultis, J. K. and R. E. Faw, "Improved Response Functions For The MicroSkyshine," Report 189, Engineering Experiment Station, Kansas State University Manhattan, KS (1987).
- Sh78 Shultis, J. K., et al., Approximate Methods in Gamma-Ray Skyshine Calculations," *Trans. Am. Nucl. Soc.*, **28**, 632, (1978)
- So75 Soffer, L., and L. C. Clemons, Jr., "COHORT-II: A Monte Carlo General Purpose Shielding Computer Code," Report NASA-TN-D-6170, Lewis Research Center, Cleveland, Ohio.
- St67 Storm, E. and H. I. Israel, "Photon Cross Sections from 0.001 to 100 MeV for Elements 1 Through 100," LA-3753, Los Alamos National Laboratory, Los Alamos, NM (1967).
- Tr61 Trubey, D. K., "The Single-Scattering Approximation to the Solution of the Gamma-ray Air-Scattering Problem," *Nuclear Science and Engineering*, **10**, 102-116, (1961).

Appendix A

Presented in this section is the computer code SKYCALC used to evaluate the skyshine dose from a shielded point source in a silo. The theoretical background for this computer code is presented in Chapters 2 and 3. This code was written for machines using ANSI-standard FORTRAN-77.

The formatted input data needed by the code is listed in the code comment lines. Most of the input data file is prepared by KSLAB [Ry79]. The computer code is designed to be run on a microcomputer.

The output data is stored in a data file whose name is specified by the user. Output data contains the skyshine dose (total and for each energy group) for each discrete radial source-to-detector distance. A second data file specified by the program user contains the skyshine dose (total) at each discrete radial source-detector distance.

The last page of this section contains an example input file for the 21-cm KSU benchmark experiment.

```

*****
*   PROGRAM TO CALCULATE THE SKYSHINE DOSE DUE TO A POINT SOURCE   *
*   LOCATED ON TOP OF A FLAT CYLINDRICAL ROOF SHIELD.  THE SOURCE  *
*   CAN BE A FUNCTION OF DIRECTION COSINES OUT OF THE SHIELD AND  *
*   OF ENERGY.  PROGRAM USES OUTPUT FROM KSLAB FORTRAN AND THE   *
*   EDITSLAB SUBROUTINE AS A DRIVER.                               *
*                                                                    *
*   WRITTEN BY MICHAEL S. BASSET                                   *
*   AS PART OF MASTER DEGREE PROGRAM                               *
*                                                                    *
*   LIST OF INPUT VARIABLES WHICH WILL BE NEEDED BY THE CODE.      *
*   IF USING EDITSLAB SUBROUTINE SOME OF THIS WILL BE INITIALIZED  *
*   IN THE OUT FILE CREATED BY THAT ROUTINE.                       *
*   NW      =  NUMBER OF ANGULAR GROUPS USED IN K-SLAB             *
*   NGRP     =  NUMBER OF ENERGY GROUPS USED IN K-SLAB           *
*   NQUAD    =  ORDER OF GAUSSIAN QUADRATURE TO BE USED            *
*               (EITHER 16 OR 32 POINT)                           *
*   THS      =  THICKNESS OF ROOF SHIELDING SLAB IN CM.           *
*   YD       =  DETECTOR LOCATION IN RELATION TO THE SILO TOP      *
*   YS       =  SOURCE LOCATION IN RELATION TO THE SILO TOP       *
*   WO       =  GEOMETRICAL COLLIMATION ANGLE FOR PARTICLES ON     *
*               THE SILO TOP.                                       *
*   RHO      =  AIR DENSITY IN G/CM3                             *
*   BP       =  SOURCE COLLIMATION BREAK POINT                     *
*   NUSCAT   =  NUMBER OF SOURCE GROUPS IN K-SLAB                  *
*   XMIN     =  MINIMUM SOURCE - DETECTOR DISTANCE (M)            *
*   XMAX     =  MAXIMUM SOURCE - DETECTOR DISTANCE (M)            *
*   XDEL     =  THE DELTA CHANGE IN X BETWEEN DOSE CALCULATIONS.   *
*   EKSLAB(I) =  THE ENERGY GROUP STRUCTURE FROM PHOGROUP FORTRAN. *
*   WKSLAB(I) =  THE ANGULAR GROUP STRUCTURE FROM K-SLAB FORTRAN   *
*   FLUX(J,I) =  THE ANGULAR FLUX DENSITIES FOR ANGULAR GROUP J   *
*               AND ENERGY GROUP I                                *
*   NCOMP(I) =  THE NUMBER OF THE ENERGY GROUP CONTAINING        *
*               AN UNSCATTERED FLUX COMPONENT.                     *
*   EXEN(I)  =  THE ENERGY OF THE I'TH UNSCATTERED FLUX COMPONENT *
*   CROSS(I) =  THE CROSS SECTION OF THE I'TH ENERGY GROUP      *
*               COMPONENT TAKEN FROM K-SLAB                        *
*   SOURCE(I) =  THE NUMBER OF PARITICLES EMITTED PER SECOND FROM  *
*               THE I'TH SOURCE GROUP.  USED TO NORMALIZE         *
*               TO DOSE/RAD.                                       *
*   NDTYPE   =  THE TYPE OF RESPONSE FUNCTION USED WHEN           *
*               CALCULATING THE SKYSHINE RESPONSE ( 1 = ABSORBED   *
*               DOSE RAD/PHOTON; 2 = EXPOSURE (R/PHOTON)          *
*****
*   INTEGER GP,GPADJ
*   CHARACTER*64 FNAME, A(3)
*   CHARACTER*79 TITLE
*   COMMON /BDATA/PRIGAM(12,30,3),EN(17),X(40),W(40),ANGLE(20),PI
*   COMMON /KSLAB/NGRP,NW,EKSLAB(25),WKSLAB(25),FLUX(25,25),NCOMP(25),
*   1NUSCAT,THS,SOURCE(25),EXEN(25),CROSS(25),BP,STOTAL,NFLAG(25);
*   2DEL(25)

```

```

COMMON /DOSED/B(25,25),STBEAM(32),YD,YS,ENDOSE(25),E,CE,GP,
CGPADJ,EFACT,RHO,MSAVE,BEAM(20),WSTOP,B1,NQUAD,A1OLD,W0
* SET INITIAL VALUES FOR NCOMP
  DO 1 I = 1,25
1    NCOMP(I) = 0
*
* OPEN FILE UNIT 8 FOR CONTROLLING DATA INPUT
*
* OPEN'S FILE TO READ IN INITIAL DATA AND THE ANGLULAR FLUX
* DENSITIES FOR ALL ENERGY GROUPS AND ANGULAR DIRECTIONS.
*
* INPUT NAME OF THE DATA CONTROLLING FILE
  WRITE (*,900)
900  FORMAT(' INPUT DATA FILE NAME ')
  READ (*,901) FNAME
901  FORMAT(A)
  OPEN (8,FILE=FNAME)
* INPUT THE NAME AND OPEN THE OUTPUT FILE
  WRITE (*,905)
905  FORMAT(' Input name of the Output file ')
  READ (*,906) FNAME
906  FORMAT(A)
  OPEN(10,FILE=FNAME,STATUS = 'UNKNOWN')
* INPUT THE NAME AND OPEN THE PLOT FILE
  WRITE(*,910)
910  FORMAT(' Input the Name of the Plot File ')
  READ(*,911) FNAME
911  FORMAT(A)
  OPEN(20,FILE=FNAME,STATUS = 'UNKNOWN')
  WRITE(*,912)
  READ(*,*)NDTYPE
912  FORMAT(' Chose Type of Dose response desired',/,20X,'1 = Rad/phot
*on',/,20X,'2 = R/photon')
  READ (8,999,END=10000)TITLE
999  FORMAT(A)
  READ (8,1000,END=10000) NW,NGRP,NQUAD,THS
  NW = NW/2
1000  FORMAT (3I4,E14.7)
  READ (8,1001,END=10000) YD,YS,W0,RHO,BP,NUSCAT
1001  FORMAT (2F12.8,3E14.7,I3)
  READ (8,1002,END=10000) XMIN,XMAX,XDEL
1002  FORMAT (3E14.7)
  READ (8,1003,END=10000) (EKSLAB(I),I = 1,NGRP)
1003  FORMAT (5F12.8)
  READ (8,1004,END=10000) (WKSLAB(I),I = 1,NW)
1004  FORMAT (5E15.8)
  READ (8,1005,END=10000) ((FLUX(J,I),I = 1,NGRP),J = 1,NW)
1005  FORMAT (5E15.8)
  IF (NUSCAT.GT.0) THEN
    READ (8,1006,END=10000) (NCOMP(I),EXEN(I),CROSS(I),SOURCE(I),
    CI = 1,NUSCAT)

```

```

1006  FORMAT (I3,F12.8,E16.8,F12.8)
      END IF
***
***  WRITE'S BACK OUT INPUT DATA CONTROLLERS TO OUTPUT FILE ON UNIT 10
***
      WRITE (10,1009)
1009  FORMAT(3(/),1X,40('*'),' INPUT AND DATA PARAMETERS FOR SKYCALC ',
      C40('*'))
      WRITE(10,1010)TITLE
1010  FORMAT(//,20X,A80)
      WRITE(10,1011)NW
1011  FORMAT(/,18X,I2,4X,'NW',5X,'NUMBER OF ANGULAR DIRECTIONS OUT OF TH
      CE SLAB FACE. ')
      WRITE(10,1012)NGRP
1012  FORMAT(18X,I2,4X,'NGRP',3X,'NUMBER OF ENERGY GROUPS FROM K-SLAB.')
```

WRITE(10,1013)NQUAD

```

1013  FORMAT(18X,I2,4X,'NQUAD',2X,'NUMBER OF GAUSSIAN QUADRATURE POINTS
      CUSED TO CALCULATE THE DOSE.')
```

WRITE (10,1035)NUSCAT

```

1035  FORMAT(18X,I2,4X,'NUSCAT',1X,'NUMBER OF ENERGY GROUPS CONTAINING
      CUNSCATTERED GAMMAS')
```

WRITE(10,1014)THS

```

1014  FORMAT(12X,F8.4,4X,'THS',4X,'SLAB THICKNESS IN (CM).')
```

WRITE(10,1015)YD

```

1015  FORMAT(12X,F8.4,4X,'YD',5X,'SOURCE HEIGHT BELOW SILO TOP (NEGATIVE
      C FOR HEIGHTS ABOVE SILO TOP).')
```

WRITE(10,1016)YS

```

1016  FORMAT(12X,F8.4,4X,'YS',5X,'DETECTOR HEIGHT BELOW SILO TOP (NEGATI
      CVE FOR HEIGHTS ABOVE SILO TOP)')
```

WRITE(10,1017)WO

```

1017  FORMAT(6X,E14.7,4X,'WO',5X,'IMPOSED MINIMUM COSINE OF THETA OVER W
      CHICH DOSE IS INTEGRATED.')
```

WRITE(10,1018)RHO

```

1018  FORMAT(6X,E14.7,4X,'RHO',4X,'AIR DENSITY IN (G/CM^3) ')
```

WRITE(10,1019)BP

```

1019  FORMAT(6X,E14.7,4X,'BP',5X,'COLUMATION ANGLE OF THE SOURCE ON THE
      CSLAB SURFACE BOTTOM.')
```

WRITE(10,1020)XMIN

```

1020  FORMAT(12X,F9.3,4X,'XMIN',3X,'MINIMUM SOURCE-DETECTOR DISTANCE (M)
      C')
```

WRITE(10,1021)XMAX

```

1021  FORMAT(12X,F10.2,4X,'XMAX',3X,'MAXIMUM SOURCE-DETECTOR DISTANCE (M
      C)')
```

WRITE(10,1022)XDEL

```

1022  FORMAT(12X,F9.3,4X,'XDEL',3X,'CHANGE IN SOURCE-DETECTOR DISTANCE B
      CWEEN DOSE CALCULATIONS')
```

WRITE(10,1023)

```

1023  FORMAT(/,25X,'***  GROUP AVERAGE ENERGIES FROM K-SLAB"S CROSS SECT
      CION PREPARATION CODE ***')
```

WRITE(10,1024)

```

1024  FORMAT(5(3X,'GROUP',5X,'AV. ENERGY'))
      WRITE(10,1025)(I,EKSLAB(I),I=1,NGRP)
1025  FORMAT(5(5X,I2,3X,F12.6,1X))
      WRITE(10,1026)
1026  FORMAT(/,20X,'*** ANGULAR QUADRATURE POINTS USED BY K-SLAB DURING
CALCULATION OF THE ANGULAR FLUXES ***')
      WRITE(10,1027)
1027  FORMAT(5(3X,'GROUP',3X,'ANG. DIRECTION'))
      WRITE(10,1028)(I,WKSLAB(I),I=1,NW)
1028  FORMAT(5(5X,I2,4X,E13.6,1X))
      WRITE(10,1029)
1029  FORMAT(/,25X,'*** INFORMATION ABOUT THE SOURCE ENERGY GAMMAS ')
      WRITE(10,1030)
1030  FORMAT(5X,'ENERGY GP CONTAINING',5X,'ENERGY SOURCE GAMMAS',5X,'TOT
CAL CROSS SECTION',5X,'GROUP SOURCE STRENGTH',/,5X,'UNSCATTERED GAM
CMAS')
      DO 5 I = 1,NUSCAT
5      WRITE(10,1031)NCOMP(I),EXEN(I),CROSS(I),SOURCE(I)
1031  FORMAT(14X,I3,18X,F10.8,13X,E14.7,13X,F10.7,5X)
***
*** CHOOSE ORDER OF GAUSSIAN QUADRATURE FOR USE IN INTEGRATING THE
*** NORMALIZED DOSE.
***
      IF (NQUAD.EQ.32) THEN
          DO 10 I = 1,16
10          X(I) = -X(33 - I)
          DO 20 I = 1,16
20          W(I) = W(33 - I)
      ELSE
*** NQUAD = 16 POINT QUADRATURE
          DO 21 I = 1,8
              X(I) = -X(41-I)
              W(I) = W(41-I)
              X(I+8) = X(32+I)
21          W(I+8) = W(32+I)
          END IF
      WRITE(*,*) 'FINISHED CALCULATING QUADRATURE POINTS'
***
*** CALL THE SUBROUTINE TO DECOMPOSE THE SCATTERED AND UNSCATTERED
*** GROUPS INTO SEPARATE GROUPS OF ONLY SCATTERED OR UNSCATTERED
*** COMPONENTS.
***
      CALL UNGRP
*** CALL SPLINE FITTING ROUTINE WHICH WILL ENABLE ALL ANGULAR
*** DIRECTIONS FOR A GIVEN ENERGY GROUP TO BE ESTIMATED.
***
      CALL SPLINE
*** LOOP OVER DESIRED SOURCE DETECTOR DISTANCES.
      DO 30 XH = XMIN,XMAX,XDEL
          WRITE(*,*) 'CALCULATING S-D DISTANCE ',XH
          TOTDOS = 0.0

```

```

        CALL DOSE(XH)
        DO 40 I = 1,NGRP
40      TOTDOS = TOTDOS + ENDOSE(I)
        IF (NDTYPE.EQ.1) THEN
***    WRITE OUT DOSE RESPONSE
            WRITE(10,1100)XH,TOTDOS
1100    FORMAT(/,' SOURCE DETECTOR DISTANCE',F9.3,3X,' IN M',/, 'DOSE FROM
        CALL GAMAS',E14.7,' IN RAD/PHOTON')
        ELSE
***    WRITE OUT EXPOSURE RESPONSE
            WRITE(10,1110)XH,TOTDOS*1.154
1110    FORMAT(/,' SOURCE DETECTOR DISTANCE',F9.3,3X,' IN M',/, 'DOSE FROM
        CALL GAMAS',E14.7,' IN R/PHOTON')
        END IF
        NLOOP = INT(NGRP/8)
        IF (MOD(NGRP,8).GT.0) NLOOP = NLOOP + 1
        WRITE(10,2000)
2000    FORMAT(48X,'*** ENERGY GROUP NUMBERS ***')
        DO 50 K = 1,NLOOP
        NEND = K*8
        IF (NGRP.LE.NEND) NEND = NGRP
        IF (NDTYPE.EQ.1) THEN
            WRITE(10,2001)(J,J=(K-1)*8+1,NEND)
2001    FORMAT(16X,8(5X,I4,5X))
            WRITE(10,2010) (ENDOSE(J),J=(K-1)*8+1,NEND)
2010    FORMAT(3X,'DOSE IN GROUP',8(2X,E12.5))
            WRITE(10,2020) (ENDOSE(J)/TOTDOS,J=(K-1)*8+1,NEND)
2020    FORMAT(2X,'FRACT OF TOTAL',8(2X,E12.5),/)
        ELSE
            WRITE(10,2002)(J,J=(K-1)*8+1,NEND)
2002    FORMAT(19X,8(5X,I4,5X))
            WRITE(10,2011) (ENDOSE(J),J=(K-1)*8+1,NEND)
2011    FORMAT(3X,'EXPOSURE IN GROUP',8(2X,E12.5))
            WRITE(10,2021) (ENDOSE(J)/TOTDOS,J=(K-1)*8+1,NEND)
2021    FORMAT(5X,'FRACT OF TOTAL',8(2X,E12.5),/)
        END IF
50      CONTINUE
        WRITE(10,2030)
2030    FORMAT(128(' '))
        WRITE(20,2040)XH,TOTDOS
2040    FORMAT(F12.3,' ',',',E15.8)
30      CONTINUE
        GOTO 150
10000  WRITE(10,1220)
1220    FORMAT (' END OF INPUT ENCOUNTERED IN INPUT DATA FILE. CHECK ')
150    STOP
        END

```

```

*****
*
* SUBROUTINE TO SEPARATE THE SCATTERED AND UNSCATTERED FLUX
* COMPONENTS. SUBROUTINE WILL NEED THE INPUT SOURCE FOR EACH
* DIRECTION COSINE AND THE TOTAL CROSS SECTION FOR EACH GROUP
* WHICH CONTAINS AN UNSCATTERED COMPONENT OF THE FLUX
*
*****

      SUBROUTINE UNGRP
      REAL MFP,NWFLUX
      DIMENSION NWFLUX(25,25),ESAVE(25)
      COMMON /KSLAB/NGRP,NW,EKSLAB(25),WKSLAB(25),FLUX(25,25),NCOMP(25),
      1NUSCAT,THIS,SOURCE(25),EXEN(25),CROSS(25),BP,STOTAL,NFLAG(25),
      2DEL(25)
      IADD = 0
      STOTAL = 0.0
***   LOOP TROUGHT ALL ENERGY GROUPS LOOKING FOR GROUPS WHICH HAVE
***   SCATTERED AND UNSCATTERED FLUX COMPONENTS.
      DO 10 I = 1,NGRP
***   CHECK TO SEE IF ENERGY GROUP CONTAINS AN UNSCATTERED FLUX COMPONENT
      IF (I.EQ.NCOMP(I)) THEN
          STOTAL = STOTAL + SOURCE(I)
          NFLAG(I + IADD) = 1
          NFLAG(I + IADD + 1) = 0
          ESAVE(I+IADD) = EXEN(IADD+1)
          ESAVE(I+IADD+1) = EKSLAB(I)
***   LOOP THROUGH ANGULAR DIRECTIONS FINDING UNSCATTERED FLUXES AND
***   SETTING FLUXES IN ANGULAR GROUPS LESS THAN THE SOURCE COLLIMATION
***   ANGLE TO ZERO.
          DO 20 J = 1,NW
              IF (WKSLAB(J).LT.BP) THEN
                  NWFLUX(J,I+IADD) = 0.0
              ELSE
                  MFP = CROSS(I)*THIS/WKSLAB(J)
                  NWFLUX(J,I+IADD) = SOURCE(I)*EXP(-MFP)/WKSLAB(J)
              END IF
              NWFLUX(J,I+IADD+1) = FLUX(J,I)-NWFLUX(J,I+IADD)
20          CONTINUE
          IADD = IADD+1
      ELSE
          NFLAG(I + IADD) = 0
          ESAVE(I+IADD) = EKSLAB(I)
          DO 30 J = 1,NW
              NWFLUX(J,I+IADD) = FLUX(J,I)
30          CONTINUE
      END IF
10      CONTINUE
      NGRP = NGRP + IADD
      DO 40 I = 1,NGRP
          DO 50 J = 1,NW
              FLUX(J,I) = NWFLUX(J,I)
          
```

```

50      CONTINUE
      EKSLAB(I) = ESAVE(I)
40      CONTINUE
      RETURN
      END
*****
*
* SUBROUTINE TO CALCULATE THE SPLINE FITTING COEFFICIENTS WHICH WILL
* ALLOW FOR ESTIMATION OF THE ANGULAR CURRENT DENSITIES AT ALL
* ANGULAR DIRECTIONS REQUIRED BY THE SKYSHINE CALCULATION PROCEDURE.
*
* B(I,J) = IS THE SPLINE FIT COEFFICIENTS FOR ANGLUAR DIRECTIONS;
*          WHERE I CORESPONDS TO AN K-SLAB ANGULAR DIRECTION AND
*          J TO THE J'TH ENERGY GROUP.
*
*****
      SUBROUTINE SPLINE
      DIMENSION XSOL(25)
      INTEGER GP,GPADJ
      COMMON /BDATA/PRIGAM(12,30,3),EN(17),X(40),W(40),ANGLE(20),PI
      COMMON /KSLAB/NGRP,NW,EKSLAB(25),WKSLAB(25),FLUX(25,25),NCOMP(25),
      1NUSCAT,THIS,SOURCE(25),EXEN(25),CROSS(25),BP,STOTAL,NFLAG(25),
      2DEL(25)
      COMMON /DOSED/B(25,25),STBEAM(32),YD,YS,ENDOSE(25),E,CE,GP,
      CGPADJ,EFACT,RHO,MSAVE,BEAM(20),WSTOP,B1,NQUAD,A1OLD,W0
      COMMON /SPLDAT/A(0:25,0:25),BB(0:25)
***      FIND THE SHARP CUTOFF ANGLE
      M = 0
      DO 10 I = 1,NW-1
      IF ((WKSLAB(I).LE.BP).AND.(WKSLAB(I+1).GT.BP)) M = I
10      CONTINUE
      MM = M
      MSAVE = M
***      CHANGE THE ANGULAR FLUX INTO AN NORMALIZED ANGULAR CURRENT
      DO 20 J = 1,NGRP
      DO 30 I = 1,NW
30      FLUX(I,J) = FLUX(I,J)*WKSLAB(I)/(4.0*PI)/STOTAL
20      CONTINUE
***
***      CALCULATE THE MATRIX ELEMENTS A AND SOURCE VECTOR BB FOR DETERMININ
***      THE CUBIC SPLINE FIT COEFFICIENTS.
***
***      LOOP OVER ALL ENERGY GROUPS
      DO 40 JE = 1,NGRP
***      CHECK TO SEE IF GROUP COMPOSED OF UNSCATTERED FLUX COMPONENTS.
***      IF UNSCATTERED COMPONENT IS BEING PROCESSED; BREAK UP INTO TWO
***      REGIONS TO AVOID IRREGULARITIES WHICH ARISE FROM SPLINE FITTING
***      SHARP CUTOFFS IN THE ANGULAR FLUX DENSITY.
      MM = MSAVE
      IF (NFLAG(JE).EQ.1) THEN

```

```

*** FIT IN REGION LESS THAN THE BREAK POINT BP
  IF (M.EQ.0) THEN MM = NW
  BY = FLUX(1,JE)-SLOPE(1,JE)*WKSLAB(1)
  IF (BY.LT.0) BY = 0
  DO 50 I = 1,MM-1
50  DEL(I) = WKSLAB(I+1) -WKSLAB(I)
*** SET FIRST MATRIX ELEMENTS IN A
  A(1,0) = 0.0
  A(1,1) = 2.0*WKSLAB(2)/DEL(1)
  A(1,2) = 1.0
  BB(1) = 6*((FLUX(2,JE)-FLUX(1,JE))/(DEL(1)**2)-(FLUX(1,JE)-BY)/
C(DEL(1)*W(1)))
  DO 60 I = 2,MM-1
  A(I,I) = A1V(I)
  A(I,I-1) = DEL(I-1)/DEL(I)
  A(I,I+1) = 1.0
60  BB(I) = BVALUE(I,JE)
  A(MM,MM+1) = 0.0
  A(MM,MM-1) = 0.0
  A(MM,MM) = 0.0
  BB(MM) = 0.0
  CALL TDMA(MM,XSOL)
  DO 70 I = 1,MM-1
70  B(I,JE) = XSOL(I)
  B(MM,JE) = 0.0
***
*** FIT FOR ANGULAR DIRECTIONS GREATER THAN BP
***
  IF (M.GT.0) THEN
  MM = M + 1
  BY = FLUX(MM,JE) - SLOPE(MM,JE)*WKSLAB(MM)
  IF (BY.LT.0) BY = 0
  DO 80 I = MM,NW-1
80  DEL(I)=WKSLAB(I+1) - WKSLAB(I)
  A(MM,MM-1) = 0.0
  A(MM,MM) = 2.0*WKSLAB(MM+1)/DEL(MM)
  A(MM,MM+1) = 1.0
  BB(MM) = 6*((FLUX(MM+1,JE)-FLUX(MM,JE))/(DEL(MM)**2)-
C(FLUX(MM,JE)-BY)/(DEL(MM)*WKSLAB(MM)))
  DO 90 I = MM+1,NW-1
  A(I,I) = A1V(I)
  A(I,I-1) = DEL(I-1)/DEL(I)
  A(I,I+1) = 1.0
90  BB(I) = BVALUE(I,JE)
  DO 95 I = 1,NW-MM
  A(I,I-1) = A(MM+I-1,MM+I-2)
  A(I,I) = A(MM+I-1,MM+I-1)
  A(I,I+1) = A(MM+I-1,MM+I)
95  BB(I) = BB(MM+I-1)
  A(NW-MM,NW-MM+1) = 0.0

```

```

      CALL TDMA(NW-MM+1,XSOL)
      DO 100 I = 1,NW-MM
100    B(MM+I-1,JE) = XSOL(I)
      B(NW,JE) = 0.0
      END IF
***
***  SPLINE FIT FOR ENERGY GROUPS COMPOSED OF SCATTERED RADIATION
***
      ELSE
      BY = FLUX(1,JE)-SLOPE(1,JE)*WKSLAB(1)
      IF (BY.LT.0) BY = 0.0
      DO 110 I = 1,NW-1
110    DEL(I) = WKSLAB(I+1) -WKSLAB(I)
      A(1,0) = 0.0
      A(1,1) = 2*WKSLAB(2)/DEL(1)
      A(1,2) = 1.0
      BB(1) = 6*((FLUX(2,JE)-FLUX(1,JE))/(DEL(1)**2)-(FLUX(1,JE)
C-BY)/(DEL(1)*WKSLAB(1)))
      DO 120 I = 2,NW-1
      A(I,I) = A1V(I)
      A(I,I-1) = DEL(I-1)/DEL(I)
      A(I,I+1) = 1.0
120    BB(I) = BVALUE(I,JE)
      A(NW,NW+1) = 0.0
      CALL TDMA(NW,XSOL)
      DO 130 I = 1,NW-1
130    B(I,JE) = XSOL(I)
      B(NW,JE) = 0.0
      END IF
40    CONTINUE
      RETURN
      END
***  FUNCTION TO CALCULATE THE SLOPE BETWEEN TWO POINTS
      REAL FUNCTION SLOPE(NF,JE)
      COMMON /KSLAB/NGRP,NW,EKSLAB(25),WKSLAB(25),FLUX(25,25),NCOMP(25),
1NUSCAT,THS,SOURCE(25),EXEN(25),CROSS(25),BP,STOTAL,NFLAG(25),
2DEL(25)
      SLOPE = (FLUX(NF,JE)-FLUX(NF+1,JE))/(WKSLAB(NF)-WKSLAB(NF+1))
      END
***  FUNCTION TO CALCULATE ONE OF THE MATRIX ELEMENTS
      REAL FUNCTION A1V(I)
      COMMON /KSLAB/NGRP,NW,EKSLAB(25),WKSLAB(25),FLUX(25,25),NCOMP(25),
1NUSCAT,THS,SOURCE(25),EXEN(25),CROSS(25),BP,STOTAL,NFLAG(25),
2DEL(25)
      A1V = 2*(WKSLAB(I+1)-WKSLAB(I-1))/DEL(I)
      END
***  FUNCTION TO DETERMINE THE SOURCE VECTOR BB9I)
      REAL FUNCTION BVALUE(I,JE)
      COMMON /KSLAB/NGRP,NW,EKSLAB(25),WKSLAB(25),FLUX(25,25),NCOMP(25),
1NUSCAT,THS,SOURCE(25),EXEN(25),CROSS(25),BP,STOTAL,NFLAG(25),

```

```

2DEL(25)
  BVALUE = ((FLUX(I+1,JE)-FLUX(I,JE))/(DEL(I)**2)-(FLUX(I,JE)-
CFLUX(I-1,JE))/(DEL(I)*DEL(I-1)))*6.0
  END
***
*** TRI-DIAGONAL MATRIX ALGORITHM TO SOLVE SIMILTANEOUS EQS.
***
  SUBROUTINE TDMA(N,X)
    DIMENSION H(0:25), AL(0:25),X(25)
    COMMON /SPLDAT/A(0:25,0:25),BB(0:25)
    H(0) = 0.0
    AL(0) = 0.0
    A(1,0) = 0.0
    DO 10 I = 1,N - 1
      H(I) = A(I,I+1)/(A(I,I)-A(I,I-1)*H(I-1))
10    AL(I) = (BB(I)-A(I,I-1)*AL(I-1))/(A(I,I)-A(I,I-1)*H(I-1))
      X(N-1) = AL(N-1)
      DO 20 I = N-2,1,-1
20    X(I) = AL(I)-H(I)*X(I+1)
    END
*****
*
* CALCULATES THE SKYSHINE DOSE FOR A DISTANCE X1 AND AND AN ANGULAR
* CURRENT DENSITY OF FLUX(I,J).
* PROGRAM USED LINE BEAM RESPONSE FUNCTIONS AND IS USABLE FOR
* ONLY FOR CYLINDRICAL GEOMETRY.
* STRBEAM(I) IS THE SPLINE FIT CALCULATED VALUES FOR THE I'TH
* DIRECTION IN THE GAUSSIAN QUADRATURE SET FOR A GIVE ENERGY GROUP.
*
*****
  SUBROUTINE DOSE(X1)
    INTEGER GP,GPADJ
    COMMON /BDATA/PRIGAM(12,30,3),EN(17),X(40),W(40),ANGLE(20),PI
    COMMON /KSLAB/NGRP,NW,EKSLAB(25),WKSLAB(25),FLUX(25,25),NCOMP(25),
1NUSCAT,THS,SOURCE(25),EXEN(25),CROSS(25),BP,STOTAL,NFLAG(25),
2DEL(25)
    COMMON /DOSED/B(25,25),STBEAM(32),YD,YS,ENDOSE(25),E,CE,GP,
CGPADJ,EFACT,RHO,MSAVE,BEAM(20),WSTOP,B1,NQUAD,A1OLD,W0
    SUMD = 0.0
*** LOOP OVER ALL ENERGY GROUPS.
    DO 10 JE = 1,NGRP
      E = EKSLAB(JE)
      CALL ENBRAK
*** DETERMINE IF GROUP COMPOSED OF UNSCATTERED RADIATION
      IF (NFLAG(JE).EQ.1) THEN
*** FIND DOSE CAUSED BY UNSCATTERED RADIATION IN REGION TWO
        AMP = (1-BP)/2.0
        AMB = (1+BP)/2.0
        DO 20 I = 1,NQUAD
          WW = AMB + AMP*X(I)

```

```

*** CALCULATE THE SPLINE CURRENT DENSITIES FOR ENERGY JE, AND ANGULAR
*** DIRECTION WW
20  STBEAM(I) = VALUE(JE,WW)
    WSTOP = BP
    B1 = 1
    CALL SKYDOS(SDOSE,X1)
    DOSE2 = SDOSE
*** FIND DOSE CAUSED BY UNSCATTERED RADIATION IN REGION ONE
    AMP = (BP)/2.0
    AMB = (BP)/2.0
    DO 30 I = 1,NQUAD
    WW = AMB + AMP*X(I)
30  STBEAM(I) = VALUE(JE,WW)
    WSTOP = W0
    B1 = BP
    CALL SKYDOS(SDOSE,X1)
    ENDOSE(JE) = DOSE2 + SDOSE
    ELSE
*** FIND DOSE CAUSED BY SCATTERED GAMMA RAYS
    AMP = (1-W0)/2
    AMB = (1+W0)/2
    DO 40 I = 1,NQUAD
    WW = AMB+AMP*X(I)
40  STBEAM(I) = VALUE(JE,WW)
    WSTOP = W0
    B1 = 1.0
    CALL SKYDOS(SDOSE,X1)
    ENDOSE(JE) = SDOSE
    END IF
10  CONTINUE
    END
*****
*
*          VERSION 2.0 NEWGAM RESPONSE FUNCTIONS
*          FROM FAW AND SHULTIS'S MICROSKYSHINE CODE
*          K-STATE EXPERIMENTAL STATION REPORT 189
*          CE      = DOSE CONVERSION FACTOR
*          GP      = ENERGY GROUP CONTAINING PHOTON ENERGY E
*          GPADJ   = ADJACENT ENERGY GROUP FOR INTERPLOATION
*          EFACT   = INTERPOLATION FACTOR = (E-EGP)/(EGPADJ-EGP)
*
*          SUBROUTINE WILL DETERMINE BETWEEN WHICH GROUP STRUCTURE ENERGIES
*          USED IN THE PRIGAM DATA SET THE ENERGY E FALLS.
*****
SUBROUTINE ENBRAK
INTEGER GP,GPADJ
COMMON /KSLAB/NGRP,NW,EKSLAB(25),WKSLAB(25),FLUX(25,25),NCOMP(25),
1NUSCAT,THS,SOURCE(25),EXEN(25),CROSS(25),BP,STOTAL,NFLAG(25),
2DEL(25)
COMMON /DOSED/B(25,25),STBEAM(32),YD,YS,ENDOSE(25),E,CE,GP,

```

```

CGPADJ,EFACT,RHO,MSAVE,BEAM(20),WSTOP,B1,NQUAD,A1OLD,W0
CE = (1.3078E-11*(RHO/0.001225)**2)*E
IF (E.GT.1) THEN
  IF (E.EQ.10.0) THEN
    GP = 1
  ELSE
    GP = 10 - INT(E)
  END IF
ELSE IF (E.GE.0.5) THEN
  GP = 10
ELSE IF (E.GE.0.15) THEN
  GP = 11
ELSE
  GP = 12
END IF
EGP = EBAR(GP)
IF (E.GT.EGP) THEN
  GPADJ = GP - 1
  IF (GPADJ.EQ.0) GPADJ = 2
ELSE
  GPADJ = GP + 1
  IF (GPADJ.EQ.13) GPADJ = 12
END IF
DELTE = EBAR(GPADJ) - EGP
IF (DELTE.EQ.0) DELTE = 1.0
EFACT = (E-EGP)/DELTE
END
* FUNCTION EBAR USE TO FINE THE MEAN GROUP ENERGY FOR GROUP I
  REAL FUNCTION EBAR(I)
  IF (I.LT.10) THEN
    EBAR = 10.5-I
  ELSE IF (I.LT.11) THEN
    EBAR = 0.75
  ELSE IF (I.LT.12) THEN
    EBAR = 0.325
  ELSE
    EBAR = 0.1
  END IF
END
*****
* FUNCTION USING THE SPLINE FIT COEFFICIENTS FOR THE JE'TH ENERGY *
* GROUP TO FIND THE FITTED CURRENT VALUES AT THE ORDINATES *
* DIRECTION WW *
*****
  REAL FUNCTION VALUE(JE,WW)
  INTEGER GP,GPADJ
  COMMON /KSLAB/NGRP,NW,EKSLAB(25),WKSLAB(25),FLUX(25,25),NCOMP(25),
1NUSCAT,THS,SOURCE(25),EXEN(25),CROSS(25),BP,STOTAL,NFLAG(25),
2DEL(25)
  COMMON /DOSED/B(25,25),STBEAM(32),YD,YS,ENDOSE(25),E,CE,GP,

```

```

CGPADJ,EFAC,T,RHO,MSAVE,BEAM(20),WSTOP,B1,NQUAD,A1OLD,W0
M = MSAVE
IF (NFLAG(JE).EQ.1) THEN
  IF (WW.LT.BP) THEN
    JJ = M - 1
    DO 10 I = 1,M-1
      IF ((WW.GE.WKSLAB(I)).AND.(WW.LE.WKSLAB(I+1))) JJ = I
      IF (WW.LT.WKSLAB(I)) JJ = 1
      SAVE = FITSP(JJ,JE,WW)
    ELSE
      JJ = NW-1
      DO 20 I = M+1,NW-1
        IF ((WW.GE.WKSLAB(I)).AND.(WW.LE.WKSLAB(I+1))) JJ = I
        IF (WW.LT.WKSLAB(M+1)) JJ = M+1
        SAVE = FITSP(JJ,JE,WW)
      END IF
    ELSE
      JJ = NW - 1
      DO 30 I = 1,NW-1
        IF ((WW.GE.WKSLAB(I)).AND.(WW.LE.WKSLAB(I+1))) JJ = I
        IF (WW.LT.WKSLAB(1)) JJ = 1
        SAVE = FITSP(JJ,JE,WW)
      END IF
      IF (SAVE.LT.0) SAVE = 0
      VALUE = SAVE
    END
  *** FUNCTION THAT FITS A SPLINE FIT AT DIRECTION WW AND FOR ENERGY
  *** JE.
  REAL FUNCTION FITSP(JJ,JE,WW)
  COMMON /KSLAB/NGRP,NW,EKSLAB(25),WKSLAB(25),FLUX(25,25),NCOMP(25),
  1NUSCAT,THS,SOURCE(25),EXEN(25),CROSS(25),BP,STOTAL,NFLAG(25),
  2DEL(25)
  COMMON /DOSED/B(25,25),STBEAM(32),YD,YS,ENDOSE(25),E,CE,GP,
  CGPADJ,EFAC,T,RHO,MSAVE,BEAM(20),WSTOP,B1,NQUAD,A1OLD,W0
  FITSP = B(JJ,JE)*((WKSLAB(JJ+1) - WW)**3/DEL(JJ) - DEL(JJ)*
  C(WKSLAB(JJ+1) - WW))/6.0 + B(JJ+1,JE)*((WW-WKSLAB(JJ))**3/DEL(JJ)
  C- DEL(JJ)*(WW-WKSLAB(JJ)))/6.0 + FLUX(JJ,JE)*(WKSLAB(JJ+1) - WW)/
  CDEL(JJ) + FLUX(JJ+1,JE)*(WW-WKSLAB(JJ))/DEL(JJ)
  END
  *****
  *
  *   FORTRAN VERSION ADAPTED BY MICHAEL S. BASSETT FROM
  *   VERSION 4.0 MICRO-SKYSHINE WRITTEN BY R. E. FAW AND
  *   J. K. SHULTIS. PROGRAM ONLY DEALS WITH UNSHIELDED
  *   SILO GEOMETRY.
  *
  *****
  SUBROUTINE SKYDOS(SDOSE,X1)
  INTEGER GP,GPADJ
  COMMON /BDATA/PRIGAM(12,30,3),EN(17),X(40),W(40),ANGLE(20),PI
  COMMON /KSLAB/NGRP,NW,EKSLAB(25),WKSLAB(25),FLUX(25,25),NCOMP(25),

```

```

1NUSCAT,THIS,SOURCE(25),EXEN(25),CROSS(25),BP,STOTAL,NFLAG(25),
2DEL(25)
COMMON /DOSED/B(25,25),STBEAM(32),YD,YS,ENDOSE(25),E,CE,GP,
CGPADJ,EFACT,RHO,MSAVE,BEAM(20),WSTOP,B1,NQUAD,A1OLD,W0
COMMON /SIMPLE/ R,D1,D2
AA = SQRT(X1*X1 + (YD-YS)**2)
R = (RHO/0.001225)*AA
D1 = X1/AA
D2 = (YD-YS)/AA
*** CALCULATE THE INTERPOLATED BEAM RESPONSE FUNCTIONS
*** BEAM(J) IS THE BEAM RESPONSE FUNCTION FOR ALL ANGULAR DIRECTIONS
*** AT THE INTERPOLATED ENERGY OF E.
DO 10 J = 1,20
BINTER = EXP(PRIGAM(GP,J,1))*R**PRIGAM(GP,J,2)*EXP(-R*
CPRIGAM(GP,J,3))
BADJ = EXP(PRIGAM(GPADJ,J,1))*R**PRIGAM(GPADJ,J,2)*EXP(-R*
CPRIGAM(GPADJ,J,3))
10 BEAM(J)= BINTER + (BADJ-BINTER)*EFACT
*** CALCULATE DOSE WITH INTERPOLATED RESPONSE FUNCTIONS
A1OLD = -4.5
CALL GAUSS0(0.0,PI,SDOSE)
SDOSE = 2.0*SDOSE * CE
END
*****
*
* NQUAD GAUSSIAN INTEGRATION TO FIND THE DOSE CAUSED
* BY ENERGY GROUP JE
*
*****
SUBROUTINE GAUSS0(A2,B2,ANS2)
INTEGER GP,GPADJ
COMMON /BDATA/PRIGAM(12,30,3),EN(17),X(40),W(40),ANGLE(20),PI
COMMON /DOSED/B(25,25),STBEAM(32),YD,YS,ENDOSE(25),E,CE,GP,
CGPADJ,EFACT,RHO,MSAVE,BEAM(20),WSTOP,B1,NQUAD,A1OLD,W0
COMMON /SIMPLE/ R,D1,D2
AMB2 = (B2-A2)/2.0
APB2 = (B2+A2)/2.0
SUM2 = 0.0
DO 10 I = 1,NQUAD
PSI = X(I)*AMB2 + APB2
10 SUM2 = SUM2 + W(I)*GAUSSI(PSI)
ANS2 = SUM2 * AMB2
END
***
*** INNER INTEGRATION DONE BY GAUSSIAN QUADRATURE.
***
REAL FUNCTION GAUSSI(PSI)
REAL INBEAM
DIMENSION BB(32),CC(32)
INTEGER GP,GPADJ

```

```

COMMON /BDATA/PRIGAM(12,30,3),EN(17),X(40),W(40),ANGLE(20),PI
COMMON /DOSED/B(25,25),STBEAM(32),YD,YS,ENDOSE(25),E,CE,GP,
CGPADJ,EFACT,RHO,MSAVE,BEAM(20),A1,B1,NQUAD,A1OLD,W0
COMMON /SIMPLE/ R,D1,D2
SUM1 = 0.0
IF ((ABS(A1OLD-A1)).LT.0.0001) THEN
  DO 10 K = 1,NQUAD
    D = 57.29577951*ACOS(COS(PSI)*CC(K)-BB(K))
    SUM1 = SUM1 + W(K)*INBEAM(D)*STBEAM(K)
10 ELSE
  AMB1 = (B1-A1)/2.0
  APB1 = (B1+A1)/2.0
  DO 20 K = 1,NQUAD
    OMEGA = X(K)*AMB1 + APB1
    CC(K) = SQRT(1 - OMEGA**2) * D1
    BB(K) = OMEGA*D2
    D = 57.29577951*ACOS(COS(PSI)*CC(K)-BB(K))
    SUM1 = SUM1 + W(K)*INBEAM(D)*STBEAM(K)
20 END IF
A1OLD = A1
GAUSSI = SUM1*AMB1
END
***
*** ANGULAR INTERPOLATION OF BEAM RESPONSE FUNCTIONS
***
REAL FUNCTION INBEAM(D)
INTEGER GP,GPADJ
COMMON /BDATA/PRIGAM(12,30,3),EN(17),X(40),W(40),ANGLE(20),PI
COMMON /DOSED/B(25,25),STBEAM(32),YD,YS,ENDOSE(25),E,CE,GP,
CGPADJ,EFACT,RHO,MSAVE,BEAM(20),WSTOP,B1,NQUAD,A1OLD,W0
IF (D.GE.100) THEN
  JVALUE = 20-INT((180-D)/20)
  IF (D.LT.ANGLE(JVALUE)) THEN
    JADJ = JVALUE - 1
  ELSE
    JADJ = JVALUE + 1
  END IF
  IF (JADJ.EQ.21) JADJ = 19
ELSE IF (D.GE.20) THEN
  JVALUE = 16 - INT((100-D)/10)
  IF (D.LT.ANGLE(JVALUE)) THEN
    JADJ = JVALUE - 1
  ELSE
    JADJ = JVALUE + 1
  END IF
ELSE IF (D.GE.15) THEN
  JVALUE = 8
  IF (D.LT.ANGLE(8)) THEN
    JADJ = 7
  ELSE

```

```

        JADJ = 9
      END IF
    ELSE IF (D.GE.10) THEN
      JVALUE = 7
      IF (D.LT.ANGLE(7)) THEN
        JADJ = 6
      ELSE
        JADJ = 8
      END IF
    ELSE IF (D.GE.7) THEN
      JVALUE = 6
      IF (D.LT.ANGLE(6)) THEN
        JADJ = 5
      ELSE
        JADJ = 7
      END IF
    ELSE IF (D.GE.5) THEN
      JVALUE = 5
      IF (D.LT.ANGLE(5)) THEN
        JADJ = 4
      ELSE
        JADJ = 6
      END IF
    ELSE IF (D.GE.3) THEN
      JVALUE = 4
      IF (D.LT.ANGLE(4)) THEN
        JADJ = 3
      ELSE
        JADJ = 5
      END IF
    ELSE
      JVALUE = INT(D) + 1
      IF (D.LT.ANGLE(JVALUE)) THEN
        JADJ = JVALUE - 1
      ELSE
        JADJ = JVALUE + 1
      END IF
      IF (JADJ.EQ.0) JADJ = 2
    END IF
    INBEAM = BEAM(JVALUE) + (BEAM(JADJ) - BEAM(JVALUE))*(D - ANGLE(
    CJVALUE))/(ANGLE(JADJ) - ANGLE(JVALUE))
  END

```

*Library Skydata v. 4.0, 20 March 87

*

*— COEFFICIENTS FOR BEAM RESPONSE FUNCTIONS — PRIGAM(12,20,3)

*— Fitted to calculations of single Klein-Nishina scattering and

*— pair production in line beams followed by infinite medium buildup

*— with the GP approximation for buildup. Faw & Shultis March 87.

BLOCK DATA RRADAT

```

COMMON /BDATA/PRIGAM(12,30,3),EN(17),X(40),W(40),ANGLE(20),PI
* 9.5 MeV
DATA ((PRIGAM(1,J,I),I = 1,3),J = 1,20) /
C-8.91568,-0.99301,0.00248,-10.14431,-0.97954,0.00243,
C-10.78282,-0.96765,0.00243,-11.43880,-0.95306,0.00245,
C-12.08827,-0.93680,0.00252,-12.73211,-0.91973,0.00263,
C-13.56202,-0.89569,0.00288,-14.38304,-0.86783,0.00329,
C-15.31173,-0.82844,0.00404,-16.22773,-0.77307,0.00518,
C-16.93617,-0.71375,0.00636,-17.55317,-0.64425,0.00752,
C-18.13527,-0.56366,0.00859,-18.67047,-0.48302,0.00948,
C-18.93738,-0.46223,0.01000,-18.90293,-0.51104,0.01016,
C-18.76997,-0.59498,0.01017,-18.69541,-0.66378,0.01013,
C-18.68741,-0.69790,0.01011,-18.68751,-0.71336,0.01010/
* 8.5 MeV
DATA ((PRIGAM(2,J,I),I = 1,3),J = 1,20) /
C-8.83156,-0.99313,0.00258,-10.06015,-0.97856,0.00253,
C-10.69426,-0.96639,0.00253,-11.34385,-0.95118,0.00255,
C-11.98481,-0.93399,0.00261,-12.62155,-0.91565,0.00273,
C-13.43509,-0.89185,0.00297,-14.25599,-0.86217,0.00338,
C-15.19481,-0.82114,0.00411,-16.13103,-0.76409,0.00523,
C-16.85502,-0.70466,0.00639,-17.47239,-0.63802,0.00753,
C-18.03689,-0.56408,0.00858,-18.54096,-0.49259,0.00947,
C-18.80175,-0.47461,0.00999,-18.77677,-0.52247,0.01016,
C-18.64283,-0.60839,0.01017,-18.56277,-0.67994,0.01013,
C-18.55371,-0.71538,0.01010,-18.55547,-0.73088,0.01009/
* 7.5 MeV
DATA ((PRIGAM(3,J,I),I = 1,3),J = 1,20) /
C-8.73586,-0.99324,0.00271,-9.96185,-0.97802,0.00266,
C-10.59345,-0.96502,0.00265,-11.23784,-0.94879,0.00267,
C-11.86703,-0.93148,0.00273,-12.48963,-0.91315,0.00284,
C-13.29309,-0.88770,0.00308,-14.10896,-0.85694,0.00348,
C-15.05540,-0.81451,0.00420,-16.01343,-0.75538,0.00530,
C-16.74823,-0.69705,0.00643,-17.36967,-0.63302,0.00755,
C-17.91529,-0.56660,0.00858,-18.39054,-0.50408,0.00945,
C-18.64464,-0.48929,0.00998,-18.63231,-0.53571,0.01016,
C-18.49817,-0.62380,0.01017,-18.41410,-0.69875,0.01012,
C-18.40158,-0.73612,0.01009,-18.40473,-0.75195,0.01008/
* 6.5 MeV
DATA ((PRIGAM(4,J,I),I = 1,3),J = 1,20) /
C-8.63775,-0.99052,0.00289,-9.87913,-0.96994,0.00284,
C-10.51728,-0.95374,0.00283,-11.16730,-0.93379,0.00285,
C-11.79500,-0.91359,0.00292,-12.41234,-0.89270,0.00303,
C-13.20231,-0.86576,0.00326,-14.00646,-0.83481,0.00365,
C-14.96438,-0.78976,0.00435,-15.92977,-0.73124,0.00542,
C-16.68261,-0.67249,0.00653,-17.31061,-0.61073,0.00763,
C-17.85307,-0.54839,0.00864,-18.35938,-0.48065,0.00952,
C-18.65002,-0.45863,0.01009,-18.59678,-0.51740,0.01026,
C-18.40481,-0.62280,0.01023,-18.31359,-0.70229,0.01017,
C-18.31056,-0.73909,0.01014,-18.31906,-0.75424,0.01013/
* 5.5 MeV

```

DATA ((PRIGAM(5,J,I),I = 1,3),J = 1,20) /
 C-8.50918,-0.99050,0.00311,-9.74493,-0.96953,0.00305,
 C-10.37903,-0.95256,0.00304,-11.02157,-0.93180,0.00306,
 C-11.64070,-0.91026,0.00312,-12.24270,-0.88884,0.00322,
 C-13.01883,-0.85984,0.00345,-13.80868,-0.82813,0.00382,
 C-14.76568,-0.78194,0.00450,-15.74444,-0.72261,0.00554,
 C-16.51249,-0.66413,0.00662,-17.14815,-0.60454,0.00769,
 C-17.67830,-0.54866,0.00867,-18.14754,-0.49304,0.00953,
 C-18.41481,-0.47923,0.01010,-18.37967,-0.53582,0.01029,
 C-18.18616,-0.64571,0.01026,-18.07745,-0.73343,0.01018,
 C-18.06301,-0.77505,0.01014,-18.06879,-0.79191,0.01012/

* 4.5 MeV

DATA ((PRIGAM(6,J,I),I = 1,3),J = 1,20) /
 C-8.35440,-0.99054,0.00342,-9.57970,-0.96997,0.00335,
 C-10.20947,-0.95221,0.00333,-10.84418,-0.93049,0.00334,
 C-11.45245,-0.90776,0.00339,-12.04056,-0.88515,0.00349,
 C-12.79416,-0.85529,0.00371,-13.56468,-0.82298,0.00406,
 C-14.51023,-0.77656,0.00471,-15.49461,-0.71747,0.00570,
 C-16.27127,-0.66035,0.00675,-16.90625,-0.60506,0.00777,
 C-17.42659,-0.55583,0.00871,-17.85917,-0.51282,0.00954,
 C-18.11836,-0.50407,0.01011,-18.11672,-0.55524,0.01034,
 C-17.92974,-0.66827,0.01033,-17.78767,-0.76929,0.01022,
 C-17.75403,-0.81884,0.01016,-17.75121,-0.83932,0.01013/

* 3.5 MeV

DATA ((PRIGAM(7,J,I),I = 1,3),J = 1,20) /
 C-8.17183,-0.98828,0.00389,-9.40385,-0.96308,0.00381,
 C-10.03899,-0.94159,0.00379,-10.67691,-0.91572,0.00380,
 C-11.28263,-0.88915,0.00385,-11.86211,-0.86334,0.00394,
 C-12.59264,-0.83133,0.00414,-13.34028,-0.79744,0.00447,
 C-14.26622,-0.75042,0.00508,-15.24439,-0.69262,0.00601,
 C-16.02860,-0.63648,0.00700,-16.66515,-0.58478,0.00797,
 C-17.17563,-0.54200,0.00887,-17.59695,-0.50551,0.00967,
 C-17.85195,-0.50092,0.01025,-17.84378,-0.55745,0.01050,
 C-17.58929,-0.69379,0.01046,-17.38142,-0.81832,0.01031,
 C-17.32045,-0.87894,0.01022,-17.30779,-0.90388,0.01019/

* 2.5 MeV

DATA ((PRIGAM(8,J,I),I = 1,3),J = 1,20) /
 C-7.92954,-0.98676,0.00464,-9.15743,-0.95848,0.00453,
 C-9.79689,-0.93304,0.00450,-10.43662,-0.90238,0.00450,
 C-11.03843,-0.87135,0.00454,-11.60502,-0.84194,0.00463,
 C-12.31311,-0.80576,0.00481,-13.02839,-0.76978,0.00511,
 C-13.91068,-0.72439,0.00565,-14.85561,-0.67139,0.00649,
 C-15.62706,-0.61920,0.00740,-16.23975,-0.57630,0.00829,
 C-16.73064,-0.54145,0.00913,-17.12407,-0.51501,0.00987,
 C-17.37571,-0.51354,0.01045,-17.41302,-0.56089,0.01077,
 C-17.13507,-0.70903,0.01078,-16.80073,-0.87415,0.01058,
 C-16.64530,-0.96460,0.01044,-16.59248,-1.00247,0.01038/

* 1.5 MeV

DATA ((PRIGAM(9,J,I),I = 1,3),J = 1,20) /
 C-7.58567,-0.98475,0.00605,-8.81580,-0.94930,0.00590,

C-9.47027,-0.91570,0.00586,-10.12112,-0.87592,0.00585,
 C-10.72606,-0.83646,0.00588,-11.28246,-0.80051,0.00594,
 C-11.95995,-0.75838,0.00609,-12.62827,-0.71931,0.00634,
 C-13.43664,-0.67503,0.00678,-14.30309,-0.62950,0.00748,
 C-14.99557,-0.59361,0.00823,-15.54272,-0.56631,0.00899,
 C-15.97945,-0.54493,0.00971,-16.32359,-0.53037,0.01037,
 C-16.58714,-0.52369,0.01095,-16.72687,-0.54101,0.01139,
 C-16.64413,-0.63341,0.01169,-16.23381,-0.81927,0.01160,
 C-15.88589,-0.96327,0.01142,-15.71597,-1.03426,0.01132/
 * 0.75 MeV
 DATA ((PRIGAM(10,J,I),I = 1,3),J = 1,20) /
 C-7.14444,-0.99694,0.00839,-8.40557,-0.94672,0.00815,
 C-9.08480,-0.90034,0.00808,-9.75001,-0.84825,0.00805,
 C-10.35795,-0.79770,0.00806,-10.90872,-0.75179,0.00811,
 C-11.55655,-0.70042,0.00822,-12.17259,-0.65601,0.00840,
 C-12.87772,-0.61438,0.00872,-13.61158,-0.58111,0.00921,
 C-14.18642,-0.56337,0.00974,-14.63111,-0.55635,0.01029,
 C-14.97583,-0.55384,0.01085,-15.24170,-0.55479,0.01136,
 C-15.46310,-0.55269,0.01186,-15.64410,-0.55038,0.01230,
 C-15.85622,-0.54637,0.01287,-16.06595,-0.53718,0.01350,
 C-16.20228,-0.52879,0.01393,-16.26594,-0.52541,0.01413/
 * 0.325 MeV
 DATA ((PRIGAM(11,J,I),I = 1,3),J = 1,20) /
 C-6.71592,-1.03172,0.01153,-8.07690,-0.94581,0.01120,
 C-8.78940,-0.88085,0.01112,-9.47427,-0.81217,0.01108,
 C-10.09263,-0.74702,0.01108,-10.63353,-0.69058,0.01111,
 C-11.25494,-0.62881,0.01120,-11.82104,-0.57826,0.01133,
 C-12.43931,-0.53484,0.01155,-13.03722,-0.51037,0.01186,
 C-13.48116,-0.50724,0.01218,-13.80129,-0.51925,0.01251,
 C-14.03747,-0.53675,0.01287,-14.21578,-0.55331,0.01323,
 C-14.35568,-0.56531,0.01359,-14.46665,-0.57279,0.01391,
 C-14.60595,-0.57434,0.01434,-14.74812,-0.56676,0.01483,
 C-14.84392,-0.55716,0.01517,-14.89213,-0.55091,0.01535/
 * 0.1 MeV
 DATA ((PRIGAM(12,J,I),I = 1,3),J = 1,20) /
 C-6.40158,-1.04235,0.01675,-7.81309,-0.92558,0.01632,
 C-8.50949,-0.85097,0.01622,-9.16255,-0.77588,0.01617,
 C-9.73855,-0.70714,0.01617,-10.23417,-0.64890,0.01621,
 C-10.78308,-0.58847,0.01631,-11.25874,-0.54288,0.01643,
 C-11.74978,-0.50890,0.01663,-12.18135,-0.50036,0.01687,
 C-12.47044,-0.51439,0.01710,-12.66152,-0.54219,0.01734,
 C-12.78589,-0.57551,0.01758,-12.86513,-0.60814,0.01784,
 C-12.91613,-0.63496,0.01810,-12.95385,-0.65299,0.01835,
 C-13.00502,-0.66188,0.01874,-13.06711,-0.65253,0.01923,
 C-13.10413,-0.64177,0.01957,-13.12132,-0.63549,0.01974/
 * energy grid for tabulated values
 DATA (EN(I),I = 1,17) /.10,.15,.2,.3,.4,.5,.6,.8,1.,1.5,2.,
 C3.,4.,5.,6.,8.,10./
 * ANGLE GRID FOR TABULATED VALUES
 DATA (ANGLE(I),I=1,20) /0.5,1.5,2.5,4.0,6.0,8.5,12.5,17.5,25.0,

C35.0,45.0,55.0,65.0,75.0,85.0,95.0,110.0,130.0,150.0,170.0/
 DATA PI /3.14159265/
 * GUASSIAN QUADRATURE POINTS FOR GUASS 32 PT QUAD
 * ANGULAR DIRECTIONS X(I)
 DATA (X(I),I=17,32) /.048307665687738,.144471961584796,
 C.239287362252137,.331868602282128,.421351276130635,
 C.506899908932229,.587715757240762,.663044266930215,
 C.73218211874029,.7944837959679421,.84936761373257,
 C.896321155766052,.93490607593774,.9647622555875059,
 C.985611511545268,.997263861849482/
 * GAUSSIAN WEIGHTS.
 DATA (W(I),I=17,32) /9.654008851472801D-02,.095638720079275,
 C.093844399080805,.091173878695763,8.765209300440401D-02,
 C.083311924226947,7.819389578707001D-02,.072345794108849,
 C.06582222776362,.058684093478536,.050998059262376,
 C.042835898022227,.034273862913021,.025392065309262,
 C.016274394730906,.00701861000947/
 * 16 POINT GAUSSIAN QUADRATURE DATA
 * ANGULAR DIRECTIONS X(I)
 DATA (X(I),I=33,40)/0.095012509837,0.281603550779,0.458016777657,
 C0.6178762444026,0.755404408,0.865631202388,0.94457023073,
 C0.9894009349916/
 * GAUSSIAN WEIGHTS.
 DATA (W(I),I=33,40)/0.189450610455,0.182603415045,0.169156519395,
 C0.14959598816,0.124628971255,0.09515851168249,0.0622535239386,
 C0.0271524594117/
 END

CO-60 GAMMAS USED IN BENCHMARK EXPERIMENTAL SET UP. 21 CM CONCRETE SHIELD.

```
26 11 16 0.2099998E+02
1.32910000 -0.21000000 0.0000000E+00 0.1250000E-02 0.2546019E+00 1
0.2500000E+02 0.1000000E+04 0.5000000E+02
1.24913500 1.08389700 0.94448430 0.83443190 0.72436540
0.61940720 0.51417040 0.40399720 0.29370560 0.19372250
0.09305161
0.28694063E-01 0.12730098E+00 0.22590786E+00 0.27773422E+00 0.37065309E+00
0.51540941E+00 0.67888516E+00 0.82364148E+00 0.91656035E+00 0.94387990E+00
0.95959461E+00 0.98009801E+00 0.99581277E+00
0.47022040E-05 0.15223846E-03 0.56299102E-03 0.95597235E-03 0.20521560E-02
0.30115084E-02 0.52521937E-02 0.88381656E-02 0.14977988E-01 0.17375331E-01
0.17090712E-01 0.48849441E-04 0.62234257E-03 0.88301837E-03 0.20534184E-02
0.28775800E-02 0.40205047E-02 0.67575760E-02 0.10567617E-01 0.16934209E-01
0.19957155E-01 0.20271797E-01 0.20578112E-03 0.14748077E-02 0.21566362E-02
0.26595094E-02 0.44032671E-02 0.52555390E-02 0.82526803E-02 0.12288887E-01
0.18553708E-01 0.22066455E-01 0.22938035E-01 0.92780311E-03 0.22236416E-02
0.28058987E-02 0.35442943E-02 0.49042068E-02 0.60939305E-02 0.91133118E-02
0.13195600E-01 0.19330963E-01 0.23080699E-01 0.24239130E-01 0.44669174E-02
0.48087537E-02 0.37399449E-02 0.54366104E-02 0.64953342E-02 0.74979737E-02
0.10756973E-01 0.14895651E-01 0.20586073E-01 0.24771806E-01 0.26455171E-01
0.18972654E-01 0.10200851E-01 0.73076747E-02 0.83342344E-02 0.95182173E-02
0.10106735E-01 0.13666026E-01 0.17567530E-01 0.22445098E-01 0.27324859E-01
0.29720094E-01 0.43765388E-01 0.19039553E-01 0.12353405E-01 0.12530528E-01
0.13439607E-01 0.13594542E-01 0.17267536E-01 0.20353712E-01 0.24325125E-01
0.30082576E-01 0.33227455E-01 0.66986382E-01 0.25518179E-01 0.17212339E-01
0.17695744E-01 0.17719690E-01 0.17160382E-01 0.20455401E-01 0.22344738E-01
0.25482006E-01 0.32345820E-01 0.36221828E-01 0.81144273E-01 0.28558638E-01
0.19103136E-01 0.21069471E-01 0.21600537E-01 0.20276256E-01 0.22555020E-01
0.22941228E-01 0.26023451E-01 0.33709206E-01 0.38112491E-01 0.84768355E-01
0.28907619E-01 0.21279372E-01 0.20921603E-01 0.22311699E-01 0.21604430E-01
0.23276970E-01 0.23180500E-01 0.26203763E-01 0.34103289E-01 0.38666334E-01
0.86422503E-01 0.30600026E-01 0.20337187E-01 0.21597095E-01 0.23381796E-01
0.21648917E-01 0.23853570E-01 0.23171041E-01 0.26310250E-01 0.34305081E-01
0.38975243E-01 0.90028822E-01 0.30385982E-01 0.19603256E-01 0.22873476E-01
0.24471726E-01 0.22968661E-01 0.24191812E-01 0.22764482E-01 0.26419207E-01
0.34568090E-01 0.39366838E-01 0.91310024E-01 0.29957492E-01 0.22471957E-01
0.21923792E-01 0.24178460E-01 0.24028271E-01 0.25184281E-01 0.22575960E-01
0.26516844E-01 0.34756698E-01 0.39668877E-01
1 1.24500000 0.12130129E+00 1.00000000
```

Gamma SkyShine Calculations for Shielded Sources

by

Michael S. Bassett

B.S., Kansas State University, 1986

AN ABSTRACT OF
A MASTER'S THESIS

submitted in partial fulfillment of the

requirements for the degree

MASTER OF SCIENCE

Department of Nuclear Engineering

KANSAS STATE UNIVERSITY
Manhattan, Kansas

1989

ABSTRACT

Radiation that is scattered in the air back to a ground target is known as skyshine and is of concern in any radiation facility. For unshielded gamma-photon sources, several accurate approximate techniques have been developed to calculate the far-field skyshine doses. However, the accuracy of these methods when applied to shielded sources remains largely unknown. Thus, the primary purpose of this work is to develop an accurate method for treating shielded sources, and then to assess the accuracy of an approximate method which uses simple buildup and exponential attenuation to account for the source shield.

The resulting composite method uses an accurate one-dimensional transport code to calculate the energy and angular distribution of photons emerging from a slab shield above the source. Then this emergent photon distribution is used as an effective point source by an approximate, but accurate, method based on beam response functions to determine the far-field skyshine dose. This composite method is capable, as shown from comparisons to benchmark experimental data, of accurately calculating the shielded skyshine dose.

The composite method is used to assess the accuracy of the approximate MicroSkyshine method which uses buildup and exponential attenuation to account for the source shield. Shield thicknesses from 0.001 to 6 mean-free-paths are considered. For broadly collimated N-16 sources, the approximate method results are within a factor of two of the composite results. For narrowly collimated N-16 sources the approximate method is generally underpredictive by more than a factor of two. At source energies of 1.25 MeV and below, the

approximate method never underestimates by more than a factor of 2, and tends to overpredict, often by a factor greater than two (especially for broadly collimated sources).

The composite method reveals two surprising features. First, increasing the thickness of a thin shield (< 1 mean-free-path length) often causes the skyshine dose to increase. This effect is especially evident for high energy photons collimated vertically into a narrow beam. Second, the skyshine dose is almost independent of source photon energies for source-to-detector distances less than 250 meters. At distances greater than 250 m, the skyshine dose increases with increasing photon energy.

